Master Thesis in physical oceanography

Ice and Brine production in Hornsund

by

Martin Arntsen

University of Bergen
Geophysical Institute

University Centre
in Svalbard

Acknowledgements

I would first of all like to thank my supervisors. Great thanks to my main supervisor Frank Nilsen, you have been a motivation and an inspiration, not only though this year of working on the Master thesis, but from my first stay at Svalbard in 2011 when I was first introduced to the fascinating study of oceanography. Your enthusiasm and positive attitude is of great help when questions seem difficult to answer. Thanks to Lars Henrik Smedsrud at Geofysen for always finding time to sit down for a discussion on your short and busy stays in Longyearbyen, as well as valuable feedback on the text towards the end of the writing period. Also great thanks, to Ragnheid Skogseth for never being to busy to use your expertise in understanding what kind of problem I have encountered and very often having a solution, and to Arild Sundfjord at the Norwegian Polar Institute who has provided interesting data and given me motivating and quick feedback when I have had questions about the water circulating, either in the ocean or on the computer screen.

Thanks to the rest of the group at the Geophysics department at Unis for good discussions and a nice working environment. And thanks to Jorie for your help with improving the language.

And finally, and important, thanks to the crew in Barrack 4, skiing and studying is even more fun together with good people! Last (but in the same order of magnitude), thanks to the dogs in the dog yard, who deserve some more attention the upcoming days.

Martin Arntsen
Longyearbyen, June 1^{st} 2015

Abstract

The Hornsund fjord system has been studied using observations of the atmosphere, ocean and sea ice, and two different types of models. The study documents significant year to year variability in sea ice formation and brine release in the fjord over the period 1978 - 2014, production of brine enriched winter water, and inflow of warmer Atlantic water in recent years.

Salt production through brine release was investigated for the winter period between 1978 and 2014 using a simple one-dimensional polynya model forced with observed wind and air temperatures. Results show that easterly winds dominate in winter, often accompanied by cold air temperature. This favour high ice production as open water is often exposed to the cold air due to the development of a polynya in the fjord. The yearly accumulated heat exchange over open water is the main driver of the year to year variations in ice production.

The effect of a fast ice cover restricting the polynya activity is included for the years 2006 - 2014, and results show that this reduces the magnitude in the year to year differences in salt production. This is a result of higher fast ice coverage in years of high polynya activity. In later years (2012-2014) indications of a warmer inflow is seen in the hydrographic observations, and in 2013 came into contact with the Brine enriched winter water that is trapped at depth behind the sill. The warm water will likely contribute to melting of the tide water glaciers in the fjord.

Simulations using the Regional Ocean Model System (ROMS) are presented and evaluated towards observed hydrography and satellite observations of the ice cover. Simulations cover the period 2005-2010 and show that inflow events generally warm the lower layer in the inner parts of the fjord before the onset of freezing.

Contents

Chapter 1

Introduction

In 1901, Captain Roald Amundsen conducted temperature and salinity measurements in an extensive survey of the Barents and Norwegian sea (Nansen, 1906). The findings of a very cold and saline bottom water at many places were by Nansen (1906) explained by intensive surface cooling, as well as a salinity increase in the surface by ice formation. Nansen (1906) further pointed out the occasional rapid cooling of surface water on the freezing point, when "lanes" of open water is developing in the ice, and exposes the water to the cold atmosphere. The cold water will mix with underlaying water masses, if dense enough sink, and can be found in depressions in the sea bed even in summer. The cold water may also spread out over the shallow banks, and, due to gravity, percolate down the continental slope until it reaches a depth of similar density. Several studies were done in the early 20^{th} century on the formation of dense water, and it was speculated that ice formation on shallow shelfs could be one of the important mechanisms driving the creation of bottom water that eventually ended up in the deep basins of the South Atlantic (Brennecke, 1921; Mosby, 1934) and Arctic oceans (Nansen, 1906, 1915)

Central Arctic and Antarctic pack ice consists of roughly 1% and 10% of open water in the form of leads (Barber and Massom, 2007). Ocean - Atmosphere heat fluxes over the leads can be over two orders of magnitude higher than through the surrounding pack ice (Smith et al., 1990). In addition to leads, greater areas of open water are found at certain locations in the Arctic and Antarctic pack ice, named polynyas. The term polynya originates from Russian, and translates to "ice hole". This hole in the ice can be kept open in two ways, either through advection of the ice cover by currents or wind, or by melting of the sea ice by upwelling of warmer water masses. It is however shown that the cause of a polynya is often a combination of the two (Morales Maqueda et al., 2004). In literature the polynyas are often referred to as "ice factories" (Morales Maqueda et al., 2004; Williams et al., 2007; Nilsen et al., 2008), because the effective heat loss over the open water results in a rapid growth of frazil ice. The frazil ice is prevented by the wind and/or wave induced turbulence to consolidate into a firm ice cover. As factories of sea ice, polynyas also have the potential to serve as great producers of dense water. This is a result of the formation of very saline water, brine, that is formed due to the inability of salt to be incorporated into the forming ice crystals. Some of the brine is trapped in pockets in the ice, and

some is immediately rejected to the underlying water mass. The density of the water produced will depend on several conditions, such as the intensity of ice formation, salinity of the underlaying water column, and the depth of the layer were the brine is diluted. The latter can be confined to a surface layer, separated from the underlaying water mass by a pycnocline, or consist of the entire water column if convection is strong enough. Through a modeling study, basing polynya dynamics on a polynya flux model originally presented by Pease (1987), Winsor and Björk (2000) estimated that Arctic polynyas accounted for ∼30% of the dense water production necessary to maintain the Cold Halocline (Aagaard et al., 1981). Winsor and Björk (2000) further showed that polynya activity in the Chukchi Sea contributed to formation of Arctic Ocean deep water. Whereas several studies, e.g. Foldvik and Gammelsrød (1988), Gordon (1998), and Baines and Condie (1998), demonstrates how enhanced ice formation give rice to production of high salinity shelf water on the Antarctic continental shelf, which in turn contributes to the formation of Antarctic intermediate and deep water in the Weddel Sea.

Storfjorden, on the eastern side of Svalbard, is one of the areas where a considerable amount of the Barents Sea high density shelf water is produced (Schauer, 1995). Variations in large scale atmospheric circulation and oceanic conditions, such as salinity modification in summer by water of Atlantic origin, are factors that influence the year to year variability in the dense water and its contribution to the deep water formation off the continental shelf (Schauer and Fahrbach, 1999; Skogseth et al., 2004).

In addition to ventilate the deep basins of the world oceans, dense water formation may also have an impact on the local circulation in smaller fjord systems. With a focus on Isfjorden, Nilsen et al. (2008) describes how fjords on the West coast of Spitsbergen can act as coastal polynyas, where prevailing easterly winds maintain an ice free fjord for longer periods with sub-freezing air temperatures. Based on the physics of other polynya studies (Pease, 1987; Skogseth et al., 2004), they estimated the dense water produced through six winter seasons, and compared this with hydrographic observations. Dmitrenko et al. (2015) studied polynya events in the mouth of Young Sound on the north east coast of Greenland during the winter of 2013. They demonstrated how the dense water produced in the polynya is ventilating the intermediate water layer of the silled fjord. On the West coast of Spitsbergen there will always be a combined effect of atmosphere and oceanic implications to whether an ice cover is developing in the fjords through winter. Most of the fjords have an open connection to the shelf that allows for warmer Atlantic type water to penetrate the fjord, something that is observed more rapidly during winter in the last decades (Walczowski and Piechura, 2011; Pavlov et al., 2013).

On his journey with Veslemøy in 1912, Fritjof Nansen took oceanographic measurements at several positions along the shelf West of Spitsbergen. On the shelf close to shore they found the coldest water temperatures in the south, in which the whole water column in the mouth of Hornsund in September was below 0°C. Nansen (1915) stated that the water had its origin in the Polar Water, and had been carried with the current around the Sør-Kapp. Because the water was closer to its origin, it was colder then the water found further north that had mixed with the Atlantic Water off the shelf. In winter, Horsund is the fjord that experience the most drift ice, which is brought around the cape by the coastal current

(Wadhams, 1981). In general a decrease in sea ice is observed northward, indicating that melting is taking place along the shelf (Tverberg et al., 2014). The local conditions in winter in the fjords of West Spitsbergen, are to a great extent related to the position and interaction between the warm water carried by the West Spitsbergen Current (Cottier et al., 2007; Walczowski and Piechura, 2011; Nilsen et al., ress) and the cold water carried by the coastal current (Cottier et al., 2005), as well as local processes going on in the fjord (Nilsen et al., 2008). The latter often being a product of the two first.

The presented work is part of the AWAKE-2 project, which aims to improve the understanding of the effect of increased Atlantic water inflow onto the shelf area, and into the Svalbard fjords, on the Svalbard climate. In this study we will present inter annual differences in both the atmospheric and hydrographic conditions in Hornsund. This will be linked to the variability in the ice cover in in the fjord. The approach of Nilsen et al. (2008) will be used, were a polynya model (Pease, 1987; Haarpaintner et al., 2001; Skogseth et al., 2004) will help in the understanding of the atmospheric contribution to dense water formation and water transformation through winter. A discussion of the impact of warm Atlantic Water in the fjord, as a reason for low ice concentration in certain years will be given. This discussion will further lead us to other implications, such as impact on the many tide water glaciers defining the shore line of Hornsund (Błaszczyk et al., 2013). We therefor investigate the likelihood of Atlantic water to come into contact with the glacier fronts in the inner part of Hornsund. Hydrographic observations in Hornsund are mostly confined to the summer months, including some measurements made in spring and fall. We therefore present results from a five year long 3-dimentional model simulation of the circulation in the fjord. The simulations are made using Regional Ocean Model System (ROMS) (Budgell, 2005), that might provide additional insight into the water circulation pattern in the fjord over the whole season.

The thesis is structured as follows:
Chapter 2 presents a general description of the circulation in the Fram Strait and its interaction with the fjords along the the West Coast of Spitsbergen. An overview of water mass characteristics and ice conditions and a description of the regional settings in Hornsund is given. Chapter 3 first presents the sources for observational data of atmosphere, ocean and ice conditions. Second a description of the polynya model is provided. Finally a brief presentation of the ROMS-model is given. In Chapter 4 results of atmosphere and hydrography observations are presented. Modelled ice and salt production results are given, and time series from selected stations of the ROMS-simulations are presented. A discussion on the results are given in Chapter 5. Here the polynya model is evaluated through comparison with satellite ice observations, and hydrographic measurements. An evaluation of the ROMS-simulations is given, and finally we discuss how all the information can be utilised in helping to understand what governs the ice production and dense water production in the fjord. In Chapter 6 some of the major findings of this work are summarised in an attempt to draw some conclusions on the major factors governing the ice situation in Hornsund and the adjacent shelf area. Some future perspective and suggestions are described in Chapter 7.

Chapter 2

Hornsund: A Fjord on the West Coast of Spitsbergen

This chapter gives a brief overview of the circulation in the Fram Strait, with particular emphasis on the western part, and its interaction with the shelf water off the coast of Spisbergen. An overview of the water masses and the transformation of these through local processes in the fjords is included. This overview provides an initial idea of the processes governing the circulation and water mass transformation in the southernmost and smallest, but still important fjord of Hornsund. A brief description of the regional features of Hornsund is given, and lastly some aspects on the variability in sea ice conditions.

2.1 Circulation in the Fram Strait

The relatively warm climate along the west coast of Spitsbergen, compared with other Arctic regions at same latitude, is to a great extent caused by the West Spitsbergen Current (WSC), which transports warm, saline water up from lower latitudes. This heat flow makes the Fram Strait the northernmost ocean area on earth, free of sea ice year round. The WSC is steered by the topography and follows the shelf break northward along the the western coast of Spitsbergen (Gammelsrød and Rudels, 1983). Gammelsrød and Rudels (1983) also found the current to steer east as it reaches north of Spitsbergen. However, WSC is found to split up in several branches as it reaches the end of the strait. Some of the water turns west, joining the East Greenland Current (Bourke et al., 1988) , and one branch goes north, following the Yermak Plateau (Gascard et al., 1995). The water in WSC continuously looses heat on its way north (Boyd and D'Asaro, 1994). Some heat is lost directly to the atmosphere, some mixes with surrounding water masses, and some is brought onto the shelf, and mixes with shelf water and local water inside the fjords on the west coast (Saloranta and Haugan, 2004; Nilsen et al., 2008; Svendsen et al., 2002). As the WSC is following the shelf break northward, a Coastal Current (CC) is running parallel to it on the shelf. This current is an extension of the East Spitsbergen current, rounding the tip of Sør Kapp, and brings colder and fresher water northward that is supplied by fresh

water originating from river runoff and glacier melt along the coast (Cottier et al., 2005). Studies have been done in order to understand the mechanisms allowing warm Atlantic water onto the shelf, and into the fjords (Saloranta and Svendsen, 2001; Svendsen et al., 2002; Nilsen et al., 2008). In winter this can be of great importance for the ice production in the fjords. Saloranta and Svendsen (2001) studied how the front between Atlantic water in the WSC and colder water in the CC takes part in controlling the exchange of Atlantic water across the shelf. Nilsen et al. (2008) showed how the density and amount of locally produced winter water can control the ability for the Atlantic water to penetrate into the fjord of Isfjorden.

2.2 Hydrography and water masses

In a silled fjord, the vertical structure can typically be divided into three layers. The bottom layer often reaching up to sill depth, being in a more quiescent state undergoes diffusive and turbulent mixing and/or occasional renewal of the water that is controlled by outer forcing (Inall and Gillibrand, 2010). The circulation above sill level is typically dominated by estuarine circulation where fresh water input at the head of the fjord sets up a pressure gradient in the out-fjord direction. This gradient initiates a surface current that mixes with underlying water masses, which results in a thickening of the surface layer from head to mouth of the fjord. A halocline (strong salinity gradient, that often defines the stratification at high latitudes) separates the surface layer from the underlaying water, which is often found to be an intermediate water mass spanning the water column down to sill depth. This water mass might consist of a mix between locally produced water and water advected from the shelf and ocean outside. Throughout fall and early winter, these layers may brake down due to a heat loss to the atmosphere, and formation of an ice cover.

In general the distribution of water masses occupying the fjords along the west coast of Spitsbergen shows a seasonal cycle. The changes throughout the year are responses to external forces from water masses existing on the shelf and their ability to intrude the fjord, to local processes such as atmospheric cooling, river run off and glacial melt, and ice production, as well as different mixing processes inside the fjord. To identify the different water masses, a classification based on summer properties presented by Svendsen et al. (2002) for the Kongsfjord/Krossfjord system has been used by several authors investigating water mass properties and exchange mechanisms between shelf and fjord (e.g. Cottier et al. (2005); Nilsen et al. (2008)). The Atlantic Water (AW), carried north by the WSC is characterised by its high salinities and temperatures ($S > 34.9$ psu, $T > 3°C$). The AW in the WSC is usually separated by a strong front from the colder water on the shelf following the CC (Saloranta and Svendsen, 2001). The colder water mass in the CC is of Arctic origin and is named Arctic Water (ArW). The freshening of this water mass as the water flows north-ward along the western coast results in a wider range of salinity characteristics. Cottier et al. (2005) defined ArW summer temperatures to be in the range $-1.5 < T < 1.0°C$, and salinities in the range $34.30 < S < 34.80$ psu.

During fall 2002, the West Spitsbergen Shelf was occupied by AW, and penetrated

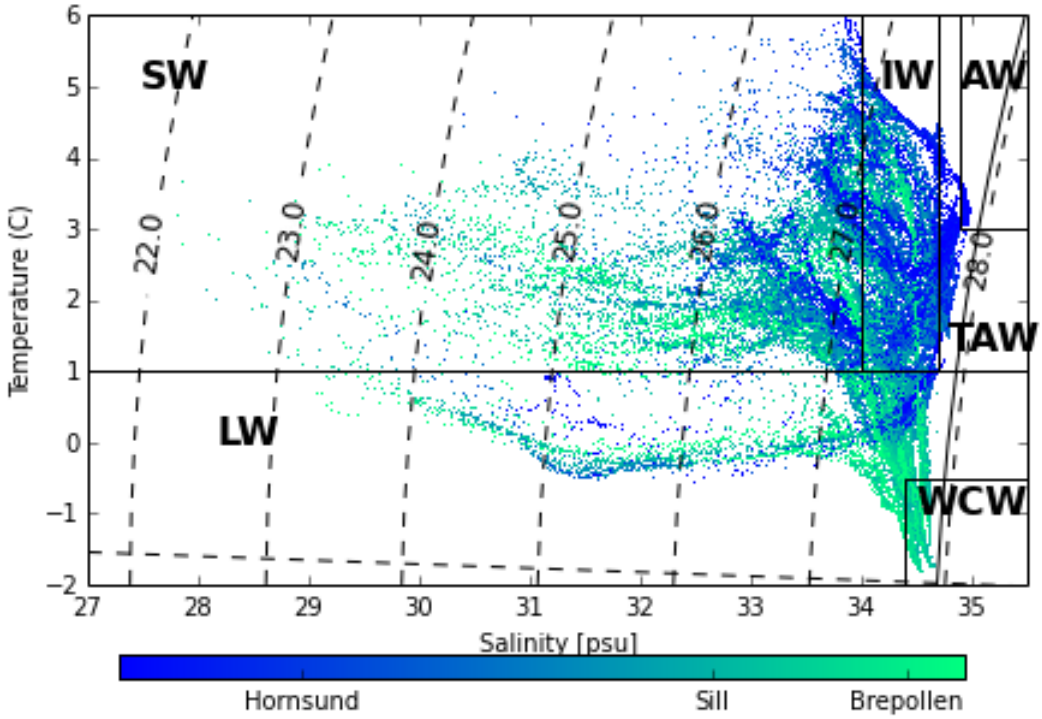

Figure 2.1: Water mass distribution in Summer in Hornsund with water mass characteristics based on Svendsen et al. (2002). WCW resulting from brine rejection is in this text denoted BWW. All data are sampled in late July (Prominska et al., Unpublished data) by the Institute of Oceanology of the Polish Academy of Science. Yearly transects are made reaching from the inner Bay of Brepollen, over the sill and further out to the mouth of Hornsund (dashed lines in map in Figure 2.2). The colors of the plot, indicate the positions of the stations relative to the sill.

into the fjords (Nilsen et al., 2008; Cottier et al., 2005). More often the water undergoes mixing with the coastal waters on the shelf. The mixing product between AW and ArW, a colder and less saline water mass, is often found in the fjord defined as Transformed Atlantic Water (TAW), with temperatures $T > 1°C$ and salinity $S > 34.7$ psu (Svendsen et al., 2002). Through summer, glacier melt, river run-off, and precipitation leads to a distinct surface layer of fresher and warmer water named Surface Water (SW). The close interaction with the atmosphere leads to a wide range of temperatures (generally $T > 1°C$), and through mixing with underlying waters salinities will increase as one approaches the fjord mouth. The entrainment and mixing between SW and the underlying AW or TAW give rise to the formation of an Intermediate Water mass (IW) that is defined as having salinities in the range $34 < S < 34.7$ psu. Approaching the end of the year, the colder air temperatures reduce the freshwater input and the surface layer starts cooling down. Throughout winter and spring this leads to formation of a water mass denoted as Local Water (LW).

Nilsen et al. (2008) describes several processes leading to the formation of LW (T < 1°C). LW can have a wide range of salinities. As it mixes with underlying TAW the salinity increases, and as soon it reaches the freezing point and ice formation starts, the corresponding brine release may cause a strong enough densification to make it convect towards the sea floor. After the freezing season, the water close to the freezing point with high salinities may be found at depth termed Winter Cooled Water (WCW; T < -1°C, S > 34.4 psu). During spring this water can mix with TAW and fall under the definition LW. The density of WCW is to a great extent determined by the ice production throughout winter. In silled fjords like Billefjorden, a side fjord of Isfjorden, it is usual to find WCW that, due to low water exchange rates has persisted through the following summer. Properties of WCW trapped behind the sill can be used as a measure of the previous winters ice production and polynya activity in the fjord (Nilsen et al., 2008).

As the amount of AW in the fjords on the west coast of Spitsbergen has increased throughout the latest years, strong cooling of this rather saline water mass can lead to formation of dense and cold water in the fjords with similar temperature and salinity characteristics as the brine enriched water produced through ice formation. In the proceeding text the water mass characteristics by Svendsen et al. (2002) will be adopted, and the term Brine enriched Winter Water (BWW) will be used to define deep water exclusively produced through the freezing process. Furthermore WCW and LW will be combined in the common term Winter Water (WW). A temperature salinity diagram is shown in Figure 2.1 which overviews the water mass definitions and the water mass distribution in Hornsund in summer.

2.3 Regional setting

Hornsund is the southern most fjord system on Spitsbergen, with its northern shore at the fjord mouth touching the 77°N latitude (Figure 2.2). The fjord axis is aligned 70° relative to north and stretches from 15.5°E at its mouth to 16.6°E at the head. The fjord system can be divided in two basins, in which a sill at 50 m depth between Treskelodden and Tranpynten separates Brepollen from the outer region. The total area is 323 km^2. The outer region does not have a prominent sill separating it from the shelf area outside, but a deeper area of about 250 m is found in the middle of the main basin. The main basin includes a side-fjord, Burgerbukta on the northern side which is 11% of the total area in size. The side-fjord of Samarinvågen is located on the southern shore, just east of the inner sill. It together with Brepollen has a surface area of about 108 km^2 and occupys 33% of the total area. As the name implies, the shore line of Brepollen is dominated by glaciers. These tide water glaciers have had a gradual retreat over the last century. Together with the retreat of the glaciers in Burgerbukta and Samarinvågen, this has led to an expansion in surface area of Hornsund of about 44% between 1899-2010 (Błaszczyk et al., 2013). In summer, glacier melt and run off give rise to a strong halocline between the surface layer and the underlying water masses.

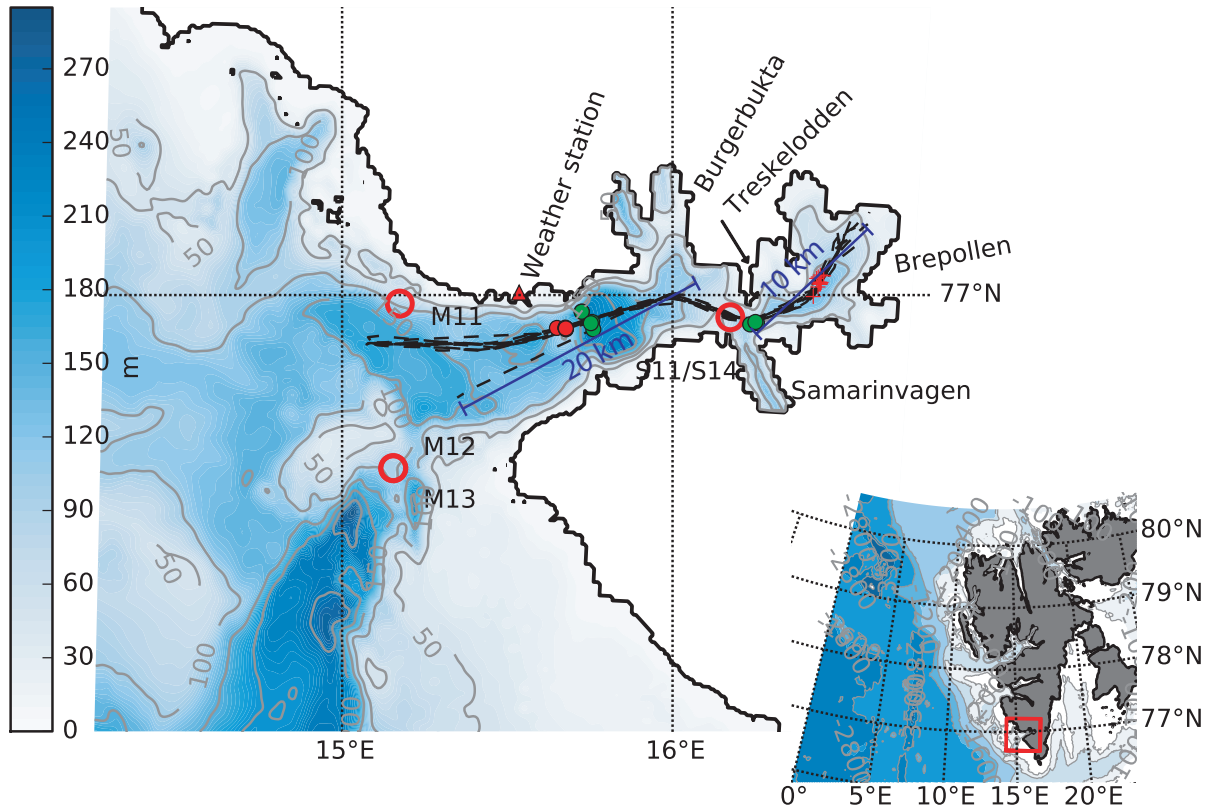

Figure 2.2: Bathymetry map of Hornsund. Position for mooring data are shown (Red rings), together with CTD longsections (dashed lines) and positions of CTD profiles (Green dots UNIS, Red dots IOPAS), both behind the sill in Brepollen and in Hornsund proper. Further description of the data is given in Section 3.1 and Table 3.1 and 3.2

2.4 Sea ice conditions

Similar to the other fjords on the west coast of Spitsbergen, the ice cover in Hornsund shows a seasonal cycle. In late summer only growlers and bergy bits from glacier calving is present in the fjord. As the freezing season starts, the more sheltered areas in the side fjords are the first locations to become ice covered. The ice cover in Hornsund main basin consists of either locally formed ice, or drift and pack ice transported into the fjord from the shelf area outside. The ice conditions show great year to year variability, both in the extent of fast ice cover and the duration of the ice season (Weslawski and Adamski, 1987). For the winter season of 2009/2010, Kruszewski (2010) reported that relatively warm temperatures prevented efficient ice growth formation in the start of the winter season. The inner areas of the fjord system were not fully covered by fast ice before mid March. On the contrary, the next year saw first ice forming in mid October, while the inner parts were fully covered by fast ice by mid December (Kruszewski, 2011). High ice concentrations lasted from January to end of March, but were interrupted by periods of strong easterly winds that transported the ice out of the fjord. Figure 2.3 shows four different representations of the ice situation in late April 2011. In the photograph (a), we can observe the polynya and the pack ice outside. (b) shows manual interpretations of the ice at the same time that are presented in Kruszewski (2011). The satellite image (c) is taken 6 days later and shows complete ice cover in the fjord. Manual interpretation of satellite imagery has been done by Muckenhuber et al. (In progress), and an example year of the produced time series is shown in (d). Ice thickness observations in Burgerbukta and in the sill area outside Brepollen in April 2004 were presented by Gerland and Hall (2006). Their measurements showed an ice thickness of around 1.2 meters. Observations done by Muckenhuber et al. (In progress) from satellite imagery show that the main basin of Hornsund is mostly occupied by open water or newly frozen thin ice or drift ice, whereas the inner parts, Brepollen, Burgerbuktan and Samarinvågen normally get an increasing fast ice coverage through out the winter.

(a)

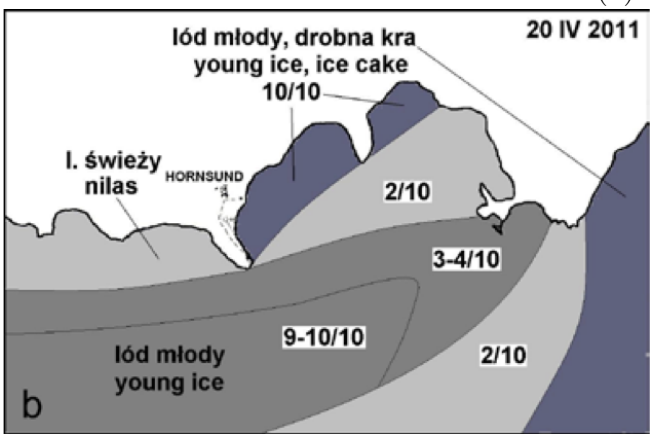

(b)

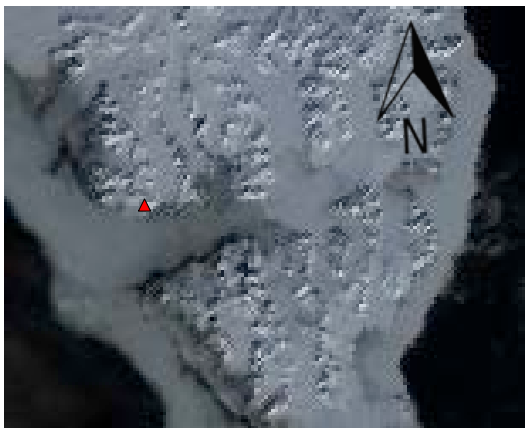

(c)

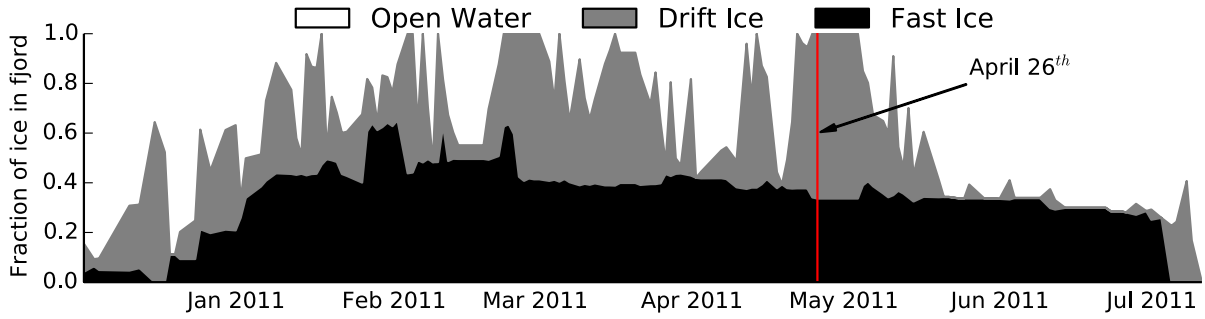

(d)

Figure 2.3: Different representations of Hornsund ice cover. (a) shows a photograph from April 20^{th} 2011, taken above the weather station in Isbjørnhavna, facing south. (b) is manual interpretation of ice classes from observations at the Polish Research Station in Hornsund from the same day. (a) and (b) are presented in Kruszewski (2011). (c) is a MODIS satellite picture from April 26^{th} 2011 (Red triangle represents the Polish weather station) and (d) is the time series established by Muckenhuber et al. (In progress) for the 2010/2011 winter season.

Chapter 3

Data and Method

In the following chapter, the different sources for ocean, atmospheric, and ice concentration data used are presented. Second, the governing equations for the polynya model are explained. Lastly, a brief description of the Regional Ocean Modeling System is given.

3.1 Hydrographical data

Hydrographic data from different sources will be presented in the results and used in the discussion. In addition, the polynya model input parameters, such as surface salinity at the beginning and the end of the freezing season, can be adjusted to enhance the model performance. Locations for the hydrographic data are shown in the map in Figure 2.2. Dashed lines are towed CTD long-sections, done late July 2006-2014 by the The Institute of Oceanology of the Polish Academy of Sciences (IOPAS). Red plus in Brepollen and Hornsund main basin are stations from the deepest point in Brepollen and Hornsund respectively that are extracted from the July long-sections. Red dots are spring data from IOPAS and green dots are UNIS stations from spring and fall (Table 3.1).

M11, M12, and M13 are IOPAS moorings with temperature and salinity data time series where specifications for the moorings are shown in Table 3.2. The moorings have provided three years of temperature and salinity time series. The three winter seasons from fall 2010 to summer 2013 have been covered. The moorings were deployed outside the mouth of the fjord with M11 on the northern side and M12 and M13 on the southern side (Red circles in Figure 2.2). One can expect water leaving the fjord to be topographically steered along the northern side of the mouth area (Cushman-Roisin and Beckers, 2011). Thereby M11 is able to capture the properties of the fjord water. Likewise, M12 and M13, on the southern side, are believed to provide information about water masses that can possibly intrude the fjord and affect the situation therein. The moorings give an indication on how the exchange between fjord and shelf evolvs throughout the year. Norwegian Polar Institute (NPI) has provided moored temperature time series from July 2011 to July 2012. The mooring (S11) was located on the sill outside Brepollen and provided a time series of the temperature profile through the 2011 winter season.

Table 3.1: Overview of the different hydrography data used. CTD-stations provided by UNIS in Hornsund are taken close to the deepest point and in Brepollen close to the sill. CTD-stations by IOPAS in Hornsund in spring are taken on the shallower area south of the weather station. The long-sections are from the inner part of Brepollen extending to the mouth of the fjord. July CTD profiles presented in Section 4.2 are extracted from these transects. Positions are are shown in Figure 2.2.

Type of Measurement	Location	Time	Provided by	Ship
CTD-station	Hornsund	2008-05-02	UNIS student cruise	Lance
CTD-station	Brepollen	2008-05-02	UNIS student cruise	Lance
CTD-station	Hornsund	2009-09-08	UNIS student cruise	Håkon Mosby
CTD-station	Hornsund	2011-09-06	UNIS student cruise	Håkon Mosby
CTD-station	Hornsund	2013-09-04	UNIS student cruise	Håkon Mosby
CTD-station	Brepollen	2013-09-05	UNIS student cruise	Håkon Mosby
CTD-station	Hornsund	2014-04-06	UNIS student cruise	Lance
CTD-station	Brepollen	2014-04-07	UNIS student cruise	Lance
Towed CTD	Longsection	July 2006-2014	IOPAS	R/V Oceania
CTD-station	Hornsund	2010-04-09	IOPAS	
CTD-station	Hornsund	2011-05-20	IOPAS	
CTD-station	Hornsund	2012-04-29	IOPAS	
CTD-station	Hornsund	2013-05-19	IOPAS	

Table 3.2: Mooring specification for M11, M12, M13 and S11. M11, M12, and M13 were deployed by IOPAS, and S11 was deployed by NPI. S11 has temperature string with 5 meter spacing between the sensors. Column 4four and five show depth of sensor and water depth at mooring position, respectively.

Name	Deployed	Recovered	Depth s. [m]	Depth w.[m]	Param.	Location
M11[a]	Jul 2010	Aug 2011	24	100	T, S	76° 59.651 N 15° 10.474 E
M12[a]	Jul 2011	Jul 2012	45	100	T, S	76° 52.898 N 15° 09.288 E
M13[a]	Aug 2012	Jul 2013	85	100	T, S	76° 52.898 N 15° 09.288 E
S11[b, c]	Sept 2010	Jul 2011	13.5 - 68.5	75	T	76° 59.000 N 16° 11.000 E

[a]SBE 37-SM MicroCAT, sampling interval of 15 minutes, and accuracy for the instrument is ± 0.1 psu for salinity and ±0.002°C for temperature.

[b]TinyTag Aquatic 2, sampling interval of 60 minutes, with a resolution of 0.01°C and an accuracy up to ±0.5°C.

[c]S11 was in spring (April 11^{th} 2011), for unknown reasons, moved in towards the deeper basin of Brepollen, from 75 m to 105 m depth.

3.2 Meteorological data

The weather data used for discussing the atmospheric conditions in Hornsund, as well as input for the polynya model presented below, was provided by the Norwegian Meteorological Institute and the Polish Polar Station in Hornsund. Wind speed and direction, relative humidity, temperature, and cloud cover have been measured at the Hornsund meteorological station since 1978. The station is located west of Isbjørnhavna, on the northern shore close to the mouth of Hornsund (see map in Figure 2.2). The data set consists of a nearly complete time series of the above mentioned parameters from July 1^{st} 1978 to May 1^{st} 2014. No data was available between July 7^{th} 1981 and August 15^{th} 1982, and wind direction was erroneous between November 29^{nt} and December 29^{nt} 2012. Therefor, information is lacking to run the polynya model for the winter season of 1982 and beginning of the winter season 2013. Observation data with a six hour time step is used. When forcing the polynya model, missing data points have been linearly interpolated between neighbouring values.

The position of the weather station at Isbjørnhavna rises the question of the validity for the input data for the fjord as a whole. When including Brepollen in the model, it is under the assumptions that the weather data, and especially temperature and wind measurements done at the weather station in Isbjørnhavna is representable also for this area. The middle of Brepollen is about 20 km east of the Polish meteorological station, and has different topographic features surrounding the basin that might influence the wind pattern over the ocean surface. A weather station at Treskelodden (See map Figure 2.2) has been recording wind speed and direction, relative humidity, and air temperature in the period August 26^{th} to October 10^{th} 2014. This will be used to compare the weather situation at the two locations

3.3 Sea ice observations

A satellite data base was established by Muckenhuber et al. (In progress) which includes high spatial and temporal resolution satellite images for Hornsund and Isfjorden for the period 2000-2014. Both Synthetic Aperture Radar (SAR) and visual/near infrared (VIS/NIR) is included in the database. In addition, a manual interpretation of the images was done by Muckenhuber et al. (In progress) to develop a time series that distinguishes between areas of fast ice, drift ice, and open water for the fjord (See Figure 2.3 (d)). They further introduce a fast ice index for the fjords, "Days of fast ice coverage" (DFI), which is the accumulated daily fraction of fast ice coverage in the fjord over a freezing season. This index quantifies the yearly amount of fast ice, and reveals the inter annual differences in fast ice coverage which can be compared between the fjords. SAR images where available after 2006, so after this the time series cover ice classifications also during polar night. In this study, the fast ice cover will serve as an input to the polynya model, as it shrinks the effective area of which we can expect polynya activity. Further, the time series and selected satellite images are used to compare model results with the drift and fast ice observations.

3.4 The Polynya Model

A polynya consists of open water or newly formed ice and/or brach ice (WMO, 1970). Polynyas occur in winter, when air temperatures are well below freezing point. This creates a large heat exchange between the relatively warm sea water and the cold atmosphere. The opening can be fully enclosed by pack ice or bordered by a shore line on one side. A polynya kept open by wind or currents that transport the pack ice away is named a latent heat polynya, and a polynya created by upwelling of warm water that melts the ice is called a sensible heat polynya (Smith et al., 1990). In coastal regions, latent heat polynyas typically develop on lee sides of islands, land, and fast ice (Haarpaintner et al., 2001). A balance between off shore ice drift, due to katabatic winds from land, and the ice production in the area exposed to the atmosphere, keeps the water ice free and can give rise to a large production of sea ice. Sea ice dominates the Arctic in winter and ice production can be estimated by Stefan's law (Stefan, 1891) as soon as a thin layer of ice is formed. The further thickening of the ice will decrease with time, as the isolating layer becomes thicker. The sea ice, often covered with snow, will then isolate the water, and, with its high albedo, also reflect short wave radiation. Polynyas on the other hand, with their low albedo, absorb solar radiation, which in spring can turn them into effective melting areas (Ohshima et al., 1997).

The opening of a latent heat polynya is determined by the wind that acts on the ice surface. The model presented and used in this work has its roots in the model described by Pease (1987). Pease (1987) states that the opening of a polynya or a lead ($\frac{dW_o}{dt}$) will be proportional to the difference between the advection rate of the consolidated ice and the freezing rate of the open water within the polynya, scaled by the collection thickness of newly formed frazil ice or nilas. Haarpaintner et al. (2001) further developed this idea to model polynya events in Storfjorden on the eastern side of Spitsbergen. In their study, they included the mechanical opening of the pack ice ($\frac{dW_p}{dt}$). The Pease equation is used to describe the ice production when the wind forces an opening in the pack ice that comprises the polynya area. The following model description is based on Skogseth et al. (2004) which is a re-implementation of the model by Haarpaintner et al. (2001). With this model Skogseth et al. (2004) modelled the opening and closing of the Stofjorden polynya in agreement with observed polynya size from SAR images. Nilsen et al. (2008) used this model to help quantify the production of BWW in the Isfjorden Polynya. In Hornsund, pack- and multiyear ice is less pronounced, with pack/drift ice of varying concentration occasionally occurring outside the fjord mouth. This results in different boundary conditions for Hornsund than for e.g. the Storfjorden system, or other polynyas reoccurring in the more closed pack ice in Arctic or Antarctic. An up fjord wind in Storfjorden will force the pack ice back into the fjord and close the polynya. The ice available for closing the polynya outside the fjord mouth of Hornsund is of varying quantity. In this case, closing of the Hornsund polynya will be determined more by the thermodynamic effects, as thin ice covers the fjord. The following section is a description of the polynya model and how a slightly different parameterization has been utilised in an attempt to better describe the physical processes that govern the ice production in Hornsund.

3.4.1 Polynya dynamics

Two equations are used by Skogseth et al. (2004) to describe the dynamics of the Storfjorden polynya. The first equation describes how the wind controlls the opening and closing of the polynya by mechanically pushing the pack ice. A second equation is used to describe the ice production and thin ice movement within the polynya. Since the ice available for closing the polynya in Hornsund, is more of a drift ice character, the opening/closing equation is committed, and the dynamics of the polynya are based on the original formulation by Pease (1987). Similarly to Haarpaintner et al. (2001) and Skogseth et al. (2004) a tuning parameter is included in our equation. This parameter is intended to represent rafting and internal friction in the thin ice, an also account for the geometric features of the fjord as the ice is moved in or out by the wind. The opening and closing of the polynya is described by the equation:

$$\frac{dW_o}{dt} = F(\phi_t - \phi_0) \times B_2 U_t cos(\phi_t - \phi_0) - \frac{W_o}{h_c}\frac{dh_f}{dt}. \tag{3.1}$$

Here W_o is the width of the open water area. The nomenclature of Skogseth et al. (2004) is used here with the term "Polynya Width" refering to the distance of open water along the fjord axis. U_t is the observed windspeed at time t, $B = 3\%$ is the ice drift factor in percent of the windspeed (Leppäranta, 2011), ϕ_t is the wind angle and $\phi_0 = 70°$ is the angle most efficiently opening the polynya along the fjord axis. $F(\phi_t - \phi_0)$ is an out fjord($-90° < \phi_t - \phi_0 < 90°$) or in fjord ($90° < \phi_t - \phi_0 < 270°$) correction factor, which is determined on the efficiency of the wind forcing to open or close the polynya. Since Horsund does not have many constrictions that restricts the ice to drift off shore, this tuning parameter is set to 1 for $-90° < \phi_t - \phi_0 < 90°$, and 3 for $90° < \phi_t - \phi_0 < 270°$.

3.4.2 Collection thickness, the transition from frazil and grease ice to thin ice

The model domain can consist of either thin ice, open water, or a combination of both. In practice this defines the whole fjord except for areas covered with fast ice. When the great heat flux over open water results in a rapid freezing, the wind forces the grease and frazil ice to collect at the lee side of the polynya. The thickness of the collection of frazil ice, h_c, defines the initial thickness of the thin ice layer, and thereby the transition from open water to thin ice. Pease (1987) used a constant value for h_c. The collection thickness is not fully understood, and data collection of the grease ice thickness under representable conditions is rather tedious and difficult. However, studies have been done in order to try developing realistic parameterisation of the process (Smedsrud, 2011). Further studies and observations on the behaviour of grease ice have shown that the thickness of this slushy layer will depend on the wind speed and also on the resistance of the ice edge on the lee side of the polynya (Winsor and Björk, 2000; Smedsrud and Skogseth, 2006). A linear dependency on the wind speed (Winsor and Björk, 2000), was used by Skogseth et al.

(2004) to parameterize the frazil ice collection in the Storfjorden polynya. Smedsrud (2011) presented a formula for h_c based on a formulation by Dai et al. (2004) on the packing of pancake ice in a wave field. His formula is a balance between the wind and current stress on the grease ice, and the packing force against the ice edge which is dependent on the thickness of the grease ice layer. This equation gives a lower collection thickness for low winds than the paramterisation by Winsor and Björk (2000), and allows for a more rapid frazil ice growth in low wind speeds. Here, the equation is given as in Smedsrud (2011), but neglecting drag from ocean currents:

$$h_g = \frac{2}{3}(V_g)^{\frac{1}{3}} \left(\sqrt{\frac{\rho_a C_a}{K_r}} U_a \right)^{\frac{2}{3}}. \tag{3.2}$$

The thickness of the grease ice layer is given as h_g. Accounting for 25% solid fraction of the grease ice (Smedsrud, 2011) the equivalent ice thickness of the concolidated frazil collection or thin ice becomes $h_c = 0.25 h_g$. C_a and ρ_a is the open ocean drag coefficient and the air density, respectively. V_g is the volume of frazil ice per unit width inside the polynya and K_r is related to the internal friction acting against further packing of the grease ice.

3.4.3 Ice production in and around the polynya

Inside the polynya ice is produced in two areas; in open water and as thickening of the thin ice cover. The length of the thin ice area is defined as $W_{p,max} - W'_o$. $W_{p,max} = 20km$ is the maximum length of the effective polynya inside the fjord (See Figure 2.2). The length of the open water area $W'_o = W_o$ if $W_o \leq W_{p,max}$ and $W'_o = W_{p,max}$ if W_o exceeds $W_{p,max}$. To obtain an area, and thereby a volume of produced ice in the two different ice classes, W'_o and $(W_{p,max} - W'_o)$ are multiplied by the average width of the fjord (P_L). Under the assumption that the rest of the fast-ice free area of the fjord is responding similarly to atmospheric forcing, the model domain is multiplied by a correction factor (fr) to include the entire fjord of Hornsund. For the winters of 2005-2014, the time series of the different ice classes provided by Muckenhuber et al. (In progress), makes it possible to let this correction factor vary accoring to the variations in fast ice cover throughout the winter. Ice production from a continuous thickening of the fast ice in the inner parts of the fjord is also included.

Figure 3.1 shows a Lansat satellite image from April 8^{th} 1988, where a polynya is evident. There is a gradual transition from the open water area to the thin ice area. Streaks of frazil ice can be noted in the open water area, directed along the wind in the out-fjord direction. Different ice classes are denoted in the Figure. It is evident from the schematic that the polynya model does not take the fast ice cover into account when calculating W_o. The correction for fast ice is made when scaling the resulting areas. Following is a description of the three different algorithms needed to describe the ice production in the three different areas.

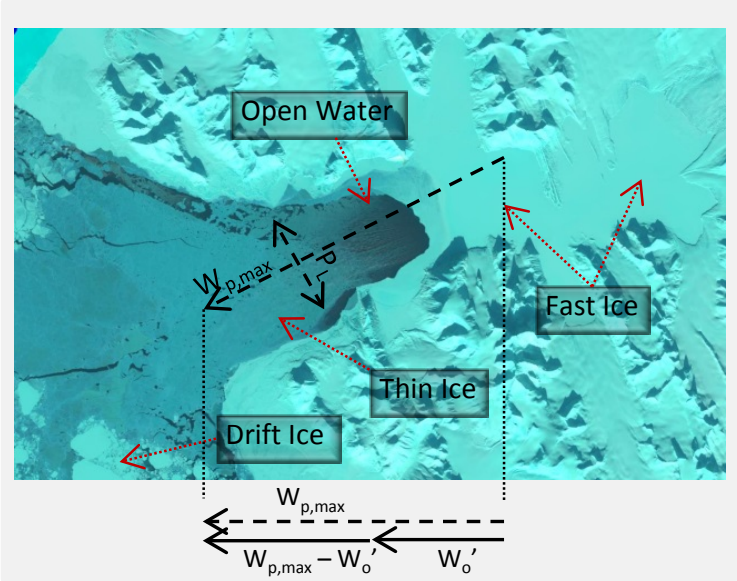

Figure 3.1: Overview of a polynya event, in a period of much drift ice on the shelf and a high fast ice coverage in the fjord. April 8^{th} 1988. This is a Landsat image provided from the database established by Muckenhuber et al. (In progress). The polynya model result does not distinguish between thin ice and drift ice. The ice occupying the model domain, can either by advected drift ice or new frozen thin ice.

Frazil ice production

The frazil ice forms in the open water area as well as in leads and cracks in the thin ice regions. Its equivalent thickness is defined as h_f, and the production rate is given by the following expression:

$$\frac{dh_f}{dt} = \frac{F_{net}}{\rho_f L_s}. \tag{3.3}$$

where production is balanced by the net heat flux over open water:

$$F_{net} = F_T + F_L - F_B - F_S. \tag{3.4}$$

F_T is the upward component of turbulent heat flux, F_L and F_B is the upward and downward long wave radiation. F_S is the downward short wave radiation. The individual terms are given in Cavalieri and Martin (1994) and Haarpaintner et al. (2001). $\rho_f = 950$ kg/m^3 in equation 3.3 is the density of frazil ice and $L = 334.1$ kJ/kg is the latent heat of fusion for sea ice (Skogseth et al., 2004). The total volume production rate of frazil ice by time is given by:

$$\frac{dV_f}{dt} = \frac{dh_f}{dt}(A_o + P_t A_t), \tag{3.5}$$

where A_o is the area of open water inside the polynya ($W_o' \times P_L \times fr$), and $P_t = 0.25$ is the fraction of the thin ice area, A_t ($(W_{o,max} - W_o') \times P_L \times fr$), that is considered open water and represents leads and openings in the newly formed thin ice or drift ice.

Growth of fast and thin ice

As long as there is a net upward heat flux, continuous ice growth will take place under the newly formed thin ice, as well as under the fast ice. The growth is in strong correlation to the freezing degree days and will decrease as the insulating ice layer gets thicker. Including snow on top, the following equation for the evolution of the thickness was given by Maykut (1986):

$$H^2 + [13.1h_s + 16.8]H = 12.9\Theta \tag{3.6}$$

and differentiated this gives us

$$\frac{dH}{dt} = \frac{d\Theta}{dt}\frac{12.9}{2H + 13.1h_s + 16.8}, \tag{3.7}$$

where H is the ice thickness in centimeters, h_s the snow thickness in centimeters, and Θ is the cumulative freezing degree days calculated from onset of freezing (further described below). The origins of the coefficients in Equations 3.6 and 3.7 are explained in Haarpaintner et al. (2001) and Maykut (1986).

Both fast ice, H_{fast}, and thin ice, H_t, thicknesses are calculated from Equation 3.7. In the fast ice area, the snow thickness is assumed to be zero initially and increases linearly by 1.2mm/d. The thin ice growth, H_t, is reset based on the dynamics of the polynya, and in the thin ice area the snow cover is neglected. The total volume of ice production under fast and thin ice can then be calculated from the following differential equation:

$$\frac{dV_i}{dt} = \frac{dH_t}{dt}[(1 - P_t)A_t] + \frac{dH_{fast}}{dt}A_{fast} \tag{3.8}$$

A_{fast} is the observed area of fast ice (Muckenhuber et al., In progress), where linear interpolation between the data points has been made to fit with the time step in the model of $\Delta t = 6h$.

Brine release

By combining Equation 3.5 and 3.8, the total production rate of ice mass can be calculated,

$$\frac{dT_{ice}}{dt} = \rho_f \frac{dV_f}{dt} + \rho_i \frac{dV_i}{dt}, \tag{3.9}$$

where $\rho_i = 920\text{kg m}^{-3}$ is the density of the consolidated ice. By knowing the surface water salinity S_0, and the fraction of salt that releases when ice freezes, the total rate of brine release can be calculated by;

$$\frac{dT_s}{dt} = \frac{dT_{ice}}{dt}(P_i + P_a)S_0, \tag{3.10}$$

where $P_i = 0.69$ and $P_a = 0.10$ (Skogseth et al., 2004), is the fraction of surface water salinity that immediately releases when ice freezes, and the fraction that releases under ice aging, respectively. The surface water salinity increases throughout the winter. In the model there is a linear increase from $S_0 = S_{01}$ at onset of freezing to $S_0 = S_{02}$ at the end of freezing period. The salt not contributing to the increased surface salinity, is by convection mixed downwards, and contributing to the production of BWW.

3.4.4 Freezing period

Based on the satellite observations, ice is first produced in the inner parts of the fjord, Brepollen, Burgerbukta, and Samarinvågen, before it starts freezing in outer parts of Hornsund. This is reflected in the correction factor that decreases the effective polynya area as fast ice grows. The model is first run with a fixed freezing period for the winters from

1978 to 2014. The fixed freezing period is assumed to be from December 1^{st} to April 30^{th} (Nilsen et al., 2008). From 2006 and onwards the satellite time series give the opportunity to estimate a time for onset of the freezing season. For these years the model has been run with a varying start date, assuming that the water is on freezing point when the first drift ice occurre in the fjord. The start of each freezing season is listed in Table 3.3. The table also show the date at which the fast ice cover reaches 40%. At this time one can assume that most of the inner bays (Brepollen, Burgerbokta and Samarinvå gen), are covered with fast ice. Ice observation time series are plotted with corresponding dates from Table 3.3 and shown in C.1 and C.2

Table 3.3: Dates for selected ice cover events. First drift ice denotes the time of first observation of drift ice in the fjord. The date for when fast ice cover has reached 40% of the total fjord area is given in the third column, and the time we have ice (drift or fast) covering more than 90% of the fjord in the last column.

Year	First drift ice	Fast ice cover > 40%	Fast + drift ice > 90%
2005/2006	18.November	24. March	Never
2006/2007	27. December	1. March	5. January
2007/2008	14. November	22. February	18. February
2008/2009	15. November	21. February	13. December
2009/2010	26. December	23. March	6. March
2010/2011	16. October	7. January	15. January
2011/2012	1. November	Never	Never
2012/2013	14. December	11. March	Never
2013/2014	15.October	never	Never

3.5 Regional Ocean Model System

Regional Ocean Model System (ROMS) (www.myroms.org, nd; Haidvogel et al., 2008; Budgell, 2005) is a three dimensional baroclinic ocean circulation model, that uses terrain-following coordinates in the vertical, and orthogonal curvelinear coordinates in the horizontal. This allows for higher vertical resolution close to the surface and the sea floor. The computational grid on which the set of equations in the ROMS model is solved has a too large spacing to solve small scale processes. The Sub-grid scale processes such as vertical mixing of mass and momentum are therefore parameterised using a turbulence closure model (Haidvogel et al., 2008). The ocean model is coupled with a dynamic-thermodynamic sea ice module (Budgell, 2005). The bottom of the sea ice layer is separated to the surface of the ocean by a molecular sub-layer. This produces more realistic freezing and melting rates than if the oceanic heat flux was dependent only on the temperature difference between the upper ocean and the bottom of the sea ice.

ROMS-simulations for Hornsund were provided by the Norwegian Polar Institute and the Institute of Marine Research for the time period between January 1^{st} 2005 to July 18^{th} 2010. The simulations have a 160 meter space resolution for the fjord and the shelf areas just outside the fjord. Oceanic boundary conditions are given from an 800 m grid ROMS-model covering the Svalbard region and large parts of the Fram Strait, which in turn gets its boundary conditions from a 4 km ROMS-model covering the Arctic and Nordic seas. The atmospheric input for the high resolution model for Hornsund is from an 11 km atmospheric model by Norwegian Meteorological Institute. Freshwater water input is included at certain locations, based on a digital terrain model for Svalbard, as well as a glaciological mass balance model for the area providing run-off from glaciers. The 160 m model for Hornsund has 35 layers in the vertical, with a high resolution close to the surface, and an increasing layer thickness deeper down. Bathymetry for the 160 m model is based on data from The Norwegian Mapping Authority Hydrographic Service. The same data is used for all bathymetry maps presented on this thesis (e.g Figure 2.2)

3.6 Polynya model code and data processing

The polynya model used in this thesis was originally written in Matlab by Ragnheid Skogseth at the University Centre of Svalbard (UNIS). As explained in Section 3.4, some changes have been made to the basic equations governing the processes involved. The Matlab routines have correspondingly been modified with the new set of equations. Further processing, statistics, plotting and map projections are done in Python, with help of scientific modules as Numpy (Walt et al., 2011), Scipy (Jones et al., 2001), and Matplotlib (Hunter, 2007). Conversions and seawater properties are calculated by using the Gibbs-SeaWater (GSW) Oceanographic Toolbox (McDougall and Barker, 2011).

Chapter 4

Results

Full winter season time series of ice concentration were available after 2006, so the polynya model has been run with different initial settings, for the different periods. First it was run with settings similar to Nilsen et al. (2008), with a constant allowable polynya area, and fixed freezing seasons in the period from 1978 to 2014. The freezing season was from December 1^{st} to April 30^{th}. Second, the fast ice concentration was used as input to let the area for polynya activity decrease as the fast ice cover increases (described in Section 3.4.3). This has was done for the winter seasons in the period 2006 to 2014. For the same time period, two additional runs were made, to look at the effect of a varying starting point (Table 3.3) and initial and final surface salinity of the winter season. Finally, the model was again run for the period before Brepollen was 100% covered with fast ice, for the years of fast ice data. In the following section, first, the input and forcing data, and the hydrographical data that is used both as input and for the discussion on the model results are presented. Second, the polynya model results are presented. Finally, results from the ROMS-simulations are described with time series and profiles of temperature and salinity from selected stations in the fjord.

4.1 Atmospheric forcing

Yearly means of Negative Freezing Degree, $\bar{\Theta}_{day}$, along fjord wind component , $\bar{U}_{\phi_0}$, and net heat flux, $\bar{F}_{net}$, gathered from the weather station at Isbjørnhavna are shown in Table 4.1. $\bar{F}_{net}$ is calculated from equation 3.4, Θ_{day} denotes the deviation from freezing temperature of sea water, $T_{freeze} = -1.865$, and the mean then indicates the cumulative forcing from these parameters over the freezing season. Since melting is not taken into account in our simulations, periods of $\bar{\Theta}_{day} \geq T_{freeze}$ are excluded from the mean. To account for this, the number of days with temperatures below freezing is included in Table 4.1. Both $\bar{\Theta}_{day}$ and the number of freezing days varies significantly from year to year. 2014, 2012, 2007, 2006 were all warm years, with 2012 being the over all warmest and 2006 having the least days of air temperatures below T_{freeze}. In the 1980s and 1990s there were periods of three to four years with colder or warmer mean temperatures following each other. 1979 and 1981 were

the coldest and 1981 had the highest number of days below T_{freeze}. In Table 4.1 a tendency of a warming after 2005 can be notized. The along fjord wind component shows positive values for all years, which gives a dominance of wind forcing in the out-fjord direction. The distribution of the wind direction is shown in Figure 4.1. In the histogram the wind data has been organised in 36° bins, in which each count within the bin is weighted with the wind speed at the same time. In this way the histogram shows that the wind forcing is dominating in the out-fjord direction, along the fjord axis, with winds approximately 70% of the time in the direction from 36° to 108°.

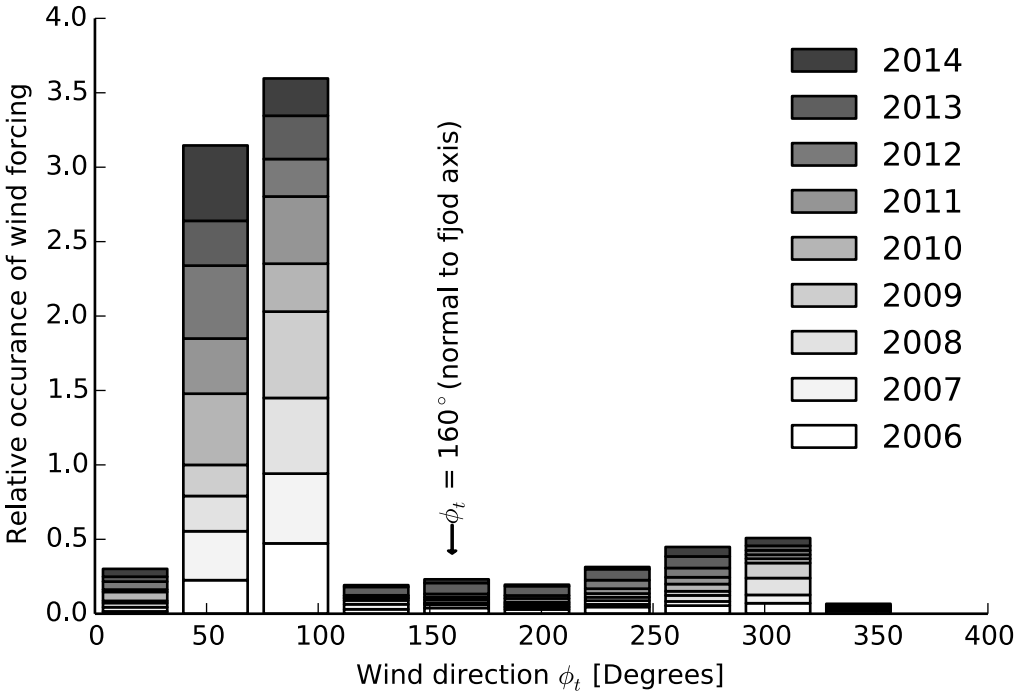

Figure 4.1: Stacked histogram showing the distribution of wind direction weighted with the wind speed from the weather station at Isbjørnhavna for the period 2006-2014.

4.1.1 Comparison with the weather station at Treskelodden

In Figure 4.2 a comparison between atmospheric data from Isbjørnhavna and Treskelodden is shown. Four different weather parameters have been plotted against each other in order to reveal deviations or similarities between the two locations. The temperature shows near one-to-one relation, while the relative humidity and the wind speed is a little more scattered. The rather high correlation, denoted by r in the plots, signifies that the temporal variations are agreeing fairly well. Most scatter in the data is seen in the wind direction, especially on low wind speeds. As seen above, along-fjord winds dominate at the station in Isbjørnhavna. For the given period in Figure 4.2, the winds at Isbjørnhavna are

Table 4.1: Mean of Negative Freezing Degree day ($\bar{\Theta}_{day} = T_{air} - T_{freeze}$), excluding days where $\bar{\Theta} = 0$, number of days with air temperature below freezing ($T_{air} \leq T_{freeze}$)), Along Fjord Wind Component ($\bar{U_{\phi_0}}$), and Net Heat Flux over open water ($\bar{F}_{net}$), from the weather station in Isbjørnhavna. Modelled Accumulated Salt release(AST) for model run with and without considering fast ice cover, Yearly mean of Thin Ice Cover (TIA) for model run without fast ice, yearly mean of observed Drift Ice area, and the Days of Fast Ice Cover (DFI), the two last from Muckenhuber et al. (In progress)

Year	$\bar{\Theta}_{day}$ day C°	# of days below T_{freeze}	$\bar{U}_{\phi_0}$ m/s	$\bar{F}_{net}$ W/m^2	AST [$\times 10^9$kg]	Fast Ice	TIA km^2	Obs. Drift km^2	DFI
2014	5.9	98	4.2	56.0	30	30	40	8.7	2.5
2013	9.4	103	5.0	164.4	55	33	37	31.9	49.9
2012	5.0	102	3.9	38.3	26	26	35	60.3	2.5
2011	8.8	128	5.0	158.6	68	47	50	101.4	76.1
2010	7.6	114	5.2	115.4	51	30	35	60.1	53.6
2009	9.3	123	4.2	146.4	60	36	50	89.5	71.4
2008	7.6	129	4.1	121.5	53	32	50	88.9	54.2
2007	6.1	125	4.5	93.1	44	30	36	97.9	51.1
2006	7.2	84	4.1	71.7	41	28	43	81.9	28.8
2005	7.6	115	5.2	120.9	55		42		
2004	10.6	124	5.5	193.8	74		52		
2003	11.1	129	3.7	187.3	73		67		
2002	9.9	123	4.9	183.6	73		55		
2001	8.8	132	4.3	157.6	64		51		
2000	9.2	132	5.8	150.3	62		39		
1999	7.8	134	6.3	157.3	68		36		
1998	11.0	136	5.9	232.4	86		47		
1997	11.2	143	4.1	202.4	68		67		
1996	10.2	118	1.7	141.3	49		76		
1995	9.5	129	6.1	176.7	73		40		
1994	9.1	127	5.6	163.0	65		44		
1993	11.3	140	4.6	230.9	87		58		
1992	9.2	133	4.9	166.5	64		50		
1991	8.3	119	3.4	130.3	55		56		
1990	9.0	117	4.9	127.3	54		44		
1989	12.7	135	3.8	208.3	72		67		
1988	12.6	143	4.7	243.0	87		64		
1987	10.6	125	3.9	182.1	70		60		
1986	11.3	133	3.3	179.1	65		70		
1985	8.5	115	2.8	111.6	48		61		
1984	9.4	128	4.2	163.0	64		58		
1983	9.8	131	4.8	180.3	72		51		
1981	13.1	144	5.5	258.6	93		54		
1980	10.5	129	3.7	156.6	61		63		
1979	12.9	140	5.0	258.1	94		64		
Sum ± std	9.5±1.9	125.1±13.1	4.5±1.0	160±51	63±15	47±12	52±11	68±29	43.3±25.2

clustered from the west-north-west (∼300°) direction and east-north-east (∼70°) direction. At Treskelodden, especially at low wind speeds, winds are more variable when it is blowing out-fjord at Isbjørnhavna. Some consistency in the wind direction at the two locations is observed. With easterly winds at Isbjørnhavna there is a tendency for a more northerly direction at Treskelodden. For westerly winds at Isbjørnhavna there is a tendency for the direction at Treskelodden to be a little more shifted to the south-west. This is consistent with winds being guided along the fjord axis, as Brepollen is angled some 20-30 degrees more towards the north then the outer basin. Onwards it is assumed that this is the case throughout the year. We thus assume that the alongfjord wind component in Hornsund proper also accounts for the Brepollen area.

4.2 Hydrography

Figure 4.3 shows selected profiles from available hydrography data from spring and fall in the period from 2008 to 2014. The locations of the profiles are shown in Figure 2.2. The July long section from IOPAS is taken on a regular basis, and the only data available which is made at approximately the same time each year. Brepollen and Hornsund July profiles in Figure 4.3 are extracted from this section. It is evident from the July profiles that behind the sill in Brepollen the water temperature is generally lower than in the outer basin. The upper water column is stratified, with a brackish layer becoming more saline down to about 50 meters, which is the sill depth of Brepollen. In the outer basin, years 2008, 2010, 2011 and, 2012 show cold temperatures at intermediate depths, with an increase in temperatures at greater depth. In Brepollen, the water below sill depth is more homogeneous both in temperature and salinity. A warmer bottom water is seen in Brepollen in 2012 and 2014, with 2014 also having a rather high salinety. The temperature below sill depth in general show a greater year to year difference in the Hornsund basin then in Brepollen. In Brepollen the bottom water salinity in July ranges between 34.37 and 34.57 psu, with temperatures between -1.3 and -0.3°C close to bottom.

In July 2010, both Brepollen and the Hornsund basin had the coldest water, while 2013 and 2014 were the warmest years. The spring and fall profiles were taken at varying times, and the positions in the outer basin is either close to the deepest point, or on the shallower area (shallower profiles are marked with red dots in the outer area of the Hornsund basin in Figure 2.2). The spring and fall profiles in Brepollen were taken close to the sill, and are thereby not covering the deepest part of the basin. Similar for all the spring profiles is a rather homogenous salinity profile which indicats low stability in the water column. In beginning of May 2008, the upper layer in Hornsund was close to freezing point, with a warmer water mass below 50 meters depth, whereas in 2010, the whole water column was at freezing point in early April. Based on the available data set, the salinity maximum in the outer basin in spring ranges between 34.47 and 34.7 psu, with temperatures between -1.9°C (2010) and 0°C (2011). In September, the upper water column is still well stratified, and the temperature has increased from summer. In 2013, the water temperature below sill level in Brepollen had increased close to 2°C from July to September, with an additional

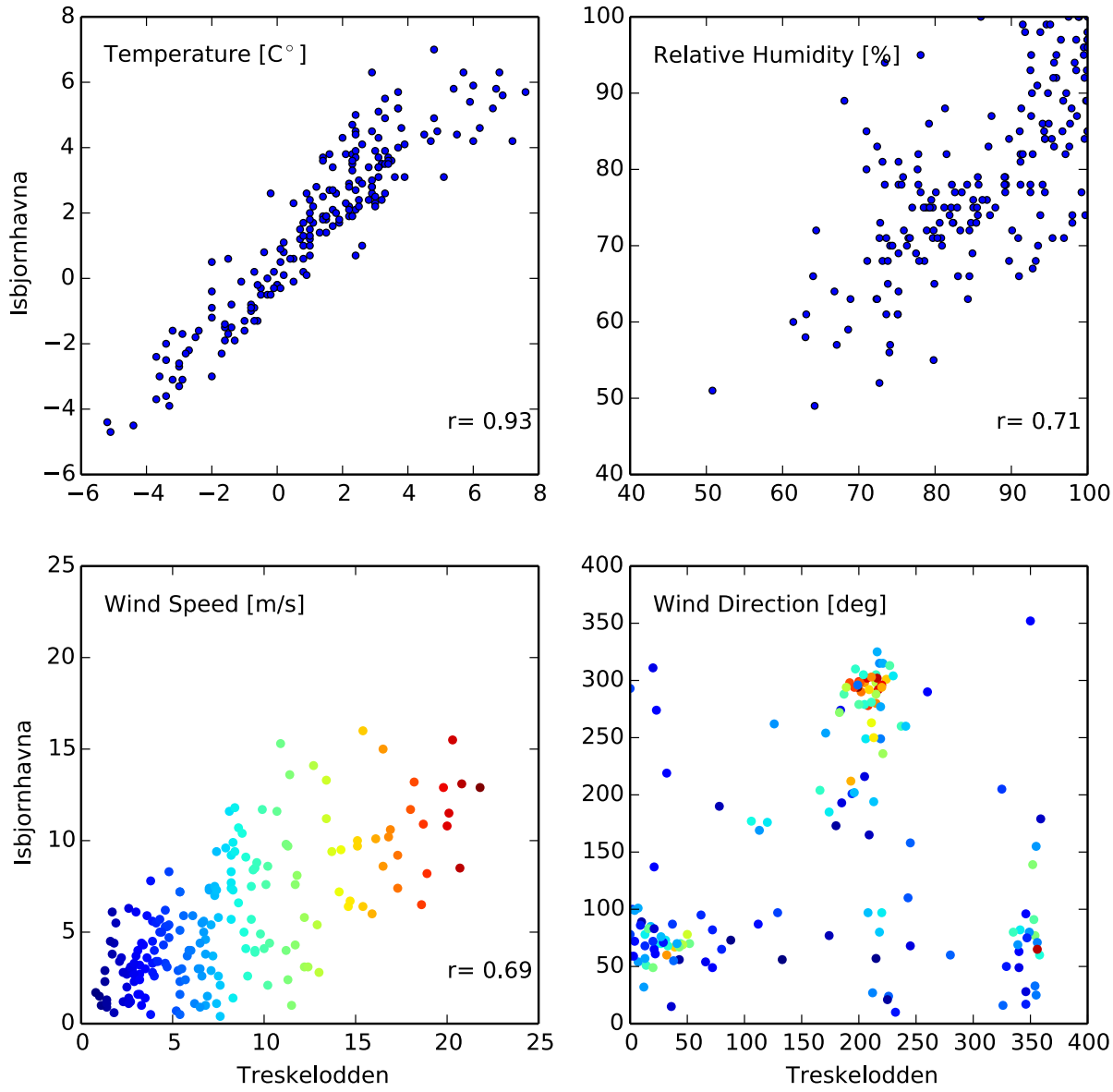

Figure 4.2: Comparison of weather parameters between Treskelodden and weather station at Polish base in Isbjørnhavna. The colors for wind speed and direction denotes the wind speed at the given data point.

increase in salinity.

Maximum salinity from the July profile behind the sill in Brepollen is used as an estimate on the salinity of the Brine enriched Winter Water, S_{bww}, produced the previous winter season and presented in Table 4.2. Assuming little exchange in the surface layer with the outer basin, the same profile can be used to give an estimate on the initial salinity at onset of freezing before each winter season. Assuming mixing of the upper 30 meters through the fall, S_{01} is given as the averaged upper 30 meters of the profile. This might be an under estimation of the S_{01}-value because the prevailing out fjord winds in Hornsund (See later discussion) may cause transport of fresh water out of the fjord after the fresh water supply has stopped, which would lead to a more saline surface layer. The two values for the 2014 season, in Table 4.2, indicate a more saline surface layer in September then in July. There is also a notable difference between 2008 and 2013, in which there was a reduction in the bottom salinity from May to July in Brepollen 2008 and an increase from July to September in 2013.

Table 4.2: Initial and final salinity values for Brepollen and Hornsund. $\sigma_{\theta,bww}$ is the density of most saline layer in the July profile for Brepollen. S_{01} in Brepollen is the salinity mean of the upper 30 meters of the water column from July before the respective freezing season (e.g. S_{01} for 2009 is the mean of the salinity profile taken July the 22^{nd} 2008). S_{01} in Hornsund is made from the available fall profiles in the outer basin. S_{02} is the mean of the upper 3 meters of the water column for the years of available spring data for the two locations. S_{bww} is the maximum salinity from the deepest point in Brepollen in July (J). April (A), May (M) and September (S) data is included for years with available data.

	Brepollen				Hornsund	
Year	S_{01}	S_{02}	S_{bww}	$\sigma_{\theta,bww}$	S_{01}	S_{02}
2006			34.62	27.85		
2007	32.51		34.52	27.77		
2008	33.14	34.5	34.63/34.55(M/J)[a]	27.79		34.55
2009	33.01		34.43	27.69		
2010	32.73		34.48	27.74	33.04	34.38
2011	32.79		34.58	27.82		34.43
2012	30.72		34.38	27.63	32.32	33.76
2013	32.19		34.64/34.68(J/S)[b]	27.87	32.85	34.25
2014	32.63/33.08(J/S)	34.69	34.74/34.82(A/J)[c]	27.69	33.76	34.87

[a]CTD profiles made in Brepollen May 2^{nd} 2008, September 5^{th} 2013, and April 6^{th} 2014, are done in a shallower area (See green dots in Figure 2.2), closer to the sill than the July profiles.

[b]See footnote *a*

[c]See footnote *a*

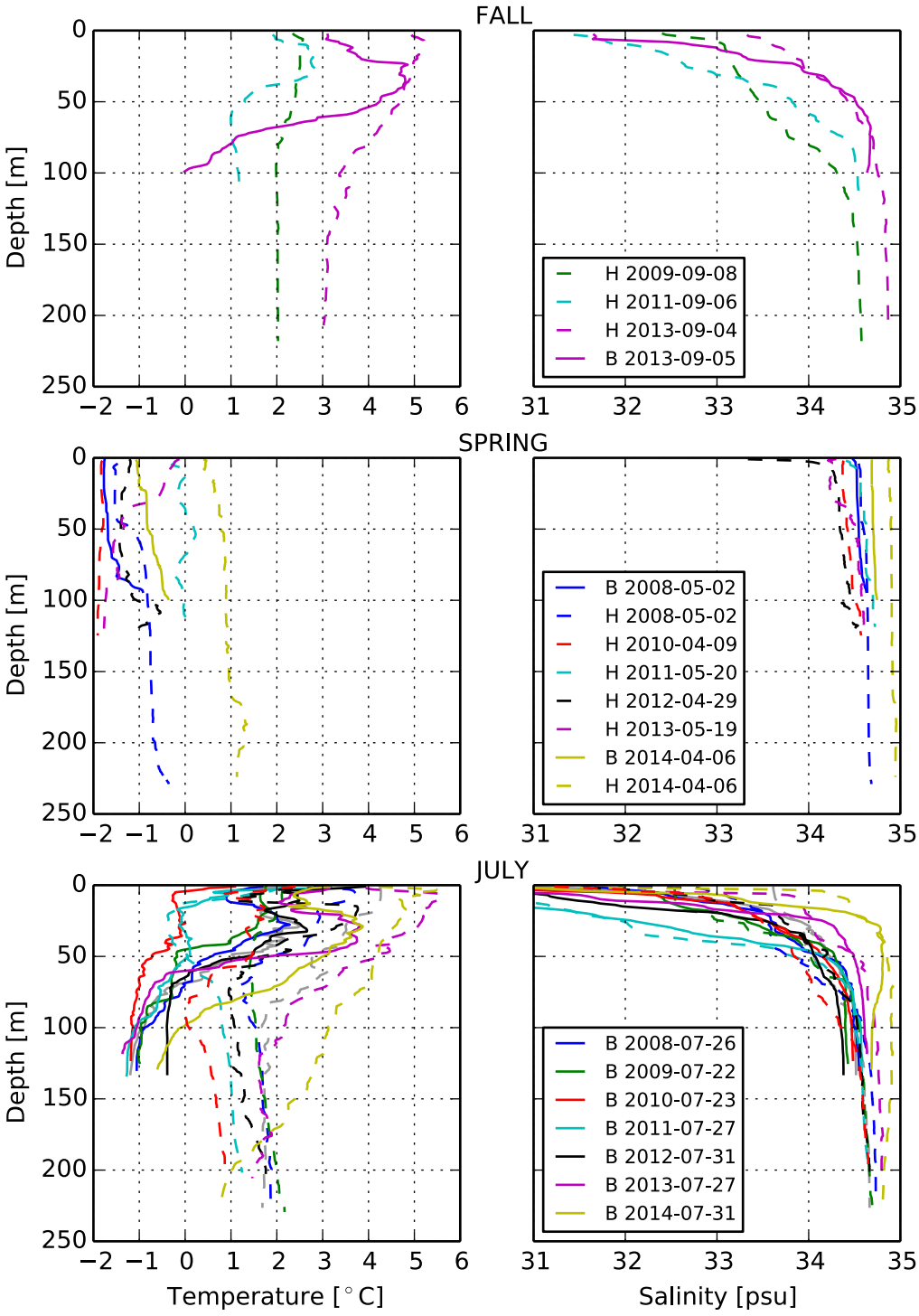

Figure 4.3: CTD profiles from the outer basin in Hornsund (H, dashed line) and Brepollen (B, solid line). Summer profiles are taken late July every year, the profiles are from the deepest point in Brepollen and Hornsund. The Fall and Spring data is more random in position and time, dependent on available data. Positions and details for the measurements are shown in Figure 2.2 and Table 3.1.

4.3 Model results

4.3.1 Example seasons

Figure 4.4 shows the model output and forcing data for the winter season 2011 (I), and for a shorter period in 2000 (II). For 2011, the along fjord wind component in a) shows a fluctuating pattern, with a dominating direction out the fjord. Maximum wind speed is 21 m/s blowing along the fjord axis. Maximum in-fjord wind component is 20 m/s. Several periods of wind speeds above 15 m/s are evident from the Figure. The temperature was mostly below freezing, and with longer periods of temperatures below -15°C. We note that colder periods are dominated by periods with easterly winds. Warmer periods, e.g. end of February and towards end the of March 2011, are both accompanied by westerly wind conditions. The net Heat Flux shown in c) shows a similar fluctuating pattern with peaks between 600-900 W/m^2 that are related to periods of low air temperature and easterly winds. From mid April F_{net} is negative, meaning no heat flux from the ocean. Figure 4.4 c) also includes the accumulated frazil and thin ice production integrated over the respective areas that are controlled by the open water width in b). We can see several occasions where the open water width exceeds $P_{w,max}$, meaning that the wind has transported all ice out the fjord. When having a closer look at the cold period at the end of March, marked by the grey shading, one can note a low open water width due to low air temperatures and calm winds. As the wind picks up half way through the period, W_o starts increasing, and eventually the domain is ice free when the wind increases substantially. The cumulative curve of frazil ice increases towards the end of the period, when both the area for frazil ice production gets bigger and F_{net} increases due to an enhanced wind speed. In general, the frazil ice, which dominates the ice production, has the strongest gradients in the cumulative curve when F_{net} is relatively high. Ice production stops in the beginning of April as a result of a negative heat flux towards the end of the season. The shorter period plotted in Figure 4.4 (II) shows the same relationship between high F_{net} and an increased frazil ice production. To periods, 15^{th} - 18^{th} and 22^{dn} - 25^{th} of March, where W_o exceedes $P_{w,max}$ can be noted. These are periods with easterly winds and a low heat flux related to rather high air temperatures and a low ice production. The blue lines in both time series mark times of certain events further discussed in Section 5.2.1.

4.3.2 Seasonal cycle in ice cover

Figure 4.5 shows three years of satellite derived ice concentration time series (Muckenhuber et al., In progress). On top of the observations, modelled Thin Ice Area (TIA) is plotted, scaled with the effective polynya area of Hornsund, i. e. the fraction (fr) of the total fjord area not covered with fast ice. The ice cover observations for these three particular years, 2011, 2012, and 2013, shows some significant differences. 2011 had the longest period of fast ice coverage, as well as the highest observed drift ice coverage of the years registered (See Table 4.1). Observed Drift Ice Mean in Table 4.1 is made by dividing with numbers of observations. The DFI value in Table 4.1 is the daily accumulated fast ice fraction, and

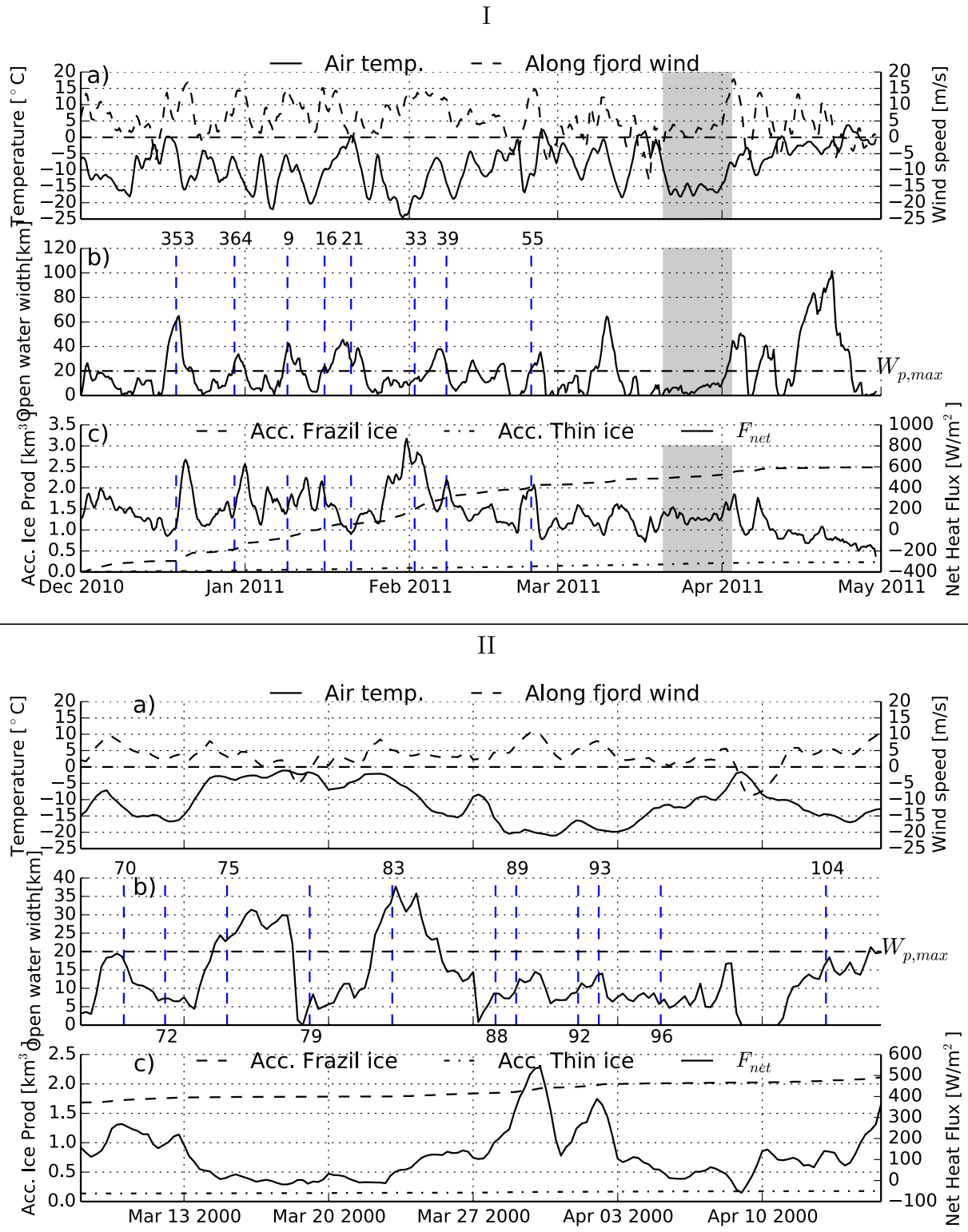

Figure 4.4: Model output and forcing data for winter season 2011 (I), and a shorter period from 2000 (II). Results are presented with no correction for fjord area or fast ice cover. One day running mean on along fjord wind(Positive out fjord) and air temperature are shown in a), b) shows the modelled open water width W_o, and c) shows accumulated Frazil Ice and Thin ice production together with a one day running mean of the Net Heat Flux over open water, F_{net}. Blue line denotes certain events further discussed in next chapter. The shaded area shows a period of opening polynya, see text.

is further explained in Section 3.3. From Table 4.1 we note that 2012 and 2014 were the years of lowest DFI, and hence lowest fast ice coverage. Nevertheless, 2012 had a higher drift ice coverage.

While ice cover in 2011 and 2012 (Figure 4.5) show a somewhat consistent situation throughout the winter season, 2011 having a prominent fast ice cover and 2012 being rather poor in the sense of sea ice, 2013 show a clear shift in the middle of February. At this point drift ice coverage started increasing, followed by a rapid increase in fast ice coverage. The general situation in the observed ice cover is that as soon as a fast ice cover has developed, it stays rather constant throughout the rest of the winter. This can be seen for 2011 and 2013 in Figure 4.5, and is also the case for the other years, presented in Figures B.1-B.9 in Appendix B. The drift ice is more fluctuating, and we see periods where it covers the whole fjord, as well as periods of only open water. For 2013 there are no periods of full coverage of drift ice, and it is the second lowest year of observed drift ice after 2014.

Similar to the drift ice observations, the modelled TIA fluctuates throughout the period. Because of erroneous wind data, the model was run for a shorter period for winter season 2013, starting 27^{th} of December. The variations in TIA for 2011 follow the same arguments as presented above, when describing at the polynya width for for the same year. We can point out the increased TIA at the end of 2011, that is a consequence of westerly winds advecting ice into the fjord, as $F_{net} < 0$ for the same period. The yearly mean of TIA follows to a great extent the yearly mean of Θ_{day}, $\bar{\Theta}_{day}$, and thus, the colder years leads to a higher TIA.

4.3.3 Year to year variations

Figure 4.6 shows the accumulated salt production from the polynya model. The red curve shows the result when the model is run without adjusting the polynya area for varying fast ice and with similar start and end dates for each season. The years 1979, 81, 87, 93, and 98 show the highest salt production, which coincides with the years of highest heat flux $\bar{F}_{net}$ (Table 4.1). On the other hand, the years having low production, 1985, 05, 96, 2006, 12 and 14, are years having low values for $\bar{F}_{net}$. By reducing the effective polynya area with the fast ice cover (Black line), the year to year variability gets dampened, although the year-to-year variation is the same. We note that the relative difference between the highest years (2011 and 2013) and the lowest years are reduced as an effect of shrinking the polynya area. By letting the freezing season vary (blue line), the inter annual variations become more pronounced. The variation of surface water salinity has little effect on the salt production.

4.3.4 The Brepollen Polynya

The results from the polynya model for the period before Brepollen is covered with fast ice are here presented. The start and end of the modelled period is based on the first observation of drift ice in the fjord, and when the fast ice cover exceeds 40%, as given in Table 3.3. Maximum polynya width $P_{w,max} = 10$ km (See map in Figure 2.2). Initial

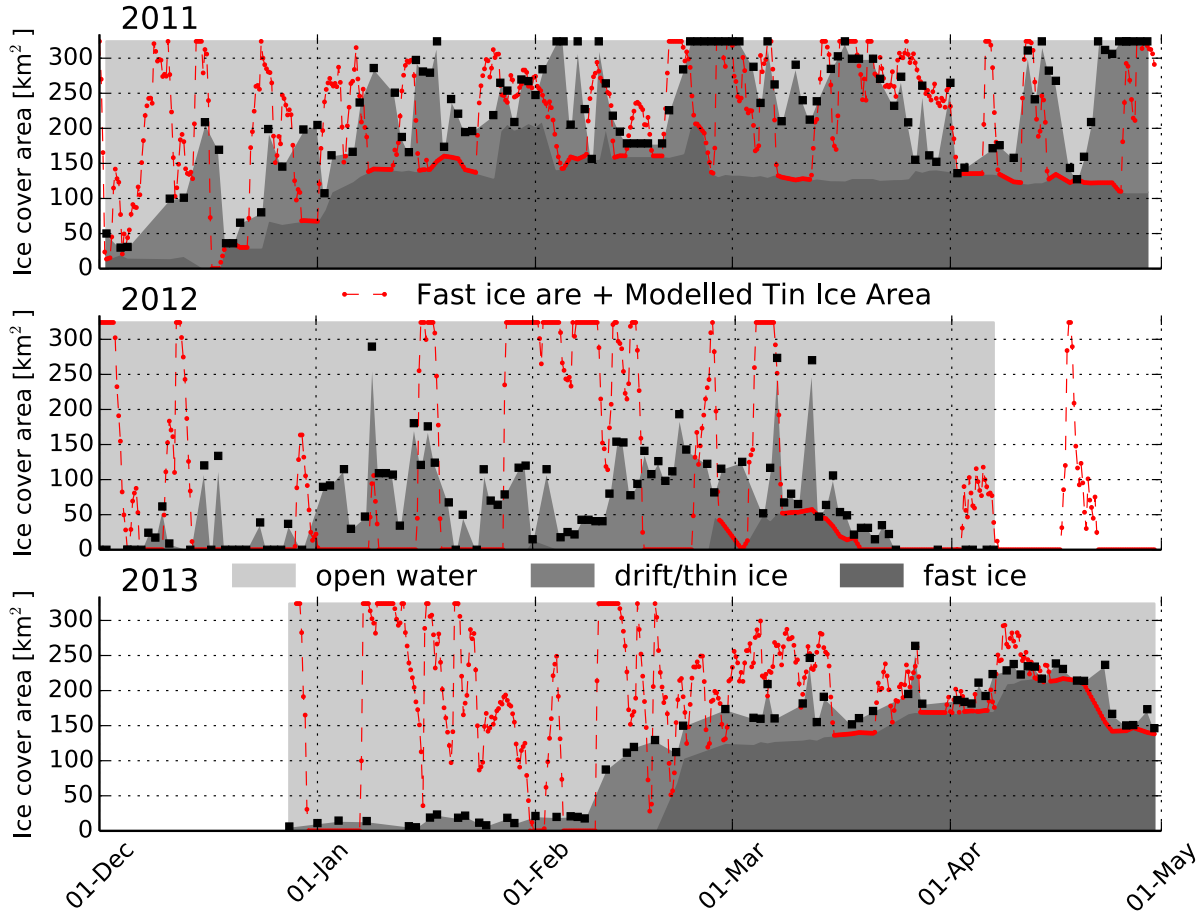

Figure 4.5: Ice observations and modelled thin ice cover for the winter seasons of 2009, 2011, and 2013. The filled areas are the observed ice cover by Muckenhuber et al. (In progress). Linear interpolation has been done between the data points, market with black dots. The red line is the modelled thin ice cover, scaled by the effective polynya area of the fjord, added to the fast ice observations

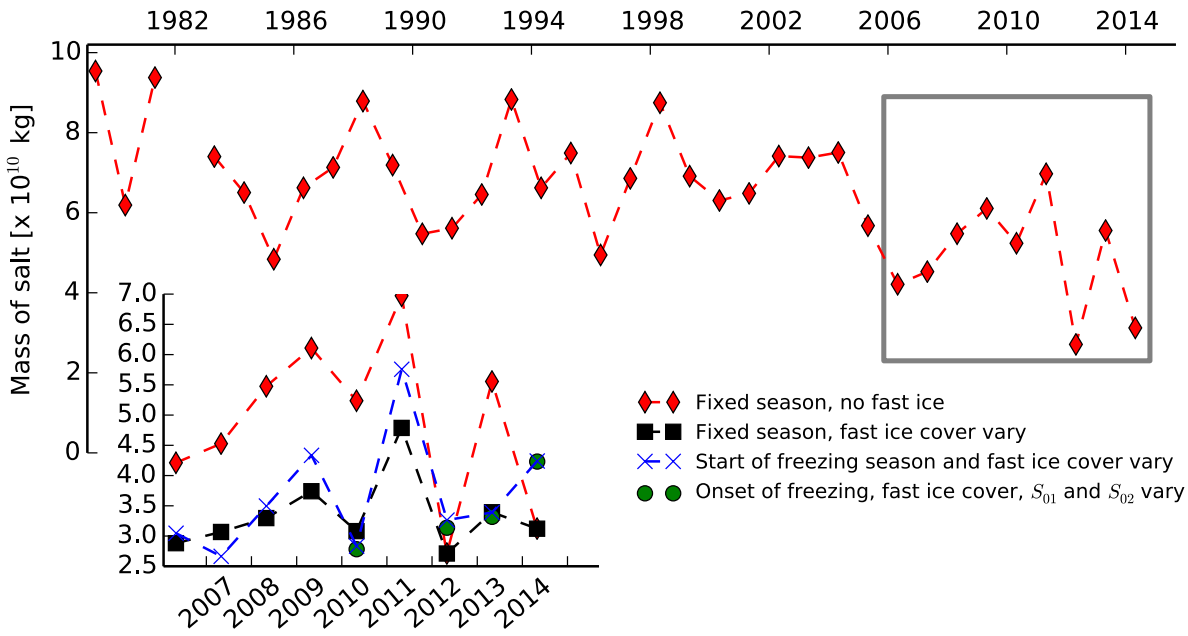

Figure 4.6: Yearly salt release, integrated over the whole fjord and different ice classes, frazil ice, thin ice, and fast ice. Red line shows model run with fixed ice season, and no fast ice cover. Black line shows model result when the allowed polynya area is dependent on the fast ice cover, and a fixed freezing season. Blue line shows results when fast ice cover is considered as well as the start time of freezing season is varying, according to Table 3.3 (First drift ice). For 2013 the model has been run from 27^{th} of December for all years.

salinity of the surface layer is similar for all the years; $S_{01} = 34.0$ and it increases linearly to $S_{02} = 34.8$ at the end of the period. Most of the ice production, and accompanied salt release is produced in open water, before a fast ice cover is established. To give the reader a picture of the freeze up process in the inner parts of Hornsund, a satellite time series is composed and shown in Figure 4.7. The images are from the Meris satellite, and show visual images for the period prior to the freeze up of Brepollen. In 2010, 40% fast ice cover in Hornsund in total was reached by March 23^{rd}. As one can see from Figure 4.7 the fjord system was more or less ice free in the beginning of March, and on the 10^{th} of March new ice was present in the fjord. By the 19^{th}, Brepollen seems to be covered with thin ice, which is thickening, and/or mostly covered with snow by the 23^{rd}.

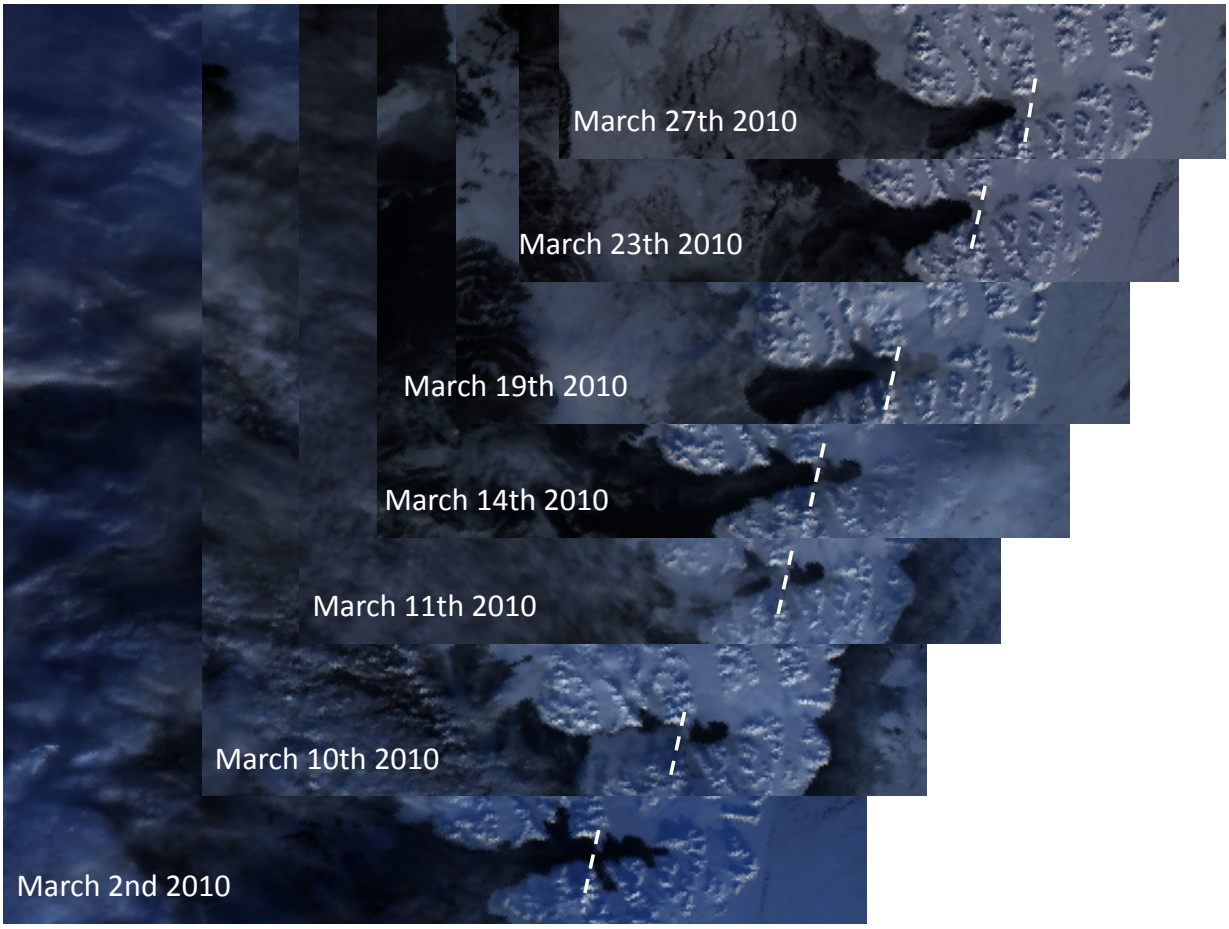

Figure 4.7: Satellite picture time series showing the period of which a fast ice cover is establishing in Brepollen in 2010. The white dashed line marks the position of the sill, separating Brepollen from the Hornsund main basin

Figure 4.8 shows the observed ice cover for the entire Hornsund, together with the model output for Brepollen. Here the model is run without considering fast ice. The modelled TIA is increasing during periods of low air temperatures and little wind. In

periods of higher winds, e.g. March 13^{th} and 22^{nd}, ice is forced out the fjord leading to a decrease in TIA. In the period March 7^{th}- 11^{th}, prevailing in-fjord winds caused a closing of the polynya, and thereby full coverage of thin ice. The rather cold air temperature for the period caused production of thin ice and a comparable production of frazil ice, which is an effect of assuming 25% of the thin ice area is open water. The frazil ice production can be noted to follow the heat flux curve, F_{net}, when thin ice coverage is low (Figure 4.8). With higher thin ice cover, the deviation between F_{net} and frazil ice production becomes somewhat bigger.

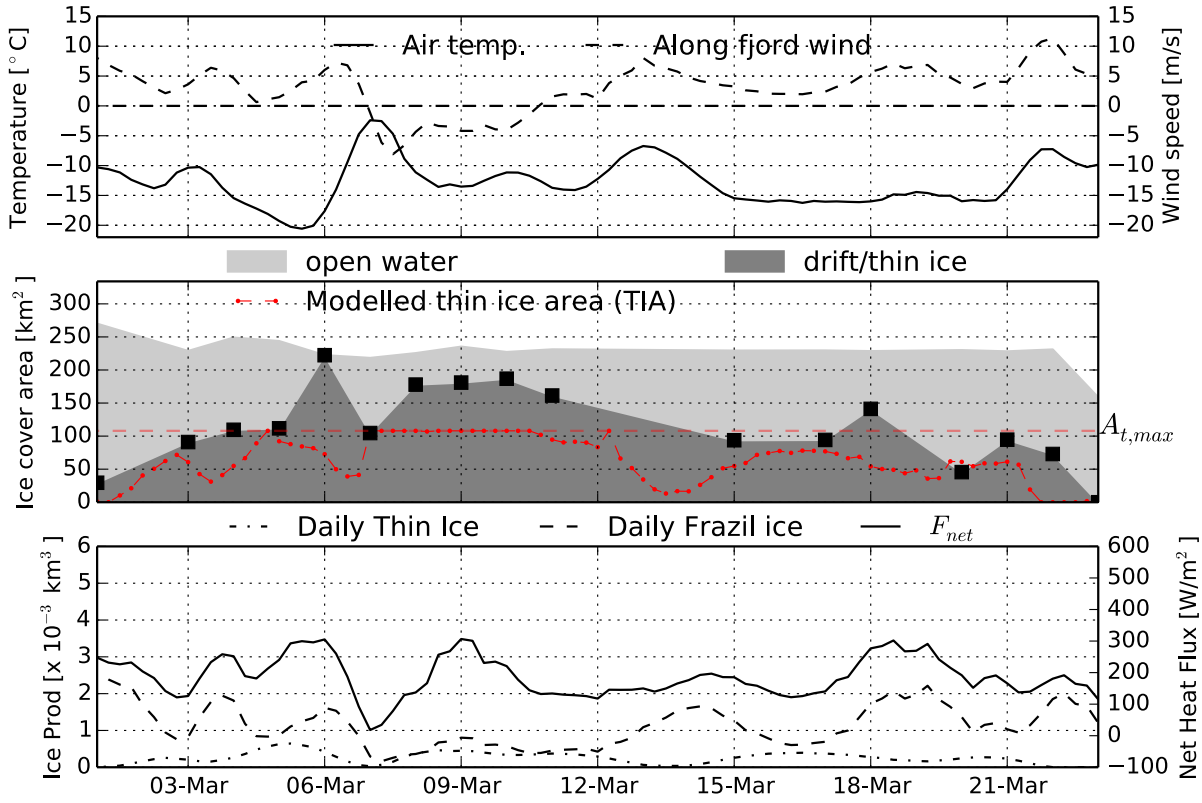

Figure 4.8: Polynya Model output for March 2010 for Brepollen. Upper panel as Figure 4.4 a). Middle panel shows observed drift ice and open water area, together with the modelled TIA (red dashed line). The fast ice cover can be seen as the the remaining white area on top of the graph. $A_{t,max} = 108$ km^2 is the surface area of Brepollen, and thereby denotes the maximum TIA. The modelled daily production of frazil and thin ice, and F_{net} is given in the lower panel. The resolution of the observed ice cover is indicated with black squares.

Figure 4.9 shows the modelled accumulated salt release for the modelled years, together with the observed maximum salinity S_{BWW} in Brepollen in July the following summer. These numbers correspond to Table 4.2, and are assumed to serve as a proxy for the changes in production of BWW the previous winter. Measurements of S_{BWW} are taken at the deepest point in Brepollen. One can note a decrease from 2006 to 2007, both in

S_{BWW} and salt production. Towards the end of the modelled period, 2011 and 2013, both the modelled salt release and the S_{BWW} salinity is increasing. Model results for 2008 are relatively lower then the observed S_{BWW}, while, in 2009 and 2010 the results are higher then expected following the trends in S_{BWW} salinity.

The cumulative forcing for the modelled periods are shown in Figure 4.10. The accumulated net heat fluxes at the end of the periods are comparable, and between 13 and 16 kW/m^2 for all years except 2007 and 2008. The same accounts for the freezing degree days. 2007 and 2008 had a somewhat lower heat flux over the respective periods. And we can also note that the two important drivers for the heat flux, wind and temperature, were lower for these years. Note that the accumulated wind in Figure 4.10 is the along fjord wind component. The salt production, given by the cumulative curve in Figure 4.9, shows the same evolution over the freezing period as the net heat flux. E.g. 2006 had a low heat flux first half of the period, whereas it increased from mid February, as did the salt production. For 2009 the heat flux had to periods of lower values due to higher temperatures (See lower and upper panel Figure 4.10). This signal is also evident in the stair case shaped salt production curve in Figure 4.9 for the same year.

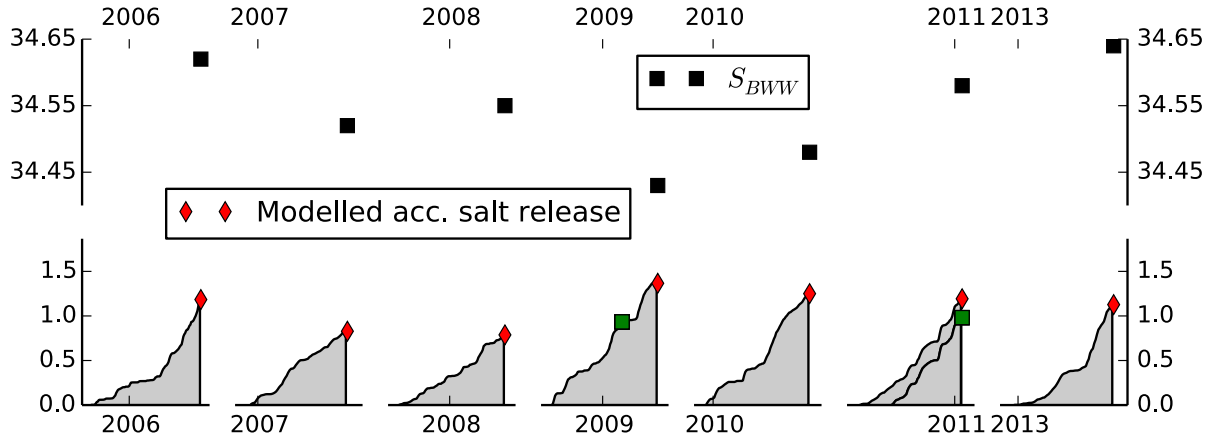

Figure 4.9: Model result of accumulated salt release red dots in the lower panel. Black line is the cumulative curve of salt production through the modelled period. Upper panel show the maximum salinity at the deepest point in Brepollen taken in July, the summer following the modelled period. The green squares show resulting accumulated salt release for an alternative model period. In 2009, ending the period before 40% is reached, and in 2011 starting it at a later point. A discussion on the latter is given in Section 5.3.2

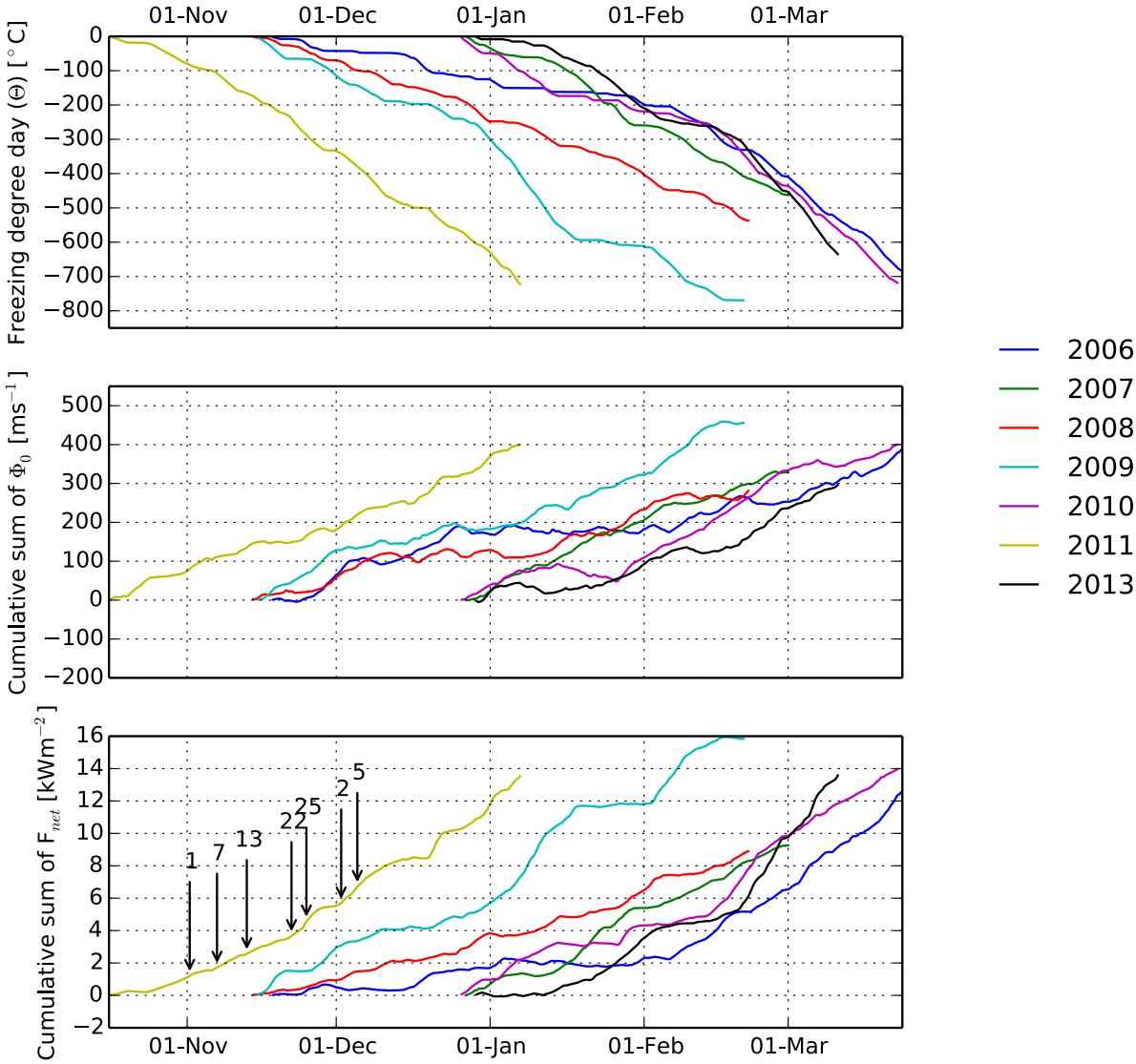

Figure 4.10: Cumulative forcing for the Brepollen Polynya. Upper panel is the freezing degree day (Θ_{day}), cumulative sum of along fjord wind component (U_{ϕ_0}) in the middle, and cumulative sum of the net heat flux (F_{net}) in the lower.

4.4 ROMS-simulations

4.4.1 Timeseries

Temperature and salinity time series for five years of ROMS simulations are shown in Figure 4.11 and 4.12. The modelled period is from January 1^{st} 2005 to July 18^{th} 2010. Five stations, HS01-HS05 (See map in Figure 4.12) are extracted from the ROMS results. The positions of the stations are selected in order to capture some of the horizontal variations that one can expect in Hornsund. Three layers are plotted for all five stations; 1 m, 30 m and the 60 m layer. The bottom layer is also plotted for station HS03 and HS05. A seasonal cycle is seen in all the presented time series in which a brackish layer in the surface becomes fresher through out summer. The temperature for the upper 60 meters also follows an annual cycle, experiencing warming through summer, maximum temperature is first reached in the upper layer and reaches the 60 m layers at varying times, depending on position. Throughout fall there is a homogenising of the water column where the brackish layer is diminishing and water temperatures decrease. The summer temperature at the bottom layer of HS03 and HS05 stays rather close to winter temperatures until the decrease in salinity of the surface layer starts in autumn. In Brepollen (HS05) the temperature increase in the bottom layer starts later then at HS03, first when the brackish layer has more or less vanished. The bottom temperature then reaches a temperature above the temperature of the surface layer. The freshest surface water in summer is found at HS05 (Brepollen). Further out, and along the northern shore of Hornsund basin (HS04, HS03 and HS01), the surface water becomes slightly more saline. Highest salinity of the summer surface water is found at HS02, along the southern shore of the main basin.

The freezing period for the polynya model, marked with the vertical lines in the HS05 time series, ranges from the time of first observed drift ice in Hornsund (Table 3.3) to May 1^{st}. For all years simulated the surface water temperature in Brepollen starts increasing at about the same time as the end of the freezing season. Before this, trough winter, the surface layer fluctuates close to freezing temperatures. The bottom layer reaches freezing point at about the same time as the rest of the water column, and the timing coincides with a salinity decrease, and the time of lowest salinity in the bottom layer. An exception is in fall 2005 where there is a period of temperature close to freezing in the upper water column, whereas the bottom layer still is close to its yearly maximum. An increase in salinity is evident through the winter season at HS05, and a further increase in bottom water salinity can be observed throughout early summer, with the yearly maximum coinciding with the temperature maximum at intermediate depth ($\sim$30 meters).

The fraction of satellite observed fast ice cover for the entire Hornsund fjord system is included in Figure 4.12, to serve as an additional indicator of the ice situation over the winter season. There are inter annual differences in when the fast ice cover establishes, which are not necessearly related to the first observations of drift ice. The timing of which the bottom water layer in Brepollen is at freezing point is changing from year to year. In 2006 and 2010 the time at which the bottom layer reached freezing point temperature and minimum salinity was in mid February, whereas for the other years it was around new year.

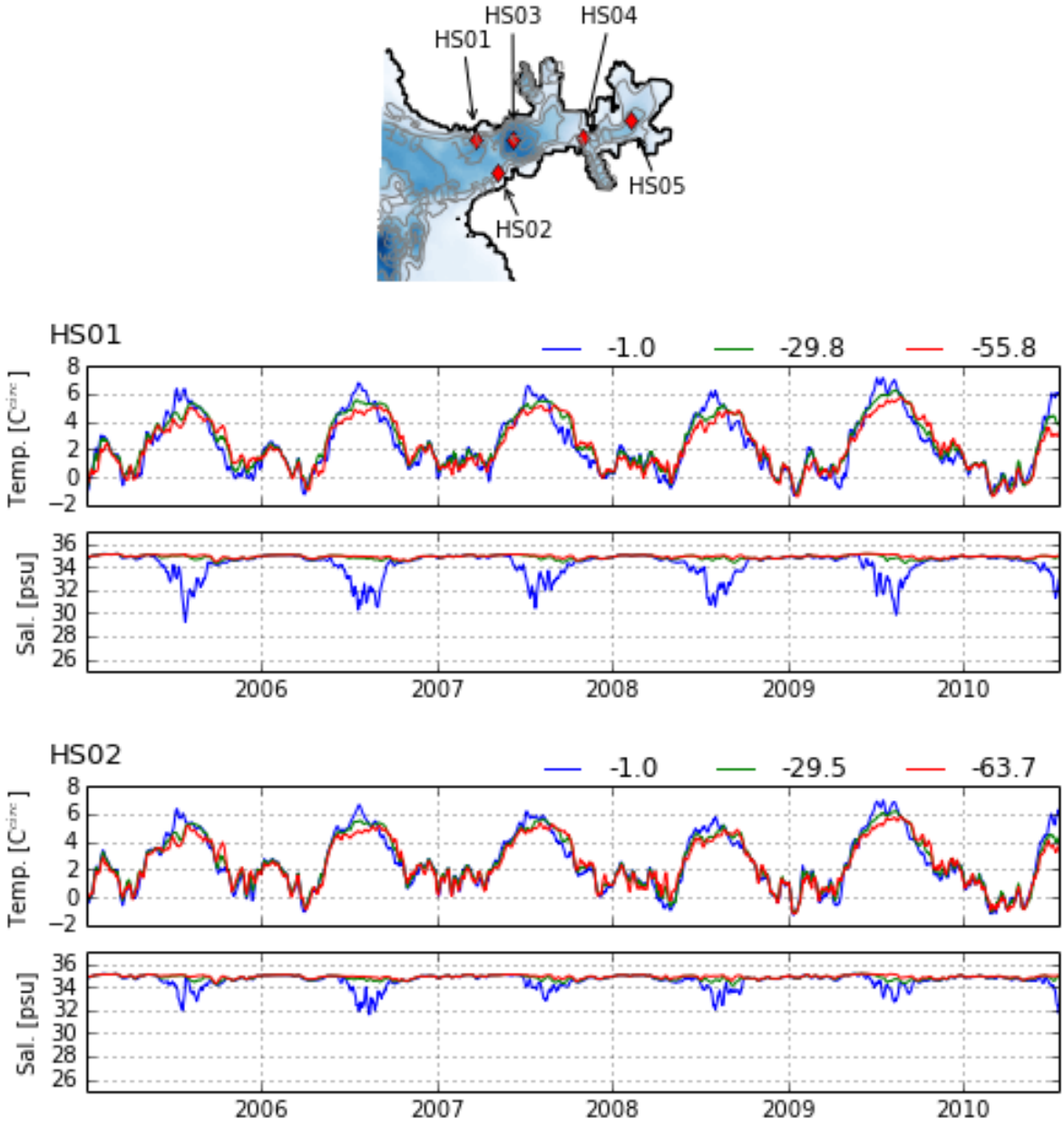

Figure 4.11: 7 days running mean of the Temperature and Salinity time series from HS01 and HS02, extracted from the 5 year long ROMS simulation. Station positions are marked in the map. Three depths are selected from each position, surface ($\sim$ 1 m), lower surface layer ($\sim$ 30 m), and intermediate layer ($\sim$60 m).

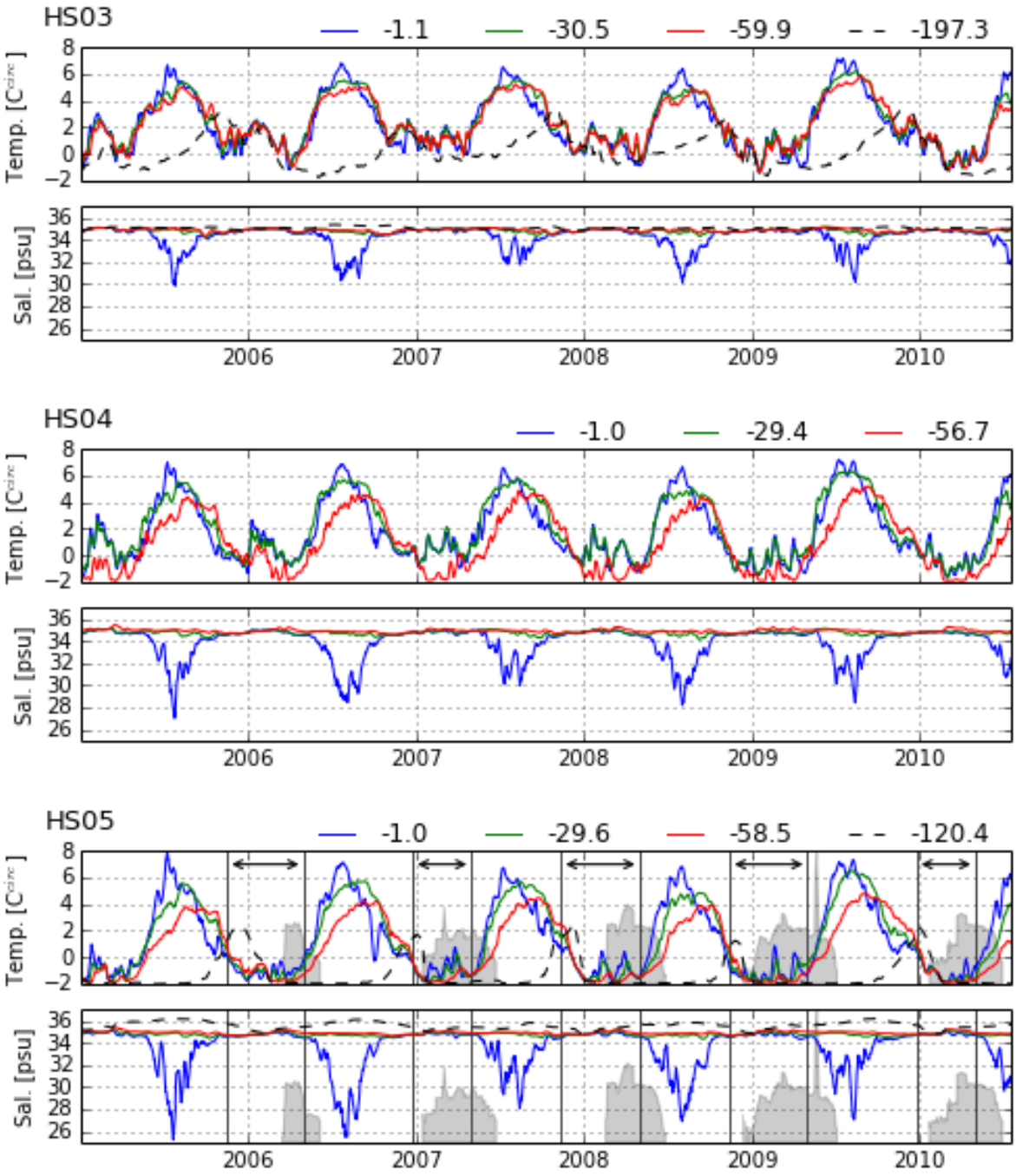

Figure 4.12: 7 days running mean of the Temperature and Salinity time series from HS03, HS04, and HS05, extracted from the 5 year long ROMS simulation. Four depths are selected from each position, in addition to the layer in Figure 4.12, the bottom layer is included for HS03 and HS05. For HS05 the arrows indicates freezing period for polynya model (Table 3.3, "First drift ice" $\rightarrow 1^{st}$ of May). The shaded area is the fast ice fraction from Muckenhuber et al. (In progress), scaled to respective axis limits.

4.4.2 Comparison with CTD observations

Temperature and salinity profiles from HS03 and HS05 (solid lines) are plotted in Figure 4.13 to compare with the observed July profiles (dashed lines), from the same location for the period 2007 - 2010. The lower panels show temperature and salinity at the date we have assumed onset of freezing for the respective years (Table 3.3). The comparison between the measured and simulated profiles reveals a thinner brackish layer in the ROMS-simulations then observed at both locations. While the observed profiles show a gradual increase in salinity down to about 120 meters depth in Hornsund, the modelled water column at HS03 has a strong salinity gradient in the upper few meters before becoming more homogeneous below 20 meters depth. An exception is 2008, where the salinity gradient is comparable to the observed profile. At both locations the modelled temperature in the upper water column is higher than the observed temperature. At depth the model does not reproduce the rather homogenous temperature evident from the observations. At HS05, there is an increase in salinity at the deeper layers that is not apparent from the observations. The modelled bottom temperature is lower at both locations, and at HS05 it is at freezing point.

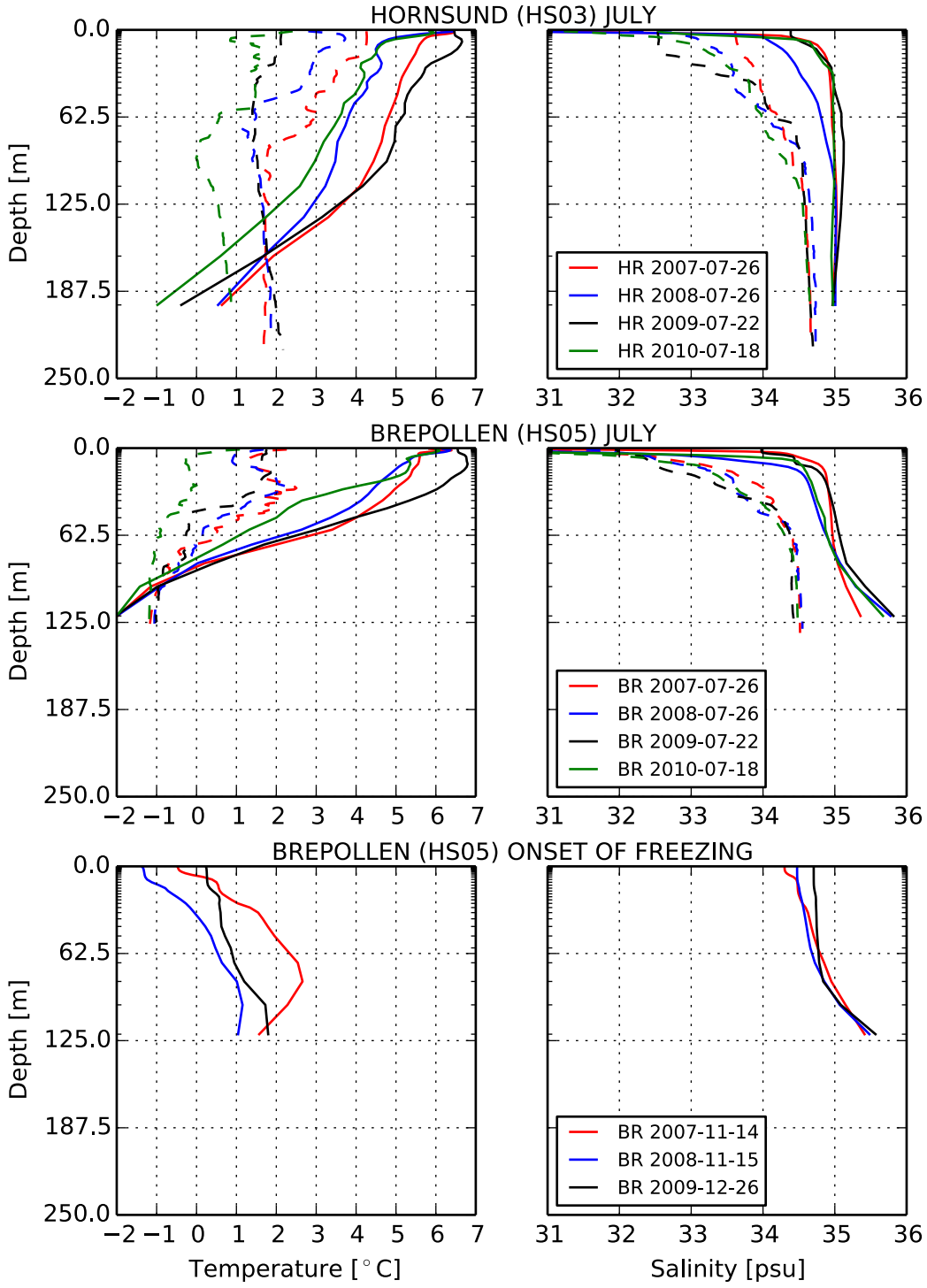

Figure 4.13: Comparison between ROMS-profiles (solid lines) of temperature and salinity to observations (dashed lines). Summer data for Hornsund and Brepollen are taken late July for the four years. Lower panels show ROMS-profiles from deepest point in Brepollen at the date were we have assumed onset of freezing (Table 3.3). Vertical resolution for the ROMS-simulations is denoted on y-axis.

Chapter 5

Discussion

In this chapter, first, the changes of the polynya model compared to Skogseth et al. (2004) and Nilsen et al. (2008) are discussed. Then an analysis of the polynya model behaviour when forced with a set of constant input parameters is made. Next, the polynya model results are compared to satellite observations of sea ice conditions during winter, with particular emphasis on polynya events. The salt production from the polynya model is also compared to ocean temperature and salinity time series in order to discuss the response in the water column. Finally, the ROMS-simulation is included, to try to achieve a better understanding of the interactive processes as a whole.

5.1 Polynya model behaviour

5.1.1 Modifications to the original model

As explained in Section 3, some changes have been made to the basic equations governing the processes involved. Here follows a discussion of what the major differences between the original model and our modified version are.

The modified Pease model

The mechanical pack ice drift opening the Storfjorden polynya is at first glance independent from the thermodynamics inside the polynya and can be considered separately with the following equation:

$$\frac{dW_p}{dt} = F(\phi_t - \phi_0)B_1 cos(\phi_t - \phi_0)U_a, \tag{5.1}$$

where F is a correction coefficient assumed to represent the deviation from the free ice drift solution represented by the B_1 drift factor. The impact from a complex coastline and internal stresses in the pack ice, and the state of the pack ice outside Storfjorden, are parameters influencing the determination of F. This parameter was tuned from year to

year for Storfjorden (Skogseth et al., 2004). Equation 5.1 is run independently on what happens inside the polynya, and the only free parameters through a modelled season are wind speed and direction. Furthermore the thermodynamics within the polynya are defined by:

$$\frac{dW_o}{dt} = B_2 cos(\phi_t - \phi_0) U_a - \frac{W_o}{h_c} \frac{dh_f}{dt}. \tag{5.2}$$

Here there is a competition between the wind and the heat flux from the open ocean, to whether the polynya area will be dominated by open water or thin ice, respectively. Note their definition of the Storfjorden polynya, to also include the thin ice area. In the present study the two equations have been reduced to one for the Hornsund polynya. Equation 3.1 is repeated for clarity:

$$\frac{dW_o}{dt} = F(\phi_t - \phi_0) \times B_2 U_t cos(\phi_t - \phi_0) - \frac{W_o}{h_c} \frac{dh_f}{dt}. \tag{5.3}$$

This equation can be viewed as a modified version of the open water equation given by Pease (1987), were a correction term, as used in Storfjorden and Isfjorden (Haarpaintner et al., 2001; Skogseth et al., 2004; Nilsen et al., 2008), is implemented in the ice drift part of the open water equation. This allows for corrections due to geographic constrains when the ice is pushed out the fjord. Without exact observations of the development of a polynya in Hornsund, we have set $F = 1$ for out-fjord and $F = 3$ for in-fjord blowing winds in the Hornsund Basin. The reasons for choosing a higher value for in fjord winds are 1) based on the observations of Skogseth et al. (2004) of a rapid closing of the Storfjorden polynya with southerly winds, due to redistribution of frazil ice that was forced under the pack ice (Drift ice/thin ice in our case) during opening, coming to the surface when the wind turns, and 2) satellite derived observations that the polynya often seems to curve northward when it extends out of Hornsund onto the shelf region. Possibly being affected by the the Coastal Current, and therefor the closing will be of drift ice south of the polynya, closer to the fjord mouth. As further discussed below, it would be plausible to vary this factor in relation to the amount of drift ice present outside the fjord mouth. And in cases of very little or no drift ice on the shore, F for in-fjord winds could be set negative because this wind has the potential to reduce the thin ice area by stacking up the new frozen ice at the fjord head or towards the fast ice that may be present. For the case study of Brepollen, F has been reduced for out-fjord winds to $F = 0.5$, as Treskelodden (See map in Figure 2.2) effectively restrict the free ice drift out of the basin.

Grease ice and collection thickness

The collection thickness, h_c, represents the transition from frazil ice to thin ice, and hence the initial thickness of the thin ice. While Haarpaintner et al. (2001) assumed a constant value, $h_c = 20cm$, Skogseth et al. (2004) used a parameterisiation by Winsor and Björk

(2000). Winsor and Björk (2000) suggested a linear relationship between the collection thickness and the wind speed, but further observations (Drucker et al., 2003; Smedsrud and Skogseth, 2006) have shown that this is not a sufficient parameterisation. Based on studies by Dai et al. (2004), Smedsrud (2011) proposed a non-linear relationship between the wind stress and observed frazil/grease ice thickness. The observed grease layer thickness, as in Smedsrud and Skogseth (2006) and Smedsrud (2011), is not the same as h_c which is the ice thickness equivalent when subtracting the water fraction difference between the slushy grease ice and a consolidated thin ice layer. Smedsrud and Skogseth (2006) found the ice concentration in their grease ice samples to be around 25% and above 60% for new solid ice. Neglecting ocean currents, the equation from Smedsrud (2011) has been used for the observed grease ice thickness h_g:

$$h_g = 0.1 + \frac{2}{3}(V_g)^{\frac{1}{3}} \left(\sqrt{\frac{\rho_a C_a}{K_r}} U_a \right)^{\frac{2}{3}}, \tag{5.4}$$

and in our model $h_c = 0.25 h_g$ accounting for 25% pure ice in the grease ice. Based on the observations of frazil ice growth and development of a grease ice layer in calm winds (1.6-2.1 m/s) in Smedsrud and Skogseth (2006), a lower boundary of 10 cm grease ice layer is assumed, and Equation 3.2 is modified thereafter. The relationship shown in Equation 5.4 considers a wider range of physical processes affecting the thickness of a grease layer packing towards the lee side of a polynya. Firstly, K_r is a proportionality constant that relates the packing force of the ice crystals to the square of the grease ice layer thickness (see Smedsrud (2011) for detailed derivation). $K_r \approx 100$ is dependent on the packing geometry, internal friction and frazil ice concentration in the grease ice. $\rho_a = 1.4$ kg/m^3 and $C_a = 1.3 \times 10^{-3}$ is the air density and open ocean drag coefficient respectively. V_g is the volume of frazil ice per unit width in the lead, and is proportional to the length of lead L_{lead}, and is further dependent on the integrated heat flux over the open water region, latent heat of fusion for sea ice, and the ice density. We have used the results presented in the simulations by Smedsrud (2011) and the value $V_g = 40.0$.

The derivation of the Equation 5.4 is complex, and the resulting curve is based on several parameters that are not easily defined and validated for our study domain. For the purpose of this study the most important difference is that this definition allows for a quicker development of an ice cover in low winds. Figure 5.1 shows the collection thickness dependency on wind speed for the two different parameterisations. The figure shows that with the use of the non-linear relationship by Smedsrud (2011), one will get a more rapid thin ice formation for all wind speeds, with the largest difference to Winsor and Björk (2000) in calm winds and high wind speeds.

5.1.2 Model behaviour and sensitivity

One of the major differences between this study and studies of conventional polynyas in the pack ice (Pease, 1987; Skogseth et al., 2004), is that our polynya is not always constrained

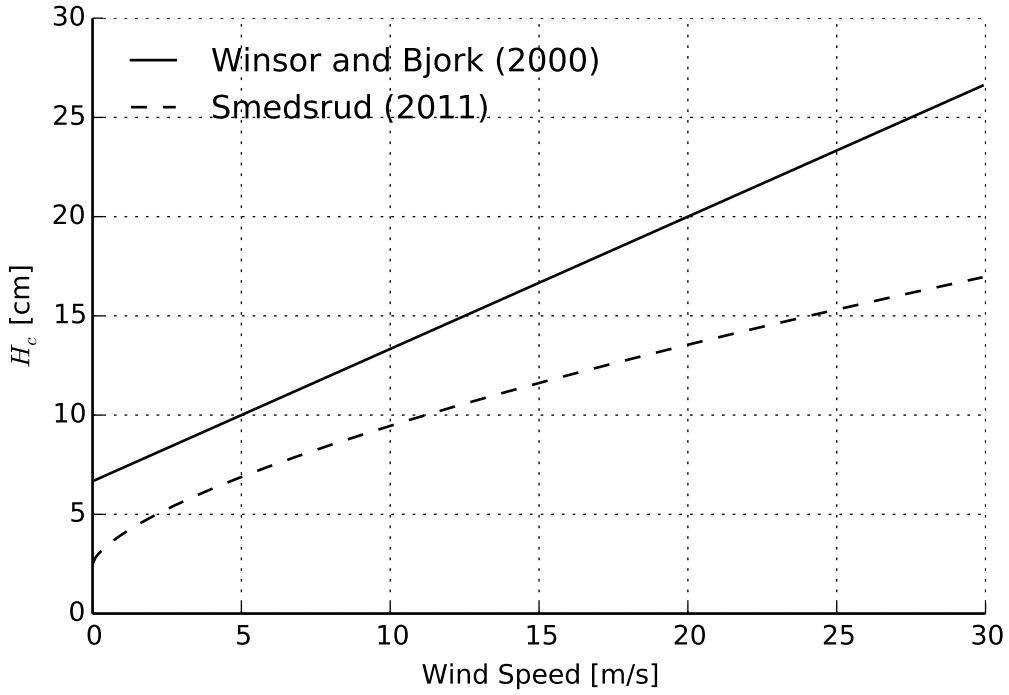

Figure 5.1: Collection thickness parameterisations. The linear relation by Winsor and Björk (2000) together with Equation 5.4 suggested by Smedsrud (2011)

by the pack ice edge on the lea side. This makes it possible for the ice produced to advect out of the model domain. Therefor the choice of the maximum polynya width, $P_{w,max}$, is of importance. In a conventional polynya the open water width will eventually come to an equilibrium, as the production rate balances the advection rate of the new frozen thin ice. In our case, the increase in production rate will be limited by the maximum length of the fjord, by the condition $W_o' \leq P_{w,max}$. If $F_{net} = 0$, and hence, there is no ice production, a rearrangement of Equation 5.3 gives the time it takes to empty a thin ice covered fjord by advection. Assuming a constant wind speed of 10 m/s we get:

$$\Delta t = \frac{P_{w,max}}{F, B_2 U_{\phi_0}} = \frac{20km}{1 \times 0.03 \times 10m/s} = 18 \text{ hours.} \tag{5.5}$$

To find the heat flux needed to sustain a maximum opening of the polynya, $W_o = P_{w,max}$, one might use Equation 5.3, set $\frac{dW_o}{dt} = 0$, and solve for F_{net}, which gives:

$$F_{net} = U_{\phi_0} \frac{h_c F B_2 \rho_f L_s}{W_o}. \tag{5.6}$$

Using values from Table 5.1, a relationship between the mechanical- and thermodynamical forcing is plotted in Figure 5.2. This gives the minimum wind speed needed to have the advection rate to overcome the production rate within the polynya. For a wind speed of 10 m/s, F_{net} of 400 W/m^2 and lower will result in an ice free fjord. Whereas for wind speed of 15 m/s we need a heat flux of 800W/m^2 to produce enough frazil ice for a thin ice cover to be apparent in the fjord. Comparing this with the polynya width calculation for 2011 shown in Figure 4.4, there are several occasions with wind speeds of 15 m/s, and heat fluxes less than 600 W/m^2, which gives maximum polynya width, $W_o \geq P_{w,max}$. The maximum F_{net}, in the end of January reaches above 800 W/m^2 at the most. With wind speeds of about 13 m/s (<15m/s) the ice production is strong is enough to overcome the advection rate, and results in a polynya width of about half the maximum width.

In order to study how the wind and temperature affect the model results, a standard case for the model is set up. Here the model is forced with an ensemble of constant temperatures and wind speeds to look at its response, and the equilibrium state, to changes in these parameters. The over all mean value for relative humidity is used, and the cloud cover is set to 50%. Constant values for the standard case are shown in Table 5.1. Because of the constant h_c in the original formulation of the polynya model (Pease, 1987), the production rate of frazil ice will increase linearly with wind speed, as the advection rate of the ice edge on the lee side of the polynya linearly increases. This makes the opening time of the polynya in their case, the time to reach an equilibrium size of the polynya, only dependent on temperature. In our case, h_c varies with wind (Equation 5.4 and Figure 5.1), and the production of thin ice which retards the opening of the polynya, will be dependent on both wind speed and air temperature. Since this study also focuses on the ability of growing thin ice in the fjord, rather then the open water, we will in the proceedings point to the Thin Ice Coverage (TIA), rather then the polynya opening.

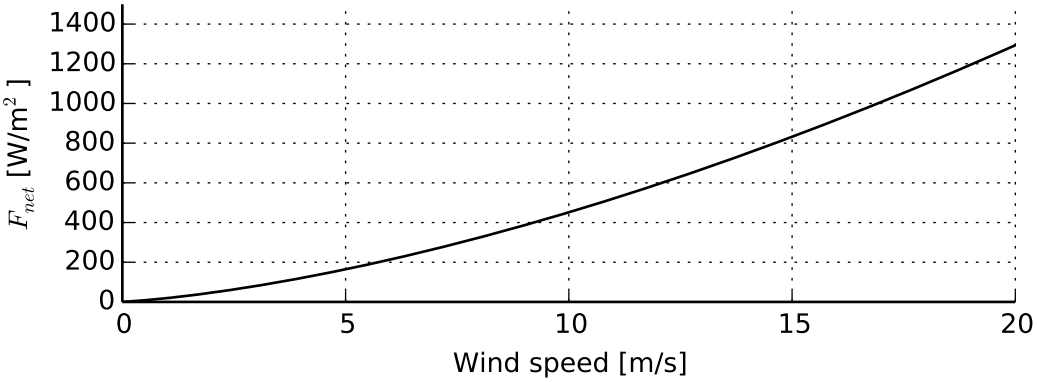

Figure 5.2: Maximum allowable F_{net} for a 10 m/s along fjord wind component to sustain a maximum Polynya Width.

Table 5.1: Model values for standard case

Parameter	Value	Definition
RH	79%	Relative Humidity
CL	4/8	Cloud cover
L_s	2.34×10^4 J/kg	Latent heat of fusion
ρ_f	950 kg/m^3	Densety of frazil ice
T_{freeze}	-1.865 C°	Freezing point of sea water
$W_{p,max}$	20 km	Max polynya opening
B	0.03	Ice drift factor
F_{out}	1 W/m^2	Ice drift correction factor

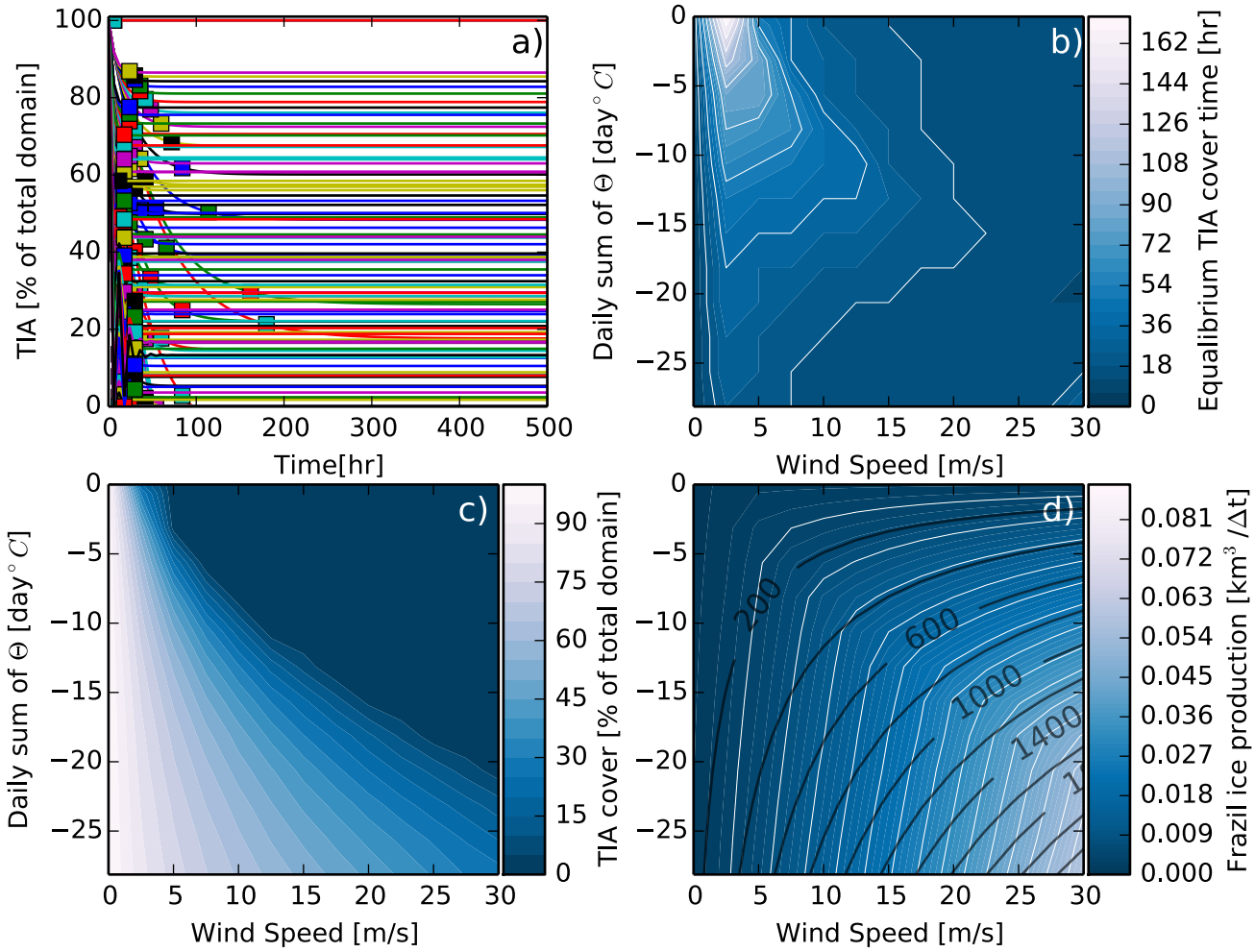

Figure 5.3: Standard case for model run. The model is forced with an ensemble of temperature and wind speeds. a) Shows the TIA coverage evolution by time for the parameter ensemble, the time it take to reach 95% of equilibrium TIA (t_{95}) is marked with squares. b) shows the t_{95} dependency on temperature and wind, c) show the TIA fraction, and d) shows the frazil ice production rate integrated over the total model domain. Overlaid in d) is the F_{net} dependency on the respective parameter ensembles.

The result for the standard case is shown in Figure 5.3. Figure 5.3 a) shows the TIA fraction of the polynya area by time from the start of the model run, for all the different runs (temperature and wind ensembles). The TIA response can be separated into three groups. Firstly, if the production rate overrules the advection rate, a complete thin ice cover will be maintained and the result will lay on the 100% line in Figure 5.3 a). Secondly, there are several combinations of air temperatures and wind speed leading to an equilibrium opening where $0 < W_o < P_{w,max}$, and hence a partially TIA covered domain. Lastly, there are combinations were the advection rate exceeds the production rate, and eventually there will be no thin ice in the model domain. The squared boxes denote the opening time, t_{95}, when TIA has reached 95% of the maximum value for the respective set of input parameters (temperature and wind ensembles). For runs in the first category the opening time is zero, while for the second case it varies between 12 and 174 hours. The opening time, t_{95}, for the different combinations are given in b). The temperature is given as Θ_{day}. Noteworthy are the 3 time steps ($3\Delta t = 18hr$) needed to reach open water for $\Theta_{day} = 0$ which is consistent with the calculation above (Equation 5.5). c) shows the TIA(t_{95}), and by comparing b) an c) it is apparent that t_{95} is lower for combinations ending with open water and for simulations with low air temperatures. Finally, the frazil ice production is shown in d). For 100% TIA the frazil ice production is low. The frazil ice production has its maximum at highest wind speeds and lowest temperatures. The production rate is a weak function of wind speed for high air temperatures, and has a strong dependence on wind speed for combinations where thin ice is present in the fjord. With TIA = 0, frazil ice production will rely only on the net heat flux, F_{net}, and becomes strongly dependent on the air temperature. Through the turbulent heat flux F_T, the frazil ice production also depend on the wind speed which dependency become more pronounced for higher wind speeds. The F_{net} [W/m^2] dependence on wind and temperature is plotted on top of the frazil ice production. For an ice free ocean (See Figure 5.3 c) to find the temperature and wind range for an ice free ocean), the frazil ice production follows the contours of constant F_{net}, which is consistent with the combination of Equation 3.3 and 3.5. When the TIA fraction increases, the heat flux needed to retain a similar frazil ice production increases, as the effective area of open water decreases.

5.1.3 Model forcing and correlations

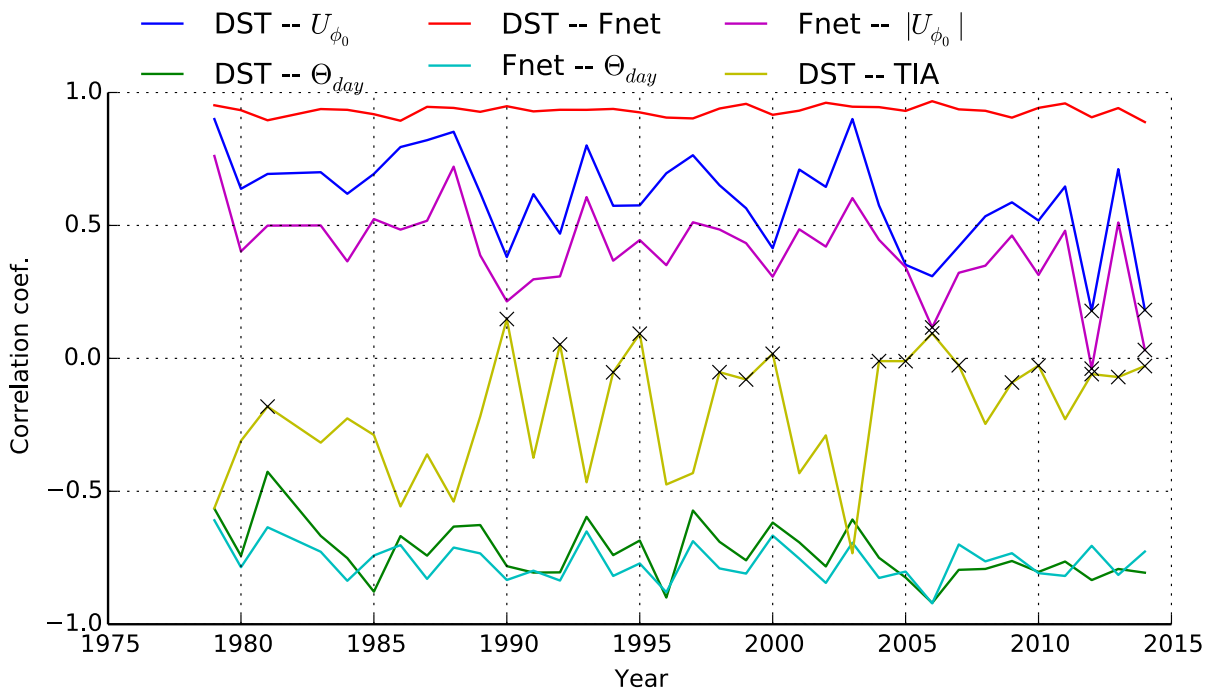

Figure 5.4: Yearly Spearman rank-order correlation coefficients between model results and major forcing parameters. DST is the Daily Salt release. "×" denotes not significant correlation values (p-value > 0.01).

To further study the relative importance of the meteorological forcing on the model result, yearly correlation values between some of the major drivers and results have been calculated and are shown in Figure 5.4. Since frazil ice growth is dominating the ice production, the daily salt release, DST, will be a direct effect of F_{net}, which controls the frazil ice growth (Equation 3.3). Figure 5.4 shows that there are inter annual differences in how well correlated wind and temperature are to the frazil ice growth. The years 1979, 1986, 1988, 1993, 2003 show the greatest correlation between wind and DST. These were rather cold years, which give the wind an importance in terms of transporting out ice, in order to increase the polynya area. This winds importance is also evident from the relatively high negative correlation with the thin ice area for these years. Warmer years, such as 1990, 2000, 2006, 2012, and 2014 have a lower correlation with wind, which coincides with the discussion above, where warmer air temperature regimes give a lower sensitivity to wind in the model. The yearly mean values for for Θ_{day} and U_{ϕ_0} and their scaled standard deviations are plotted on top of the frazil ice production in Figure 5.5. The years pointed out above are marked, and one can note how the years having a higher correlation with winds, are the colder years, whereas the warmer years lay in the less wind-dependent area. Colder years show a significant negative correlation between DST and TIA, which relates

to these years having mean values well into the partly TIA covered range in Figure 5.3. The variance in DST due to wind forcing is in general higher then the variance in F_{net} to this parameter. The latter is an effect of DST being the integrated effect of F_{net} and open water area, whereas F_{net} it self is pr unit area in the open water region. To eliminate the effect of warmer weather often related to westerly winds, the absolute value is used on U_{ϕ_0} in the correlation between F_{net} and U_{ϕ_0}.

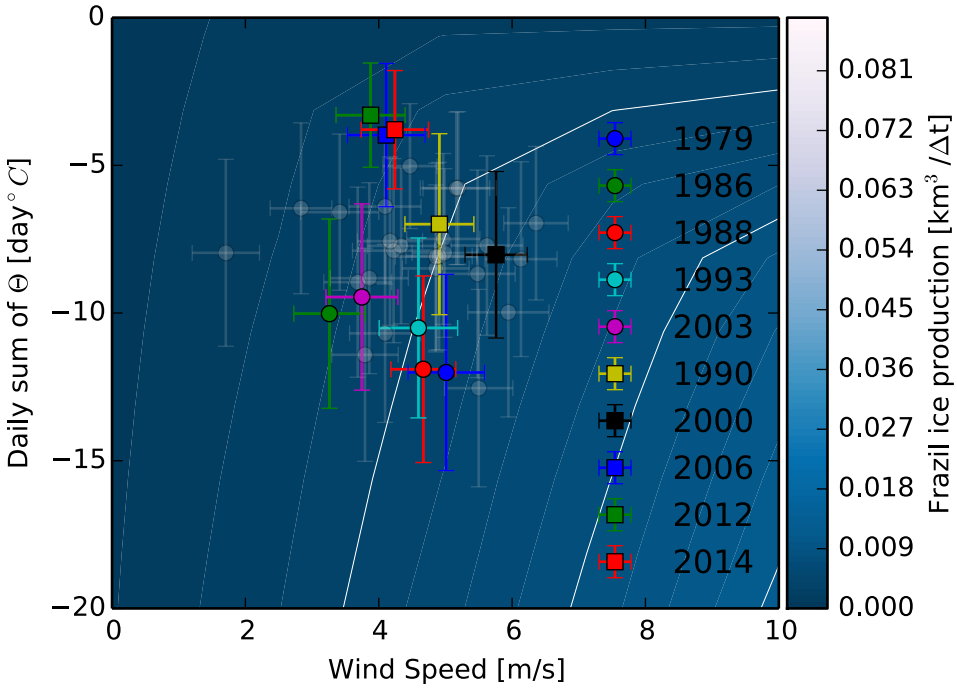

Figure 5.5: Mean values of Θ_{day} and U_{ϕ_0} for all years, selected years are coloured. Scaled standard deviations for the means, where temperature is scaled by a factor 0.5 and the wind speed by a factor 0.1. The contoured lines are the frazil ice production, derived from standard case presented in Figure 5.3

5.2 Polynya Model evaluation

5.2.1 Validation and tuning parameters

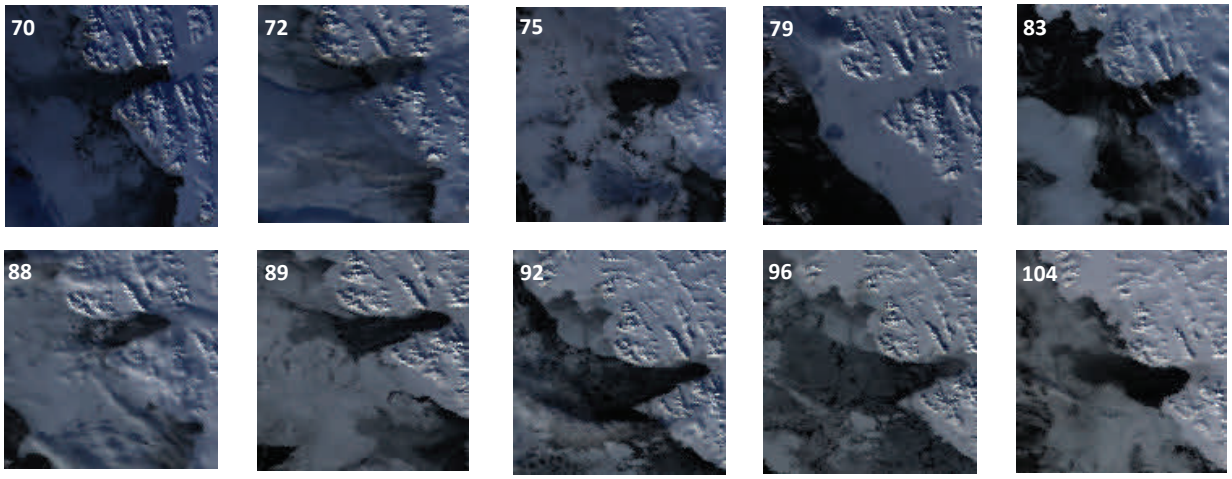

Figure 5.6: MODIS satellite pictures from selected dates in 2000. Day Number of the year in right corner of each image correspond to the number and blue lines in Figure 4.5.

Figure 5.6 shows MODIS satellite images from Hornsund for a period between March 10^{th} to April 13^{th} 2000, and is used in comparison with the model result from the same period. This is rather late in the season, and a decent amount of drift ice is evident on the shelf outside the fjord mouth. An open polynya is evident on Day 70, which is closing partially on Day 72, due to ice production in the fjord. This is comparable to the model results (Figure 4.4 II a)-c)), where a decrease in wind speed together with a sustained positive heat flux leads to a decrease in open water width W_o. On Day 75, W_o increases in our polynya model result. This is due to a combination of easterly winds, and a low heat flux. Little or no frazil ice is evident from the satellite image from the same day. A shift to westerly winds packs the ice towards the shore before Day 79. From the satellite image one sees how the ice area off shore has decreased and leads to a more closely packed drift ice along the coast. The model responds similarly to the shift in wind direction and closes the polynya. The low heat flux on Day 75, 83, and 104 leads to little frazil ice formation and, even in relatively low winds, a wide opening which is captured by the model. The highest frazil ice production for the given period is modelled between Day 89 and 93 in which the modelled open water width is fluctuating around half the fjord length. The high frazil ice production gives a smaller modelled open water area then what can be observed from the satellite images for the respective days, and leads to a discussion of the uncertainties in one of the model parameters. The transition from open water to thin ice is determined by the collection thickness (h_c). A higher value would have retarded the formation of a thin ice layer and resulted in a larger polynya opening. Proposed by Alam and Curry (1998), the length of the lead where frazil ice is produced is among the factors controlling the

collection thickness, as the stress on the grease ice layer increases with an increase fetch which is the along wind distance of which wind forcing acts on the frazil ice collection. V_g in Equation 3.2 is the total volume of grease ice produced per unit width, and is proportional to the opening of the lead were the grease ice is produced. In our case V_g is set constant, and hence there is no dependence for h_c on this length, which in this case would be W_o. Nevertheless, Smedsrud (2011) shows that this choice of V_g holds for a range of heat fluxes and open water widths, and thereby is a valid assumption.

A deflection of the open water area towards the north, as the polynya extends out of Hornsund on several of the example pictures in Figure 5.6 can be noted. There are several possible reasons for this deflection. It could be a result of a current contributing to the opening that is likely to follow the isobaths (f/depth = const (Cushman-Roisin and Beckers, 2011)) out of the fjord, and give an additional ocean drag which will also result in a wider opening. When the ice is no longer restricted to follow the fjord axis it is as well believed to follow the typical free drift direction with a $\sim 20°$ to the right of the surface wind (Nansen, 1915; Leppäranta, 2011). Moreover, the drift ice on the coast follows the general flow of the CC, which in turn forces the whole ice field north-ward, and thereby is expected to be an additional factor pushing the polynya in the same direction. The

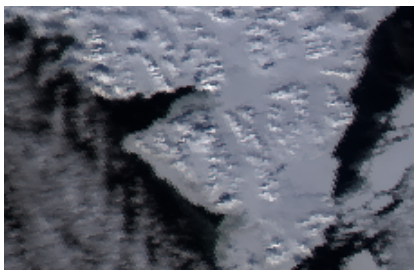

Figure 5.7: MODIS satellite pictures from April 22^{nd} 2008 were winds were blowing into the fjord.

northward deflection further explains the choice of the tuning parameter $F = 3$ which for westerly winds is three times the factor for easterly winds, as more ice is available to penetrate the fjord from the southern side of the mouth after the wind turns. The closing of the polynya is therefore, in reality, related to the amount of drift ice following the CC northward. For periods with less drift ice evident on the coast, e. g. earlier in the season, this model formulation has the potential to lead to an over estimation of drift ice in the fjord when westerly winds are not accompanied by advection of drift ice into the fjord. The satellite image in Figure 5.7 shows an example of a period of westerly winds, where the model suggests complete ice cover in the fjord (April 22^{nd} 2008 in Figure B.3, Appendix B). Because there is little ice in the water outside the fjord, the available ice is packed at the head of the fjord. This occurrence illustrates one of the limitations with the model since the ice situation undergoes great variation throughout a season and from year to year. When compared to the situation in Storfjorden (Haarpaintner et al., 2001; Skogseth et al., 2004) with more persistent the pack ice throughout the modelled season,

the situation in Hornsund may seem more complex because it is influenced indirectly by large scale atmospheric circulation and shelf circulation which have a direct effect on both the amount of drift ice in the CC and the oceanic heat flux into our system. The latter leads to the discussion on the necessary conditions for sea ice to be locally produced in Hornsund.

5.2.2 On water masses and Latent/Sensible heat polynya

After having compared the examples from the model result with ice cover observations, the focus will now be on the effect of the ice production on the underlying water, how it influences the water masses present in the fjord, and the effect the water properties has on the ice production. Temperature and salinity time series from three years of mooring data outside the mouth of Hornsund is presented in Figure 5.8. The position of M11 is likely to capture some of the processes also evident inside the fjord, as it is positioned along the northern shore in the mouth area. Before onset of freezing, in fall 2010, the measurement at 25 m depth represents values in the SW to IW domain. Throughout October and November, the water cools down. Salinity also increases in the surface layer when SW is mixed with underlying water masses. At the beginning of December, water approaches freezing point and ice production starts. A gradual increase in salinity, from 34.1 to 34.7 psu can be seen from the beginning of December to the beginning of February. This corresponds to the polynya model results for the same period with high frazil ice production (Figure 4.4 (I) c)). The blue lines denote short term events of decreased salinity at the mooring. These events coincide with periods of wide polynya opening, and high heat flux shown in Figure 4.4 (I). SAR images for some of the events are shown in Figure 5.9. An increase in wind together with a fall in temperature from Day 361 to 362 opens the polynya and increases the frazil ice production, prior to the disturbance in the salinity signal at M11 on Day 364 in Figure 5.8. Similarly, between Day 7 and 9, an enhanced frazil ice production occurs as the polynya opens which is seen both in the model results and the satellite images. White streaks in the SAR images are interpreted as streaks of frazil ice, generated by Langmuir circulation during wind events (Drucker et al., 2003). On Day 362, the polynya area extends over the position of M11 (Figure 5.9), and it is plausible to connect the salinity signal to polynya activity. The salinity decrease can be a result of wind induced mixing of the upper water mass, or a depression of the haloocline that leads to decreased salinity at 24 meters depth. When strong out fjord winds opens the fjord polynya, ekman transport of the surface layer to the right (north for easterly wind in Hornsund) of the wind direction, forces a downwelling along the northern shore (Cottier et al., 2010), and subsequently results in a lower salinity at M11 on the norther side of the polynya. Studies in summer in Kongsfjorden (Cottier et al., 2005; Ingvaldsen et al., 2001) have shown how the surface layer show a rapid respons to down fjord winds in terms of downwelling on the northern side of the fjord. For this to be the case in winter in Hornsund, there needs to be a surface layer of lower salinity present also in winter. Lower salinity close to surface might be remnants of the well salinity stratified surface water observed in summer in Hornsund (Figure 4.3), but probably more well mixed down

to a certain intermediate level in fall. Tverberg et al. (2014) observed a cold halocline on the shelf west of Prins Karls Forland on the west coast of Spitsbergen in the same period in early 2011. They partly explain this by melting of drift ice in the CC by warmer AW type water in the WSC, and this cannot be neglect as a possible factor contributing to a freshening in the upper water layer in the mouth of Hornsund in winter. If a halocline still is present before onset of freezing, it is likely to believe that M11 at 23 m depth is situated in the halaocline. It is thereby plausible to link the increase in salinity from Day 353 to Day 39 in Figure 5.8 to a salinification of the lower part of the surface layer, interrupted by occasional downwelling events of the overlying water mass. After day 39 the surface layer has vanished, and the salinity stays more constant as the brine that is released will be mixed over a deeper water column. Consequently the wind event on Day 55 is not accompanied by the same decrease in salinity as earlier. In their conclusion, Tverberg et al. (2014) suggested that the density of AW outside the shelf sets up an upper salinity limit of the shelf water, close to 34.8 psu. This is consistent with the constant salinity at M11 after Day 39. If saltier water is produced on the shelf it is likely to disappear from the shelf sliding down the continental slope (Tverberg et al., 2014). At M11, there is an increase in both temperature and salinity in late March. This is reflected in the drift ice observations (Figure 4.5 and B.6) were there is a distinct decrease in drift ice in the fjord over the same period. End of March and beginning of April 2011 experienced cold air temperature, with two weeks of about -15°C at the same time as the sea ice decreases (Figure B.6). A gradual production of BWW prior to this period can have caused a strong enough density difference between the shelf water and the AW type water further out for it to initiate a down flow of BWW down the continental slope, over which warmer AW type water could flow in on the shelf and cause the reduction in sea ice and the increase in water temperature and salinity at M11.

Satellite pictures from the Day 21 and 22 are included in Figure 5.9 to show how the wind opens a polynya in the morning on Day 21 at the same time as an enhanced heat flux due to a temperature drop. This is increasing the frazil ice production during the next day, filling the fjord with frazil or thin ice. This is not captured by the model that simulates an open polynya the whole period. There is however no notable effect from this on the M11.

The temperature and salinity time series from M12 sampling at 45 meters is shown in Figure 5.8. The mooring is located on the southern side of the fjord mouth, and differs significantly from M11 in 2011. The position of the mooring is assumed to provide information on the properties of the intermediate layer water masses entering the fjord. It thereby gives an indication of the initial state of the water circulating in the fjord.

The beginning of the time series shows the same characteristics as the previous year, with SW to IW. In fall water cools and mixes with under lying water which results in lower temperatures and higher salinities. Unlike winter 2011, the water at M12 does not reach freezing point in 2012. The water cools gradually throughout December, but then warms when approaching new year. Highest temperatures ($T > 3°C$) are reached in February. Accompanied with high salinities (up to 35 psu) this water mass has a strong signature of Atlantic type water, which may have penetrated all the way into the fjord and prevented

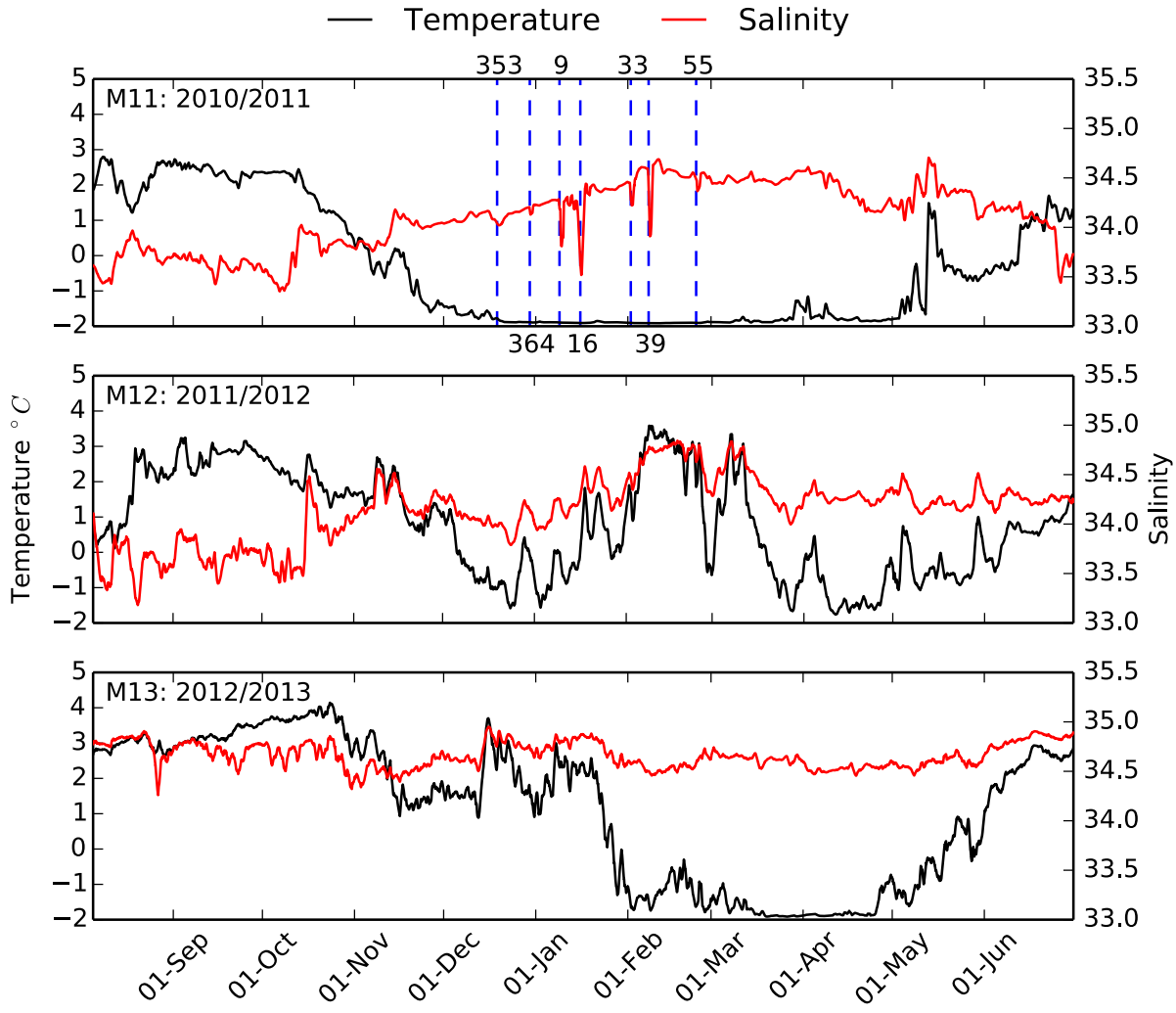

Figure 5.8: One day running mean of the Temperature and salinity time series from M11, M12 , and M13. M11 located on the northern side of the mouth area, M12 and M13 on the southern(See Figure 2.2 and Table 3.2)

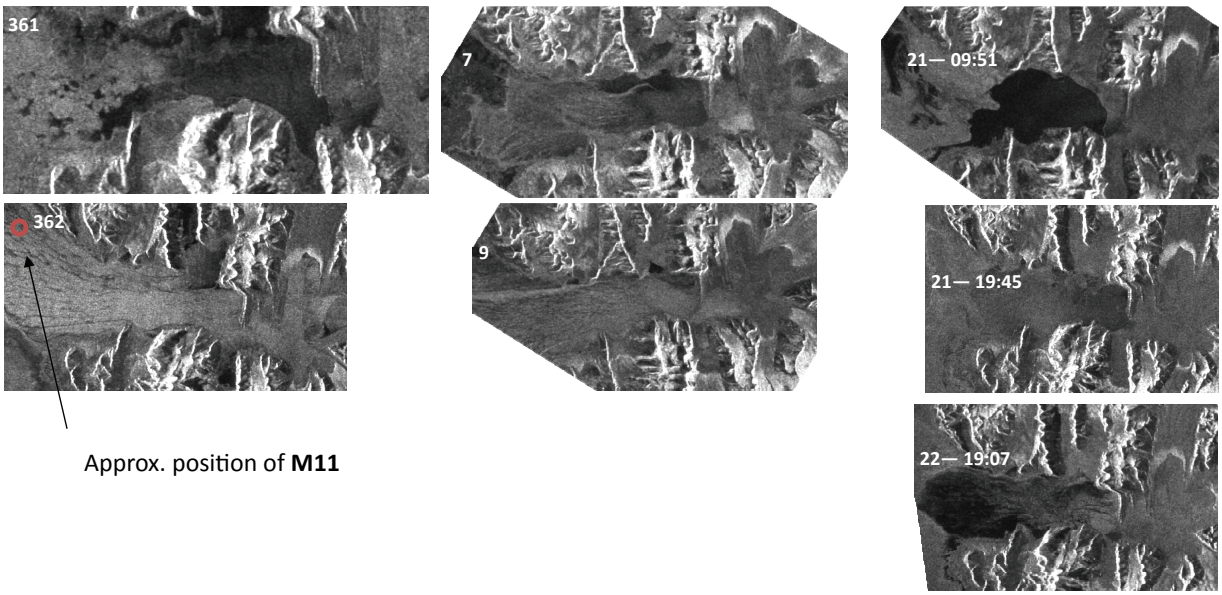

Figure 5.9: SAR images from selected days winter season 2011.

effective ice formation this in 2012. In March, this water is replaced by Arctic type water (ArW). A switch to ArW for a shorter period can also be seen between February and March. The effect on the sea ice is seen in Figure 4.5. During 2012 little ice was observed in Hornsund and fast ice was not observed before end of February. The establishment of a fast ice cover corresponds to the switch in water mass characteristics at M12, and might be related to less oceanic heat input from the shelf. In conditions similar to the general situation in 2012, with a vast amount of Atlantic type water on shelf, the polynya model fails to provide a realistic estimate on the ice production. The assumption about water on freezing point is in general not satisfied, and the ice production and related salt release become heavily over estimated.

In winter 2013, relatively warm Atlantic type water occupied the area around M13 until the end of January (Lower panel in Figure 5.8). The mooring position is the same as M12, but positioned at 85 meters depth. In the end of January there is a shift to Arctic type water. This is in correspondence to the observed ice concentration in Hornsund (Figure 4.5), in which a pronounced increase in drift ice cover was observed in mid February. In the beginning of the 2013 winter season, the polynya model must be considered invalid as it produces ice as soon as we have a positive heat flux. Nevertheless, the modelled ice production is lower in warmer periods, e. g. 2012, and beginning of 2013, as warmer sea surface temperatures often correlate well with higher air temperature (Walczowski and Piechura, 2011) that reduces the modelled ice production rate. This results in a lower ice production in time periods such as 2012 and the beginning of 2013. Furthermore, higher air temperatures are often a result of southerly wind patterns in the Fram Strait that bring warm humid air over Svalbard (Førland et al., 2011), which locally causes westerly winds

in Hornsund. This closes the polynya, and thereby decreases the effective area for frazil ice production. In this way, the yearly accumulated frazil ice production and the resulting salt release give a somewhat realistic year to year variation even though the assumption for the polynya model is not always fulfilled.

The clear shift in atmospheric forcing by the end of January 2013 (Figure B.8), of colder air temperatures and a higher occurrence of easterly winds, is yet an example were we of enhanced frazil ice production over a period of favourable oceanic conditions. The frequent high out fjord winds after mid February may have caused the low concentration of drift ice in the fjord for the rest of the season, as both modelled thin ice production and observed drift ice concentrations are low (Figure 4.5 and B.8). Another aspect worth mentioning here is that the whole water column inside the fjord may not have been occupied by ArW after February, but warmer water masses could have been present deeper down. This could lead to warmer water being mixed up during a polynya event. Through turbulent mixing, it is possible for the warmer water to turn the latent heat polynya into a sensible heat polynya for a for a period of time. Both wind induced mixing and mixing through convection of brine enriched water can contribute to lifting warmer water masses to the surface, and an additional heat loss is thus required before freezing on the surface can start again.

To have a deeper look into the complexity of the counter play between the atmospheric and oceanic forcing, on the ice situation along the West Spitsbergen Shelf, an exceptional case was demonstrated by Cottier et al. (2007). They presented an example of high northerly winds along the West Spitsbergen Shelf that induced upwelling of AW on the shelf, and a significant increase in water temperature close to the mouth of Isfjorden in February 2006. Simultaneously, northerly winds brought colder air masses to the area of West Spitsbergen. This is a situation where the polynya model clearly fails. January had been dominated by high temperatures, and the polynya model results show little frazil ice production before the beginning of February (Figure B.1). At this time, frazil ice production increased as heat fluxes got higher in responds to lower air temperatures and stronger winds. Fast ice was nevertheless not observed before mid March, which is consistent with a flooding of AW on the shelf, and possibly also a high amount of warm water inside the fjords in February that prevented ice formation. Northerly winds ceased by the beginning of March, after which water temperatures dropped, and favourable conditions for ice production were established. It is plausible to conclude that the polynya model overestimates the frazil ice production in February and the beginning of March, as the assumption about surface water on the freezing point before this was most probable not fulfilled.

5.2.3 Year to year variability

The main result of the polynya model is the yearly production of salt through brine rejection. The 35 years time series of yearly accumulated salt release (AST) shown in Figure 4.6 is made using constant tuning parameters, so the fast ice variability is not captured. Nevertheless we have briefly touched, and will further argue, that the year to year variations

are somewhat preserved, and the long time series thereby provides a valuable indication of the inter annual variations in salt production. Further, Skogseth et al. (2004) showed a similar development between yearly AST and the total volume of produced dense water. With the lack of reliable initial salinity values, the AST variations in Figure 4.6 will serve as the best estimate on year to year variations in BWW production.

With constant initial settings, the 35 year AST time series is strongly related to the total heat loss (Table 4.1 and Figure 5.4). A reduction in AST after 2005 is noted and may be related to some of the same mechanisms reviewed in other studies that observe a general change in the weather and oceanic conditions during the last decade (Pavlov et al., 2013; Nilsen et al., ress).

When comparing the AST results for Hornsund to the yearly salt release in Storfjorden for the period 1998-2001 (Skogseth et al., 2004), one can note that Skogseth et al. (2004) present 2000 as the most effective year of salt production and 1998 at the least effective year in their study. This is opposite to the results for Hornsund results for the given period. A similar situation is seen when comparing AST results for Hornsund with the similar study in Isfjorden (Nilsen et al., 2008) for the period 2000-2005. Similarly to Skogseth et al. (2004) they estimate high salt release 2000. Furthermore, Nilsen et al. (2008) found a notable increase from 2004 to 2005, which is somewhat opposite to the situation in Hornsund, showing moderate production in 2000 and a clear decrease from 2004 to 2005.

When trying to find a physical explanation for the differences, a first thing to notice is the geometric difference between our study area and the studies in Isfjorden and Storfjorden, where Hornsund is a much smaller fjord. The larger area of the Storfjorden and Isfjorden makes the polynya area more dependent on the wind conditions, as the ice is not as easily advected out of the fjord. This leads to higher variations in open water area, and thereby a higher sensitivity to ice cover on the frazil ice production for Storfjorden and Isfjorden. For Hornsund we have shown several examples were strong polynya events, which dominates the yearly frazil ice production and thereby the AST, empties the fjord of drift ice or newly formed thin ice. This is reflected in the low correlation between thin ice cover and daily salt release shown in Figure 5.4.

The atmospheric forcing in Isfjorden (Nilsen et al., 2008) in the period 2000 - 2005 is comparable to the observations in Hornsund. 2005 was the year of lowest heat exchange (F_{net}), while 2000 was the year of highest out fjord winds. In Isfjorden, the relatively high estimation of AST in 2000 is related to higher occurrences of out fjord winds this year compared to the other years included in their study, leading to this being the year having the largest average polynya area in Isfjorden. In Hornsund, the strong F_{net} dependency of the ice production results in a lower value in 2000. Similarly, the lower heat exchange in 2005 results in a lower salt production in Hornsund in 2005, while the the relatively high occurrence of out fjord winds compensated for this in Isfjorden and gave a higher AST production there.

The same argument explains the difference in AST production between Hornsund and Storfjorden for the period 1998-2001 (Skogseth et al., 2004). Skogseth et al. (2004) found the total ice production and corresponding AST to follow the yearly averaged along fjord wind ($\bar{U}_{\phi_0}$). As a higher $\bar{U}_{\phi_0}$ would give a higher averaged polynya area, this would in turn

compensate for a lower $\bar{F}_{net}$. This explains the somewhat different AST pattern found in Hornsund, in which the AST is closely related to $\bar{F}_{net}$. Even though F_{net} is driven both by the air temperatures and wind stress, the relative effect of the wind is less in Hornsund than in other studies (Nilsen et al., 2008; Skogseth et al., 2004), as less wind is needed to open the polynya, and thereby less variation in polynya area during high ice production events are expected.

Skogseth et al. (2004) used observations of surface salinity before and after the freezing season, making it possible to change the initial settings from year to year for this period. For the given period these observations are not available for Hornsund. We however demonstrate the effect of varying the surface salinity for selected years in the proceedings.

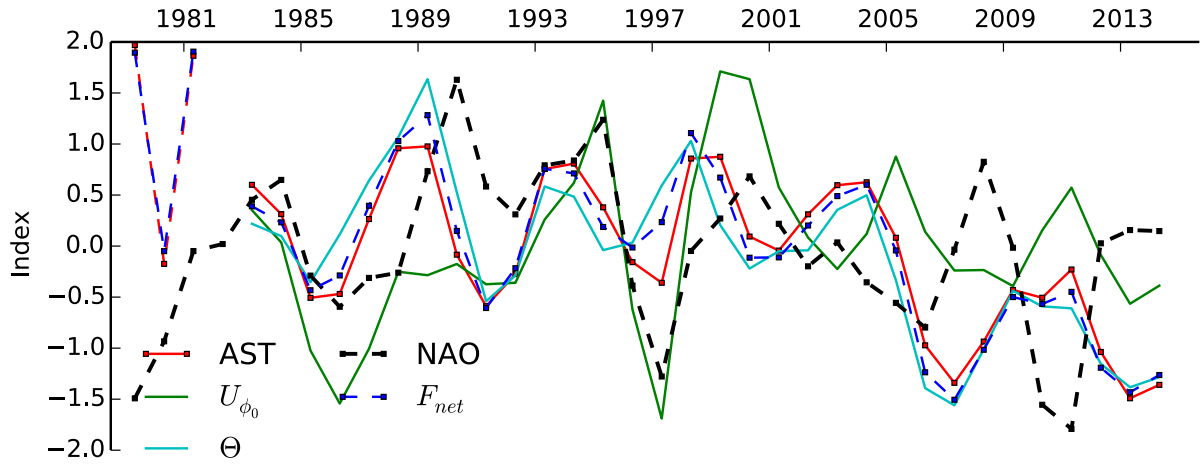

Figure 5.10: Three year running mean of normalised anomalies of yearly accumulated salt release (AST), NAO index, yearly means of along fjord wind component ($\bar{U}_{\phi_0}$), Freezing degree day ($\bar{\Theta}_{day}$), and net heat flux ($\bar{F}_{net}$).

Muckenhuber et al. (In progress) present monthly averaged fast ice cover for Hornsund from 2006-2010. The monthly means ranges from 10-33% of the total fjord area. When including fast ice in the polynya model the AST calculations will reduce similarly. The amount of fast ice cover, represented by the DFI-value in Table 4.1, relates well to the AST, whith years of higher fast ice cover being years of higher modelled AST. However, there may be a slightly different explanation for the two similar patterns. AST is governed by the frazil ice production that is dependent on a high heat flux over open water. This is governed by wind events opening the polynya in cold conditions. These easterly winds may then also prevent fast ice formation. In Hornsund, the fast ice occupies, at the most, about half the fjord, and mostly the inner, more protected parts of the fjord. When in first order neglecting oceanic heat input, the wind is the factor that prevents fast ice cover in the main parts of the Hornsund basin. The wind events that open the polynya, and moving the ice off shore are often accompanied by cold air temperatures, which together lead to high heat fluxes and thereby high salt production. In the more protected areas, the

ice export is not as efficient, but nevertheless these areas experience the same heat flux, and a fast ice cover is eventually established.

The fast ice concentration varies from year to year, and one would expect it to have an effect on the inter annual variations in brine release. From Figure 4.6 one can see how including the fast ice cover in order to shrink the polynya area reduces the year to year differences, which is a result of years of having the highest heat fluxes also being the years of higher fast ice coverage. The relative difference in AST when including the fast ice cover is highest for 2013. This is related to the frazil ice production, which had a pronounced increase in the period after the fast ice cover was established, which was rather late this year. This further supports a theory of fast ice cover being a good indicator for the amount of frazil ice produced.

When including a varying date for the onset of freezing, the year to year differences become somewhat more pronounced, when years such as 2009 and 2011 having both high ice production and an early start of the ice season. However, the onset of freezing is one of the big uncertainties since observations are uncertain. The use of drift ice observations in the fjord as an indicator for freezing conditions may be invalid as the ice could have been imported to the fjord from the CC, without giving direct evidence of necessary conditions for ice formation in the fjord. Nevertheless, drift ice observations in Hornsund can be an indicator of whether the water masses occupying the shelf is of Arctic or Atlantic type, as drift ice is likely to follow the CC around the southern tip of Svalbard (Wadhams, 1981). This is evident from the situation already discussed in 2013, where a switch in water mass characteristics at M13 was followed by an increase in drift ice and, eventually, fast ice formation in the fjord. In 2012, there was an increase in drift ice cover in the beginning of January (Figure 4.5), which could be related to colder water on the shelf (M12 Figure 5.8). Drift ice is then lower when the water temperature increases substantially in the beginning February, whereas fast ice starts forming at the same time as there is a period of colder water on the shelf in beginning of March.

Four years of observations of surface salinity measurements in fall and spring for the Hornsund main basin were used to make a rough estimate on the initial and final surface water salinity S_{01} and S_{02}, for the winter seasons 2010, 2012, 2013, 2014. Figure 4.6 shows that including the change this parameter in the polynya model does not induce a big difference in the total salt production. There is a slightly lower AST value for all four years that results from the estimates of S_{01} and S_{02} all being less then the values used for the other model runs ($S_{01} = 34.0$ and $S_{02} = 34.8$). On the basis of the discussion done in Section 5.2.2 an estimation of the increase in the surface layer salinity can be made on the basis of the salinity increase at M11 during the first part of the freezing season 2011. This gives a salinity increase from 33.5 to 34.5 psu, where the lowest salinity is found during the downwelling event on the Day 16. A salinity increase of 1 psu in 2011 corresponds roughly to the increase of 0.8 psu used in the polynya model. Moreover, according to Equation 3.10 a change in the average surface water salinity of say 2 psu would lead to an average change in the AST production of 126×10^6kg, based on the averaged AST production in Table 4.1. This would not have a notable influence on the inter annual AST pattern in Figure 4.6

Table 5.2: Spearman rank-order correlation coefficient (r) and corresponding p-value (p) between yearly mean on forcing parameters, and NAO index, on the time series presented in Figure 5.10. Correlation is made for two separate periods of the time series, as well as for the entire period.

	1983 - 2002		2002 - 2014		1983 - 2014	
	r	p	r	p	r	p
NAO - $\bar{U}_{\phi_0}$	0.68	0.001	-0.47	0.15	0.36	0.044
NAO - $\bar{F}_{net}$	0.17	0.47	-0.44	0.15	0.05	0.80
$\bar{\Theta}_{day}$ - $\bar{F}_{net}$	0.90	7×10^{-8}	0.98	9×10^{-9}	0.96	7×10^{-18}
$\bar{U}_{\phi_0}$ - $\bar{F}_{net}$	0.22	0.319	0.44	0.239	0.23	0.199
AST - $\bar{F}_{net}$	0.93	1×10^{-10}	0.99	8×10^{-7}	0.97	1×10^{-19}

To try and relate the AST results with the atmospheric circulation in the North Atlantic, the NAO (Jones et al., 1997) winter index is shown in Figure 5.10. The December-March averaged NAO is shown together with the index anomalies of AST, $\bar{F}_{net}$, $\bar{U}_{\phi_0}$, and $\bar{\Theta}_{day}$. The anomalies are made by subtracting the 35 year mean and scaling by the respective standard deviation. The corresponding correlation between the anomalies are presented in Table 5.2.

Studies have shown that the winter NAO index partly explains the variability of heat export to the Arctic through the WSC in the Fram Strait (Dickson et al., 2000; Schlichtholz and Goszczko, 2005). Saloranta and Haugan (2001) found a low but significant correlation between autumn AW temperature along the shelf break on the north-western corner of Spitsbergen for the period 1970-1994. Furthermore, Beszczynska-Møller et al. (2012) showed records of the AW layer in the WSC over the period 1997 - 2011. Compared to the AST estimate for Hornsund for the same period, they show a warming of the AW temperature in 2005 and 2006 which correspond to a reduction in the AST estimates in same period.

Skogseth et al. (2004) found a negative correlation between NAO index and yearly polynya area, resulting in higher production of Brine enriched Shelf Water in years of low NAO, induced by higher occurrence of northerly winds in Storfjorden. From Figure 5.10 the AST anomalies variations bear some of the same variation pattern as the NAO index, but from the correlation calculations in Table 5.2 no correlation is seen between the NAO index and F_{net}, which is the main driver for salt production in Hornsund. A significant correlation is however found between the NOA index and the alongfjord wind, in the period 1983-2002. This indicate that the NAO index has a different impact on the Hornsund fjord system then in Storfjorden, where the prerequisite of alongfjord wind to open the polynya is positively correlated to NAO, whereas in Storfjorden it was negatively correlated (Skogseth et al., 2004)

From Figure 5.10, a shift in the beginning of 21^{st} century is evident, where the NAO before this is following a similar pattern as $\bar{U}_{\phi_0}$, and after there seems to be more of a negative relationship between the two. This is also evident from the correlation coefficients

in Table 5.2, where there is a positive correlation before 2002 and a negative, but not significant, after 2002. The non significant correlation between NAO and the major drivers for polynya activity in Hornsund after 2002 might be a result of NAO having become less directly related to the local climate on Spitsbergen the last decade (Førland et al., 2011; Overland and Wang, 2010).

5.3 Water mass transformation

5.3.1 Model result before a permanent fast ice cover in Brepollen

In Storfjorden, the model was calibrated and validated against satellite observations of the pack ice movement on the windward side of the Polynya (Skogseth et al., 2004; Haarpaintner et al., 2001). Moreover, a comparison of modelled ice production over a 33 year period in Storfjorden, was compared with observations of Brine enriched Shelf Water (BSW) salinity from the deep basin (Skogseth et al., 2005) that had comparable year-to-year variability, indicating that the model was capable of reproducing the salt rejection leading to BSW production. Since the basin behind the sill in Brepollen is the only place were the water signatures are likely to be stored after a winter season in Hornsund, this is used in evaluating the salt production results from the model for Brepollen.

To understand the dynamic responds of the ice cover prior to fast ice coverage, we focus on the satellite images in Figure 4.7, and compare them to the interpreted ice concentration and model output in Figure 4.8. On March 2^{nd}, some of the fast ice had started forming on the northern side of Brepollen. All other areas of the fjord was in general was ice free. Even though temperatures were well below freezing (Figure 4.8), easterly winds prevented possible new ice formed from consolidating into a thin ice cover. The wind turned and brought warmer air masses in to the fjord by March 7^{th}. Before this, the minimum temperature for the considered period, on the 5^{th}, had led to thin ice formation that covered the whole fjord. This is well captured in the model, as the frazil collection and consolidation overruled the wind forces pushing ice out the fjord, and a nearly complete modelled thin ice cover is seen in Figure 4.8 for the same day. Due to decreasing heat flux from March 6^{th} to 7^{th} there was a decrease in modelled thin ice cover. When the wind turned on the 7^{th}, the model predicts a closing of the polynya, and a complete thin ice cover. This is not comparable to the observations of drift ice, were the drift ice concentration is reduced at the same time (Dark grey in Figure 4.8). A possible explanation for the reduction in observed drift ice on March 7^{th} is that in-fjord winds in this case compressed the ice cover towards the fjord head. And as little ice was available on the coast, the polynya remained open. The satellite image in Figure 4.7 from March 10^{th} shows more ice in the fjord. After the March 12^{th}, the wind was again easterly, reaching a maximum speed during the 13^{th}. The response to this can be observed in the satellite images from the 14^{th}, as the fjord was again ice free, and ice can be observed in the open ocean west of the shore. This is captured by the model, as the thin ice area reduces. The reduction of the thin ice area also increases open water area, and one can observe how the frazil ice

production increases as a response to a larger area for frazil ice growth. Towards the end of March, the ice cover behind the protecting Treskelodden was restricted from leaving the fjord, and a fast ice cover developed in Brepollen. This marks the end of the modelled period.

In Figure 5.11, polynya model results for Brepollen in 2011 are presented, together with water temperature time series from S11. As for the 2010 results discussed above, there is a reasonable agreement between model results and observed ice cover observations. A difference to the previous year is that the fast ice cover is coming earlier and the model run ends 7^{th} of January. The mooring was positioned on the sill separating Brepollen from the outer basin (See Figure 2.2 and Table 3.2), and shows how the temperature of the water column developed over the modelled period. The vertical lines in the plot marks periods with pulses of cold water measured at the mooring. This can be compared to periods of intense cooling at the surface, and it is plausible to relate this to convection of cooled surface water.

The data presented in Figure 5.11 gives evidence that the polynya model is capable of reproducing these events, as the convection events are accompanied, and possibly caused by high ice production. Furthermore, it gives trust in that the use of forcing data from Isbørnhavna is also valid in the sill area, about 17 km east of the weather station. In the beginning of the period, the strong cooling at the surface has not necessarily caused frazil ice formation, but rather convection of cooled water and upward mixing of warmer water in the intermediate layers. This is evident in the lack of observed thin ice during the two first convection events (November 1^{st} and 7^{th} 2010).

5.3.2 Year-to-year variability in Brepollen

The maximum salinity of the water behind the sill in Brepollen was shown in Figure 4.9. Since these measurements were taken in late July or the beginning of August, one would expect the salinity to have decreased after the end of the freezing period through mixing with over laying water masses. Nevertheless, since the measurements are made at the same time of the season, one would expect this desalinisation to be somewhat similar from year to year, and therefore give a representable picture of the year to year variability. Using maximum salinity of Brepollen as a measure for the efficiency of winter time brine water production requires that the initial salinity of the deep water in Brepollen is relatively low. This ensures that the convection of next year's winter water overcome the water laying there before the freezing season sets in. Nilsen et al. (2008) used the convection depth of Billefjorden as a measure of the ice production previous winter. Their TS-diagram for the deepest station in Billefjorden revealed how far down the brine enriched water had convected, as this would be the depth of the coldest water. In Brepollen, the assumption is that the mixing and diffusive processes through late summer and fall will reduce the salinity to such an extent that the salinity of the deepest point following spring will represent the latest produced Winter Water of BWW. These assumptions can be justified by looking at the temperature profiles in Figure 4.3, where the coldest water in the July profiles is always found at the bottom. Furthermore, the water temperature

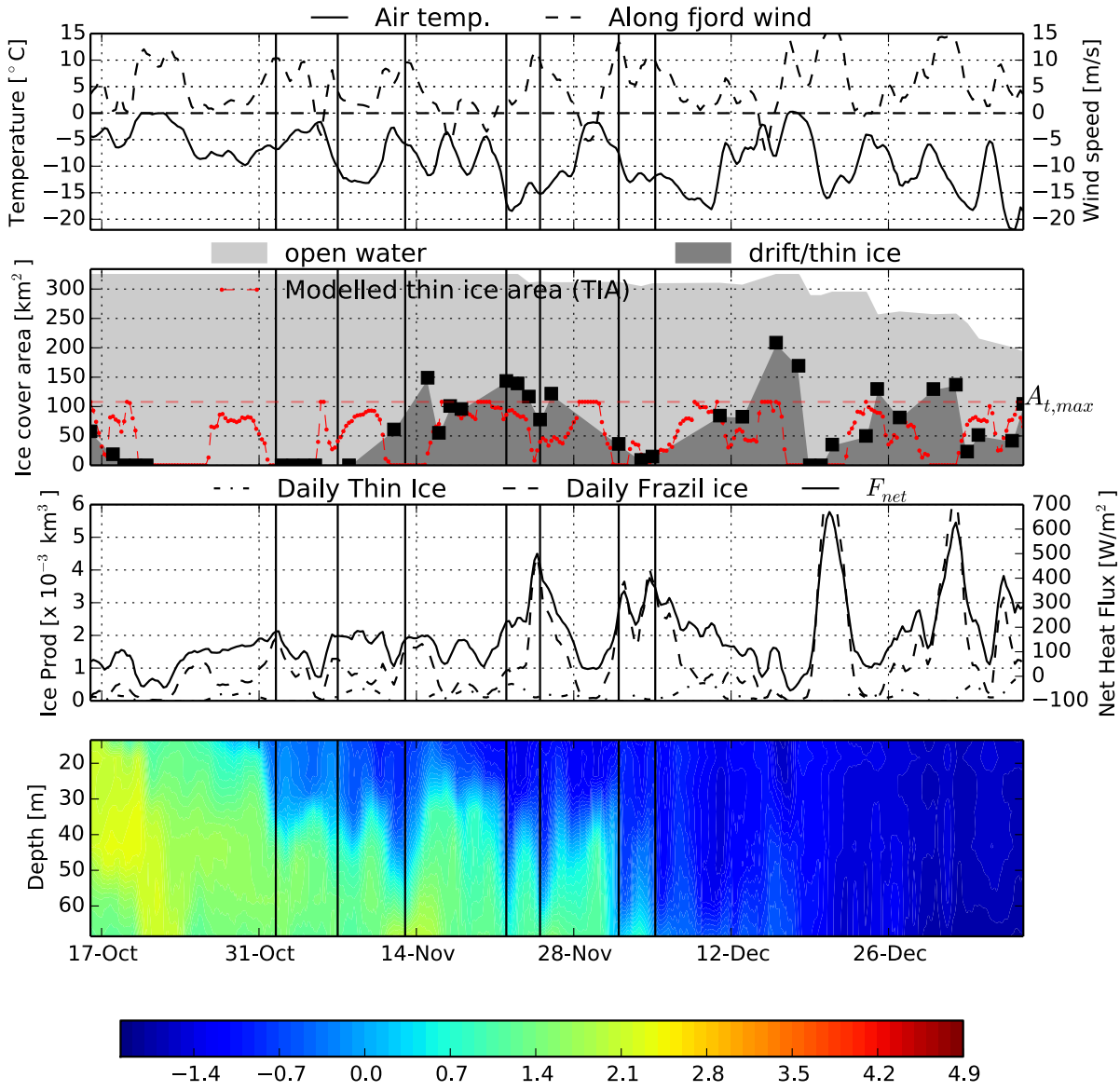

Figure 5.11: Model result, forcing parameters and hydrographic time series for the period before fast ice cover is reached in Brepollen the 2010/2011 season. The upper three panels as in Figure 4.8. The lower panel show temperature at S11, on the sill outside Brepollen.

is mostly above freezing level which indicates that mixing or diffusion has taken place since the water was formed. 2012 and 2014 can be noted as the years with the warmest bottom water. These were years with low ice production, and hence a lower production of BWW. They were also not included in the model runs for Brepollen as the fast ice cover never extended over Brepollen. Comparing the observed S_{BWW} in Brepollen with the salt production over the assumed freezing period (Figure 4.9) one notes that from 2006 to 2007 both observations and modelled result show decreasing values. Further, there is a consistent increase from 2011 and 2013. The years inbetween show little agreement between modelled results and observations. On the basis of our expectations of the S_{BWW} as a proxy for the salt production from previous winter, this may not be a very promising result. However, there are plausible explanations justifying the underestimation of AST in 2008 and over estimations in 2009 and 2010. For the winter seasons 2009 and 2010, Brepollen was partially covered with fast ice most of the modelled period. This would in reality indicate a lower salt production when compared to the modelled result where it is not corrected for a fast ice cover. The adjusted end date of the 2009 model period, denoted with green squares in Figure 4.9, reduces salt production this year. We then assume little frazil ice growth in Brepollen after January 19^{th}, when most of Brepollen was covered with fast ice. However, 2009 is still not the least effective year, as indicated by the low S_{BWW} value. Moreover the 2008 season showed a rather low modelled salt production compared to the S_{BWW} observations. Together with 2006, these were the only years where the fast ice cover had a very rapid growth, expanding from zero and crossed the 40% limit in a very short time. This make the freezing period especially efficient, because of the relatively big polynya area at the end of the modelled period.

The first observation of drift ice in the 2010/2011 season might not be representative for the onset of freezing, as no ice was observed between this and November 11^{th}. This is further supported by the rather warm water on the S11 mooring present until the beginning of November. By choosing a later start of the model period the this year, a lower salt production result (green squares in Figure 4.9), which makes the difference to 2013 more consistent with the S_{BWW} differences for those two years.

5.3.3 ROMS-simulations

To further investigate the Hornsund fjord system, ROMS simulations will be used. This will also guide some of the choices of the initial values and assumptions, such as surface layer and BWW salinity, onset of freezing, and horizontal homogeneity. The results presented here are from the first successful runs of the model, and have not been thoroughly validated against observation data, thus, we have to be careful when using it in the discussion. We will nevertheless do a discussion on the reliability of the data before we compare it to our results. When referring to the model, in this section, it is the ROMS-simulations that are addressed, whereas the term "polynya model" will be used when talking about the analytical 1-D polynya model.

The time series in Figure 4.11 and 4.12 show the strong seasonality in the water column, were a fresh brackish layer is dominating the surface layer in summer. The freshest water

is found in the inner parts of the fjord (HS05). This consistent with the July observations in Figure 4.13 where the surface layer in Brepollen is fresher and becoming slightly thicker with a weaker salinity gradient in the Hornsund basin. This is typical for estuarine circulation (Gade, 1986), where a surface flow is set up by freshwater input in the inner parts of the fjord and by entraining the underlying water masses down stream becomes thicker towards the fjord mouth. When comparing HS01 and HS02 a cross fjord variability is is also evident, where HS01 on the northern side in general has a fresher surface layer than HS02 on the southern side. The cross fjord variability might be a result of higher run-off on the northern side of the fjord, as all Hornsund glaciers are located east of the position of HS02 (Swerpel, 1985). In addition, rotational effects are expected to play a role in the circulation pattern, especially in periods with a well defined surface layer (Cottier et al., 2010; Svendsen, 1995; Svendsen et al., 2002), forcing the out flowing surface water towards the norther side of the basin. Svendsen et al. (2002) found that the surface water current in Kongsfjorden follows the norther side of the basin, under out-fjord winds this current was intensified as wind induced ekman transport of the surface layer will contribute to the pile-up of the surface water along the norther shore. This is also believed to enhance the cross fjord variability in Hornsund, as prevailing wind throughout the whole year (more than 80% from NE, E SE (Błaszczyk et al., 2013)) is in the out fjord direction.

In winter the general situation is that the stations in the main basin (HS01, HS02, and HS03) shows fluctuating temperatures close to 0°C. The lower layer at the sill (HS04) shows periods of water on freezing point whereas the entire water column in Brepollen is at freezing point at several occasions.

It is interesting to compare the time series to the above mentioned incident in early 2006. Cottier et al. (2007) observed an increase in water temperature inside Kongsfjorden at 210 m depth starting late December 2005, as a response to southerly winds on the coast, together with high air temperatures. The southerly wind pattern lasted until the end of January when a sudden shift to strong northerly winds was observed. Northerly winds lasted until the end of February. The interesting findings in their study were that the water temperature inside Kongsfjorden kept increasing until the northerly winds ceased at the end of February, after which water temperature dropped and reached freezing point by the end of March. The ROMS simulations, for Hornsund, for the given period are shown in Figure E.1, and one can note that the temperature at HS02 and HS03 is increasing from mid December 2005 until late February. At this time, however, it starts a gradual decrease until the beginning of April, interrupted by jumps in the temperature in the beginning and late February as well as a notable increase for a period in the middle of March. The temperature evolution in the ROMS-simulations are then in contrast to the observed water temperature in Kongsfjorden. One can nevertheless relate the period of increased temperature from late December and the mentioned jumps to the wind stress measurements in Cottier et al. (2007). These events of increased water temperature in the simulations tend to be in good comparison to southerly wind stress observed in Konsfjorden (See Figure 3. in Cottier et al. (2007)). This however needs deeper analyses of the forcing mechanisms and responses for the mentioned incident. A further thing noted is that HS04, close to the sill, experiences the same warming, but a bit later (beginning of January), whereas HS05

inside Brepollen seems to be more or less undisturbed of what is going on in the outer basin.

The bottom layer of HS03 and HS05 differ from the three other stations where the coupling to the upper layers at HS03 and HS05 is different. Here the temperature stays rather cold through out summer. The water temperature first sees a notable increase when the upper layers start cooling later in the season, and reaches its maximum when the water column is homogenising in late summer. At HS05 the increase in the lower layer temperature corresponds well with the time of which the brackish layer is vanishing, which is around 1^{st} of October every year. It is shown that strong stratification might confine the wind stress to a shallow surface layer (Svendsen and Thompson, 1978; Myksvoll et al., 2014). The wind effect on the surface circulation is thereby, in summer, possibly confined to the upper few meters of the water column. The ROMS simulations and observations of the water column in July show a rather shallow brackish layer in Brepollen (Figure 4.13). A weakening of the stratification in fall, due to a decrease in freshwater supply to the basin, can on the other hand create a deepening of the layer that will be affected by the wind stress (Gillibrand et al., 1995). Deep water renewal in a Scottish fjord was by Gillibrand et al. (1995) found to relate to periods of out fjord winds, and low run-off causing weak stratification. We might relate this to our ROMS-simulations and conclude that a possible explanation for the warming of the bottom layer in late fall is an effect of weaker stratification, allowing for a deeper surface layer current during katabatic winds in fall. If rotation is not important, something that is a reasonable assumption for Brepollen, this thicker surface layer current might in turn induce a compensating in flow in the lower layer over the sill. This inflow can then consist of warmer water masses from outside the sill, and if dense enough renew the deeper layer of the Brepollen basin in fall. In November 15^{th} 2010 there was observed an increase in the water temperature at the lower layers at S11 (Figure 5.11). This is an incident of rather strong out fjord winds ($\sim$10m/s), possibly inducing a surface current seaward transporting cold surface water from Brepollen over the sill. The warming of the lower layer might be a resulting inflow of warmer water from the outer basin, that if dense enough is able to penetrate the lower layers of Brepollen. To further investigate these assumptions, an analysis of the current structure over the sill and density differences between the basins should be performed.

During winter the model produces an increase in salinity of the lower layer of HS03 and HS05. As soon as the whole water column is at freezing point, and the minimum salinity is achieved, the bottom water salinity starts increasing, and this is likely to be a result of brine rejection through freezing on the surface. The salinity however continuous to increase at depth after freezing season, over a period where the temperature stays on freezing point. This is physically not realistic, as there is no water mass on freezing point that is likely to enter the basin and cause this to salinity increase. Both HS04 and HS03 show higher temperatures and lower salinity during summer, and thereby it is not expected that the bottom water at HS05 is water advected from Hornsund main basin. HS05 might however not be representative for the entire Brepollen, and a more saline water mass at freezing point may be present in the basin, causing the salinity increase through summer.

5.3.4 Sea ice in the ROMS-simulations

The modelled ice concentration and corresponding ice thickness are shown in Figures 5.12 and 5.13. Figure 5.12 shows the fraction of ice in each grid cell, and the corresponding ice thickness is presented in Figure 5.13. The period shown corresponds to the period in which a fast ice cover is establishing in Brepollen, and corresponding satellite images are shown in Figure 4.7. The simulations show that little ice formed before the beginning of March in 2010. This is in contrast to the observed ice situation, where a fast ice cover was established in beginning of January and drift ice occasionally occurred in the fjord from mid December 2009 (Figure B.5). The first patches of ice in the simulations are produced in the north-western part of Brepollen. In March the ice cover is seeing a notable increase, and the thickest ice cover is formed in the northern parts of Brepollen and Burgerbukta, which is comparable to the satellite images (Figure 4.7) where fast ice was first formed in these areas. March the 14^{th} and 23^{rd} are examples of polynyas, where the simulations show a decrease in ice concentration in the middle part of Brepollen. From the satellite images it is clear that out fjord winds emptied the the fjord of drift ice, but at the 23^{rd} the fast ice in Brepollen was strong enough to withstand the wind, and Brepollen remained covered in fast ice. From the 23^{rd} the model is not capable of reproducing the fast ice cover observed in Brepollen. The fast ice cover in the model must be governed by onshore winds, as the model has no way of attaching ice to land (Smedsrud et al., 2006).

Figure 5.14 and 5.15 show the water column in the ROMS simulations compared with the frazil ice production and F_{net} from the polynya model for the winter season 2010. From the figure it is evident that events of high frazil ice production in the polynya model corresponds to periods of convection in the ROMS simulations. In the beginning January the heat loss at the surface is not causing ice production. In late February the salinity increase at depth in water column at both HS03 and HS05 indicates brine rejection through freezing on the surface. The late onset of freezing in the ROMS simulations might be related to some of the above mentioned characteristics in the water column. Due to the low stratification of the simulated water column in fall for the whole fjord system, cooling leads to convection of the surface water through the whole water column. It is reasonable to believe that a more stratified water column in the beginning of winter allowed for the earlier development of an ice layer seen from observations, which is not captured by the ROMS simulations. For the winter season of 2011, we have earlier argued that some stratification is retained after onset of freezing, on the basis of observations from the mooring M11. With a stratified fjord a thermal convection in fall can be confined to a shallower surface layer, and freezing on the surface might start earlier. We do not know if the simulations of warm water occurrence in fall in Brepollen is overestimated. It might as well be a phenomenon dependent on density differences between the two basins (Gade and Edwards, 1980), and thereby not happen every year. If this is the case, that might explain the earlier observed ice formation in Brepollen in 2010 compared to the ROMS simulations.

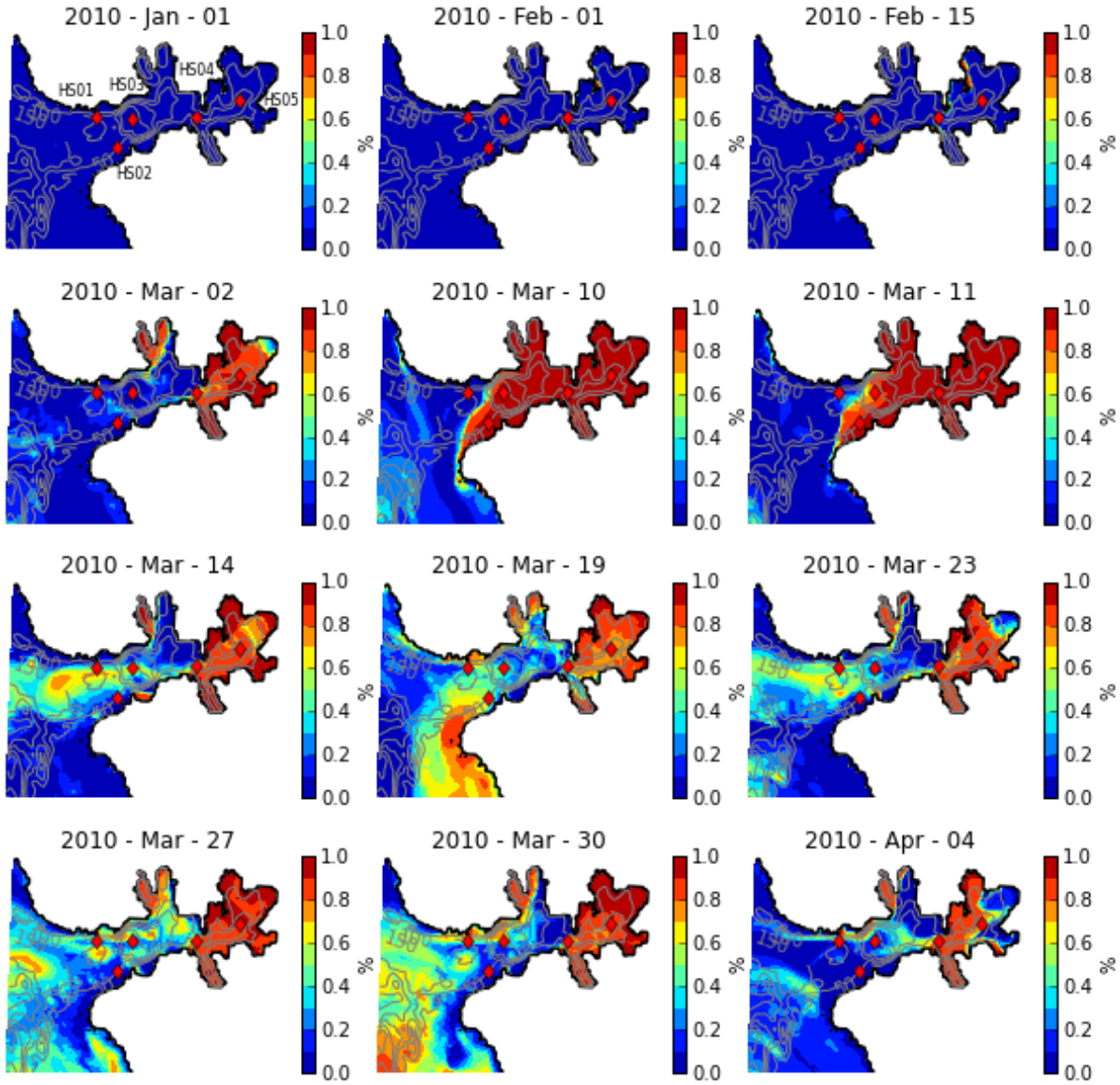

Figure 5.12: ROMS ice concentration March 2010, corresponding to the time when a fast ice cover is established in Brepollen. HS01-HS05 denotes the stations where extracted time series of temperature and salinity are presented. Satellite pictures for the same period are shown in Figure 4.7.

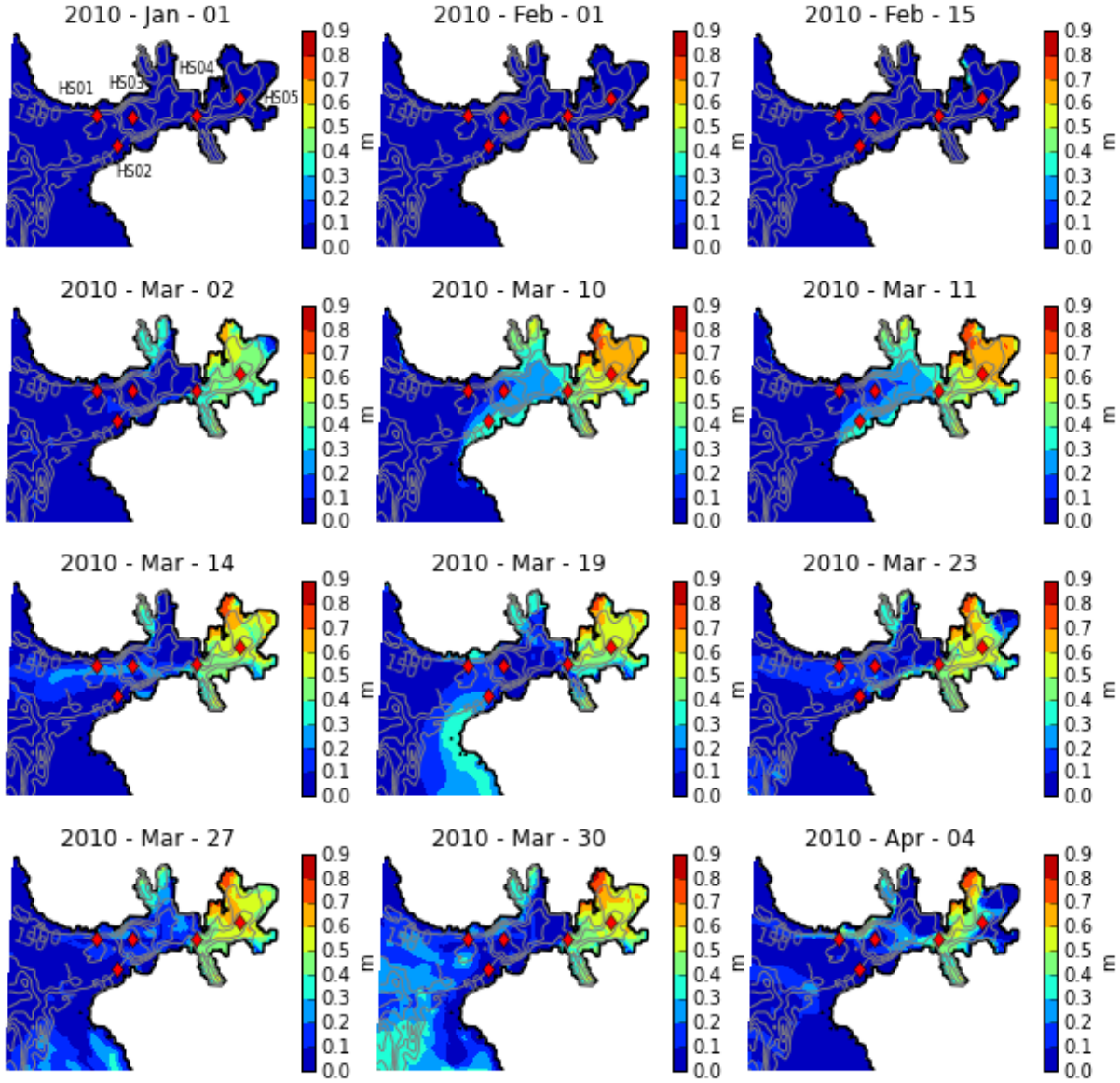

Figure 5.13: ROMS ice thickness March 2010, corresponding to the time when a fast ice cover is established in Brepollen. HS01- HS05 denotes the stations where extracted time series of temperature and salinity are presented. Satellite pictures for the same period are shown in Figure 4.7.

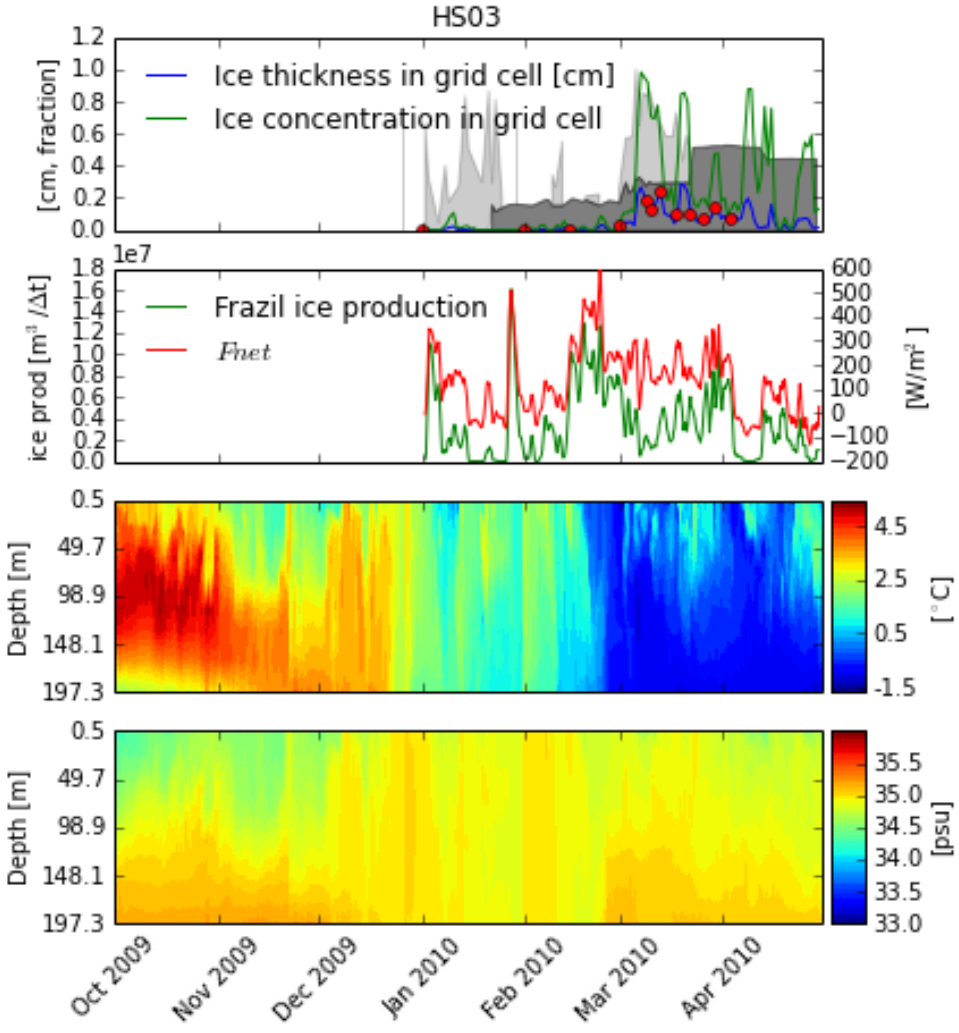

Figure 5.14: ROMS temperature and salinity evolution from station HS03 over the winter season 2010. Upper panel shows ice thickness and concentration in same grid cell HS03. The shadings are observed ice cover from Muckenhuber et al. (In progress). Red dots marks the times, corresponding to the ice field snap shots in Figure 5.13, in increasing order. Second panel shows the net heat flux and frazil ice production from the polynya model

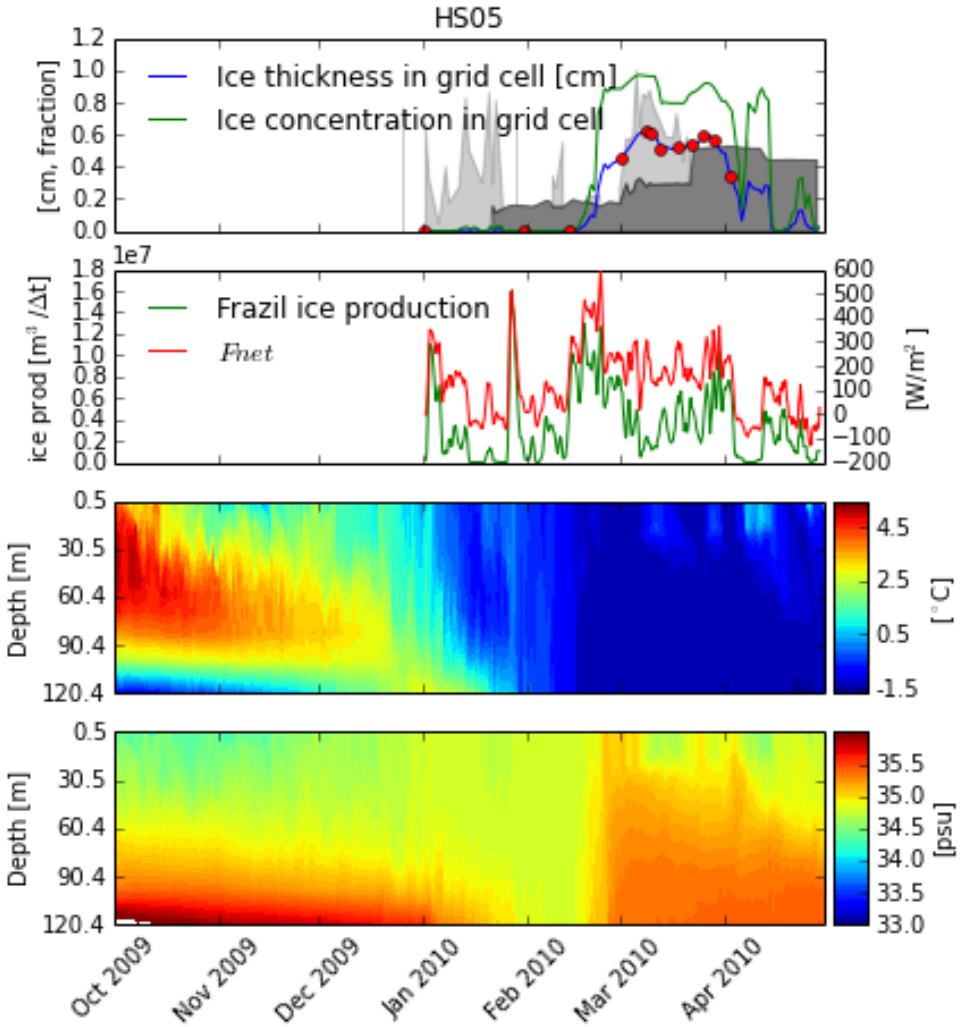

Figure 5.15: Same as Figure 5.14, but for HS05

5.3.5 Water renewal

Warming of Brepollen deep water

In July 2014, observation show a water column in Brepollen with a signature of Atlantic water (Figure 4.3). The high salinity, and the absence of sea ice the previous winter, indicate that the basin might have been occupied by Atlantic water during the previous year. In addition to the continuous mixing taking place below sill level in Brepollen causing the temperature increase and desalination through summer, Figure 4.3 show evidence of a warmer water mass present in September 2013. This is the only year with observations this late in the season in Brepollen, and we can not exclude the possibility of warmer water of Atlantic origin to enter Brepollen late in the season for other year as well. The ROMS simulations also suggest an enhanced warming of the bottom layer in fall. The presence of warmer water in Brepollen may be important for the basal melting and calving of the tide water glaciers in the fjord (Błaszczyk et al., 2013; OLeary and Christoffersen, 2013). Błaszczyk et al. (2013) found the calving rate and hence the fastest retreat of the Hornsund glaciers to take place between August and November. Their study further showed a connection between air and sea temperature to the calving rate of the sea terminating glaciers. An increase in the retreat rate was found during the first decade of the 21^{st} century, where 2012 was a year with intense calving which they explain with anomalously high air and water temperatures. This underlines the importance of understanding the circulation and water mass transformation in Brepollen late in the season. If the ROMS-simulations are reflecting the actual situation, with a significant increase in water temperatures before onset of freezing, this can be important for the dynamics of the glaciers enclosing the basin.

5.3.6 Dense water production in Brepollen and Hornsund

The total volume of water in Brepollen is 9.69×10^9 m^3 (See Hypsometric curve in Appendix D). Without water exchange with the outer basin, the salt released in Brepollen before fast ice is established can be calculated given the salt released in Figure 4.9. This gives an increase in the salinity of the water column for the given years between 0.81 ppt (2008) and 1.41 ppt (2009). We have little observations to compare these numbers with, but we can note that the ROMS- simulations (HS05) for the the period before fast ice is established in Brepollen has a salinity increase in the bottom layer between 0.2 ppt (2006) and 0.68 ppt (2009). Furthermore, the salinity increase at intermediate depth at M11 in the mouth of Hornsund, showed an increase of 0.6 psu over the period between Day 353 and 39 in the winter season 2011. And we have above argued that the salinity increase in the surface layer was about 1 psu. Over the given period the total salt release from the polynya model with fast ice was 1.44×10^{10} kg. Assuming that this salt was evenly distributed over the area not covered with fast ice (~ 200km^2), $\rho = 1000$ kg/m^3, and mixed over a surface layer of 50 m thickness, this would result in a salinity increase in the water column of $\sim$1.44 ppt. These rather rough calculations indicate that the polynya model produces a realistic estimates on the salt production. If the hydrographic situation is known the polynya model is an efficient tool for estimating production of dense water.

Chapter 6

Summary and Conclusion

This section summarizes our conclusions from the Hornsund fjord system study based on the two models, and observations of the atmosphere, ocean and sea ice. Overall the meteorological forcing that governs sea ice production in the fjord has been identified, and hydrographic observations confirm increased salinities for some years with large sea ice production. A shift in general conditions for the fjord seems to have occurred in recent years.

With use of a simple 1-D analytical polynya model, we have estimated the yearly accumulated salt release from sea ice production in Hornsund over the period 1978 to 2014. For the total fjord system this value shows large year to year variations, and ranges from 26 Mt (Megaton) in 2012 to 94 Mt in 1979. The yearly mean heat exchange between ocean and atmosphere shows similarly large year to year variation and ranges between 38 W/m^2 (2012) to 258 W/m^2 (1979, 1981). For the period between 2006 and 2014 we have further shown the importance of including the fast ice cover in these calculations, as years of high fast ice coverage corresponds to years with high salt release. Including the fast ice cover then reduces the relative differences in salt production between the years.

Limitations to the polynya model are the uncertainties related to onset of freezing and the unknown quantity of warmer water in the fjord. Warmer water masses that either are being mixed up during a polynya event, and thereby turning it into a sensible heat polynya which in turn makes the model over estimate the ice production, or warmer water circulating in the (outer) parts of the fjord leading to a decreased area of where frazil ice can be produced.

The salt release is very well correlated with the total net heat exchange, F_{net}, through a freezing season (r = 0.93 on average). Since 25% of the thin ice area is assumed to be open water there may also be a considerable frazil ice growth when the polynya is closed. We have further shown that there is a strong connection between F_{net} and easterly winds. The main basin of Hornsund is for the most time free of fast ice, which is a result of polynya activity. The years 1979, 1986, 1988, 1993, 2003 show the greatest correlation between wind and daily salt release. These are rather cold years, which give the wind an importance in terms of transporting out ice in order to increase the polynya area. Nevertheless, the short length of Hornsund makes the year to year differences more dependent on the variation

in heat flux, rather then differences in along fjord wind forcing. The latter give rise to a different year to year variability for salt production in Hornsund compared to similar studies in Isfjorden and Storfjorden (Nilsen et al., 2008; Skogseth et al., 2004). In a larger fjord, the frazil ice production will be more sensitive to the wind forcing, as it is the dominating factor defining the polynya area. In Hornsund, the polynya width is found to often stretch over the entire fjord length, and thereby variations in the frazil ice production will be strongly related to the variations in F_{net}.

In some years Hornsund becomes more of a sensible heat polynya than a latent one. This has occurred in recent years, 2012, first half of 2013 and 2014 are examples. These are periods where the polynya models also fails. Nevertheless, the connection between warmer water, warmer weather and westerly winds, makes the model produce less ice under these conditions, and the year to year variations are somewhat realistic. An exception is 2014 where most of the heat loss went into cooling of AW and little ice production took place.

It would be desirable to connect the polynya activity in Hornsund to the formation of dense water, which could give a contribution to the Arctic intermediate and deep water (Martin and Cavalieri, 1989), as well as its influence on the local water circulation in Hornsund. As was shown by Nilsen et al. (2008), dense water formation is likely to have played a role in the observed year to year differences in the circulation pattern in Isfjorden. Under given assumptions and simplifications we have argued that the polynya model gives a realistic estimate of the salt released to the underlying water column. To further use this to estimate the dense water produced, better information of the structure of the water column throughout winter is needed.

The Regional Ocean Model System (ROMS) simulations for the years 2005 - 2010 give valuable information about a fjord system that undergoes rapid changes that is hard to map with observations. The results presented in this study has shown evidence for the ROMS-model being capable of modelling an ice cover that is comparable to satellite observations. Furthermore, there is a consistency between salt rejection in the polynya model and bottom layer salinity increase in the ROMS-results. In fall 2013 and 2014, Atlantic type water was observed in Brepollen. The ROMS-simulation further indicate possibilities of warmer water in the deep layer of Brepollen before the winter season. This is of importance to the heat balance toward the many sea terminating glaciers in Brepollen.

Throughout this study observations and model simulations have given insight into the complexity governing the water circulation in a fjord on the west coast of Svalbard. We have touched upon aspects already studied in other fjord system (Nilsen et al., 2008; Cottier et al., 2007) that deals with the interaction between fjord and shelf. The use of a simple polynya model with only atmospheric input parameters is a cheap and efficient way to estimate salt production from sea ice. We aimed to use this information to quantify the amount of Brine enriched Winter Water produced throughout a winter season which could be compared to other studies (Nilsen et al., 2008; Skogseth et al., 2004; Schauer, 1995). Without sufficient information about the water column throughout the winter, this question is not fully answered. Nevertheless, we argue that the year to year variability is resolved.

Chapter 7

Future Perspective

The year to year variability and its strong correlation with F_{net} would possibly have changed if salt production on the shelf had included the , as the polynya opening often exceeds the fjord length. This could give a better estimate of the total salt production, and hence BWW production over the entire system. Nevertheless, this would rise the question whether the assumptions for the model are fulfilled on the shelf as well as in Hornsund. The open connection to the shelf makes it plausible to believe that periods of favourable conditions for ice growth in Hornsund would coincide with surface water on freezing point also on the shelf. This is also supported by the comparison between the moorings in the fjord mouth (M11, M12, and M13), where the ice concentration in the fjord has been shown to relay on the water properties in the mouth area.

The comparison with the deep water properties in Brepollen can be improved by doing a better analyses of satellite images, and get a fast ice cover dependency on the total polynya area. The possibility of warm water to penetrate into Brepollen is of importance for the dynamics of the sea terminating glacier in the basin (Błaszczyk et al., 2013), as well as the start of sea ice formation in fall. A further analyses of the current structure over the sill could provide deeper insight and understanding of the circulation here in fall.

Appendices

Appendix A

List of definitions and abbreviations

Sea ice[a]	Any form of ice found at sea which has originated from freezing of sea water.
Fast ice[a]	Sea ice which forms and remains fast along the coast, where it is attached to shore.
Drift ice[a]	Observed ice of any type drifting in the ocean, not attached to land.
Brach ice[a]	Accumulation of floating ice that are the wreckage of other forms of ice.
Frazil ice[a]	Fine spicules of ice suspended in water.
Grease ice[a]	A later stage of freezing of frazil ice when the crystals coagulated to form a soupy layer on the surface.
AW	Atlantic Water (S > 34.9 psu, T > 3°C)[b]
TAW	Transformed Atlantic Water (T > 1°C, S > 34.7 psu)[b]
ArW	Arctic Water (-1.5 < T < 1.0°C, 34.30 < S < 34.80 psu)[b]
LW	Local Water (T < 1°C)[b]
WCW	Winter Cooled Water (T < -1°C, S > 34.4 psu)[b]
BWW	Brine enriched Winter Water. Cold water mass produced through mixing of brine with
MERIS[c]	Medium Resolution Imaging Spectrometer on ENVISAT
MODIS[c]	Moderate Resolution Imaging Spectroradiometer on Terra and Aqua
ASAR[c]	Advanced Synthetic Aperture Radar on ENVISAT
Thin ice	Newly grown thin ice, or consolidated grease ice. local water masses.
TIA	Thin ice are modelled by the polynya model.
AST	Accumulated salt release from brine rejection through freezing of sea water, calculated with the polynya model.
DST	Dayily salt release from brine rejection through freezing of sea water, calculated with the polynya model.
DFI[c]	Days of fast ice coverage ($DFI = \Sigma_{days} \frac{\text{fast ice area}}{\text{total area}}$)
f	The Coriolis parameter

[a] Ice nomenclature is based on international standards (WMO, 1970)
[b] Summer water mass definitions from Svendsen et al. (2002)
[c] From Muckenhuber et al. (In progress)

Appendix B

Model output for all years with fast ice cover time series.

Results from polynya model in the period 2006 -2014, when the polynya model is run including fast ice cover in the fjord.

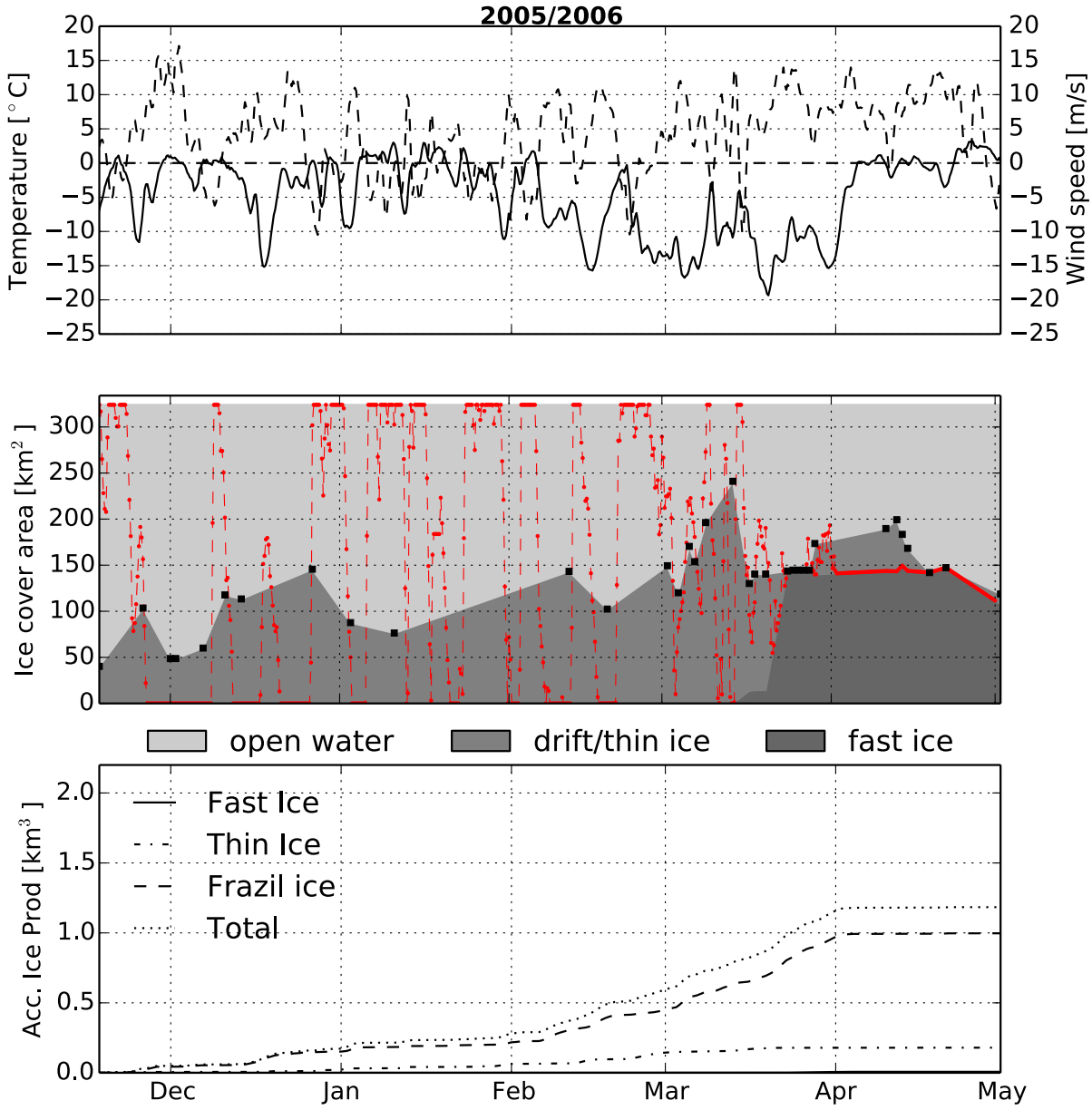

Figure B.1: Polynya Model output for winter season 2006 for. Upper panel show one day running mean on along fjord wind (Positive out fjord) and air temperature. Middle panel shows observed fast ice, drift ice and open water area, together with the modelled TIA (red dashed line). The modelled accumulated ice production in the different ice classes are shown in the lower panel. The resolution of the observed ice cover is indicated with black squares.

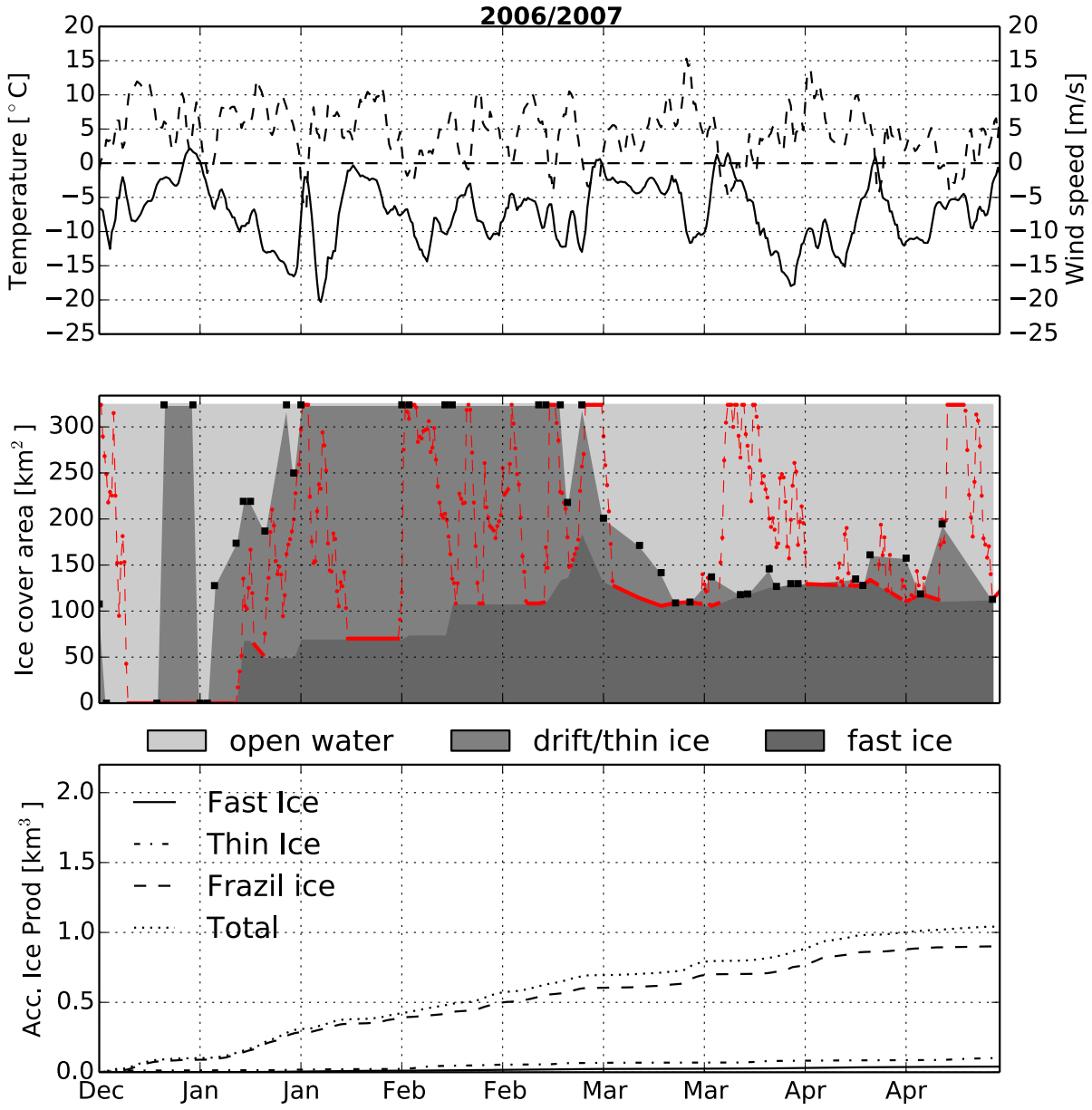

Figure B.2: Model output winters 2007. See caption of B.1 for further explanation

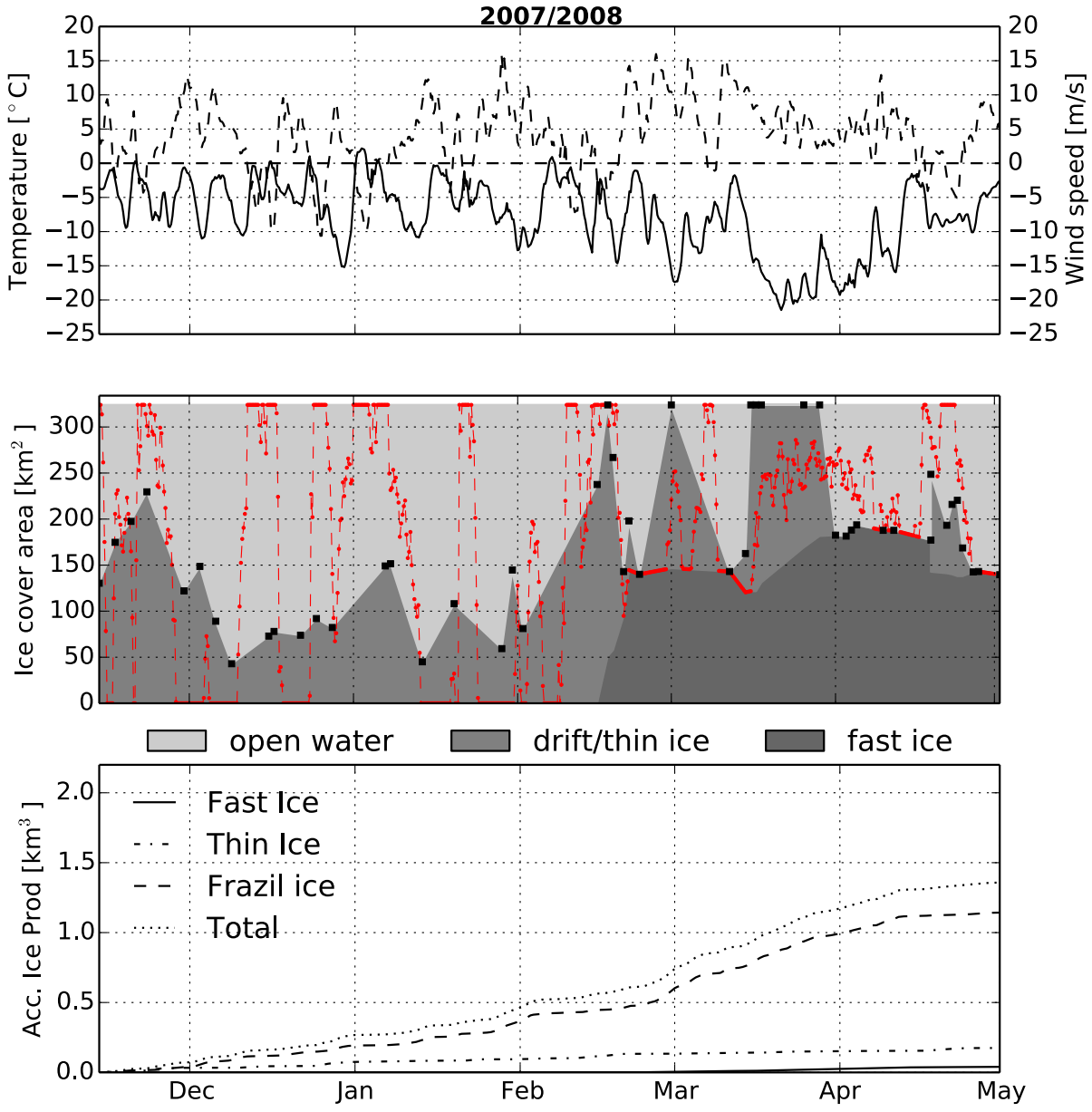

Figure B.3: Model output winters 2008. See caption of B.1 for further explanation

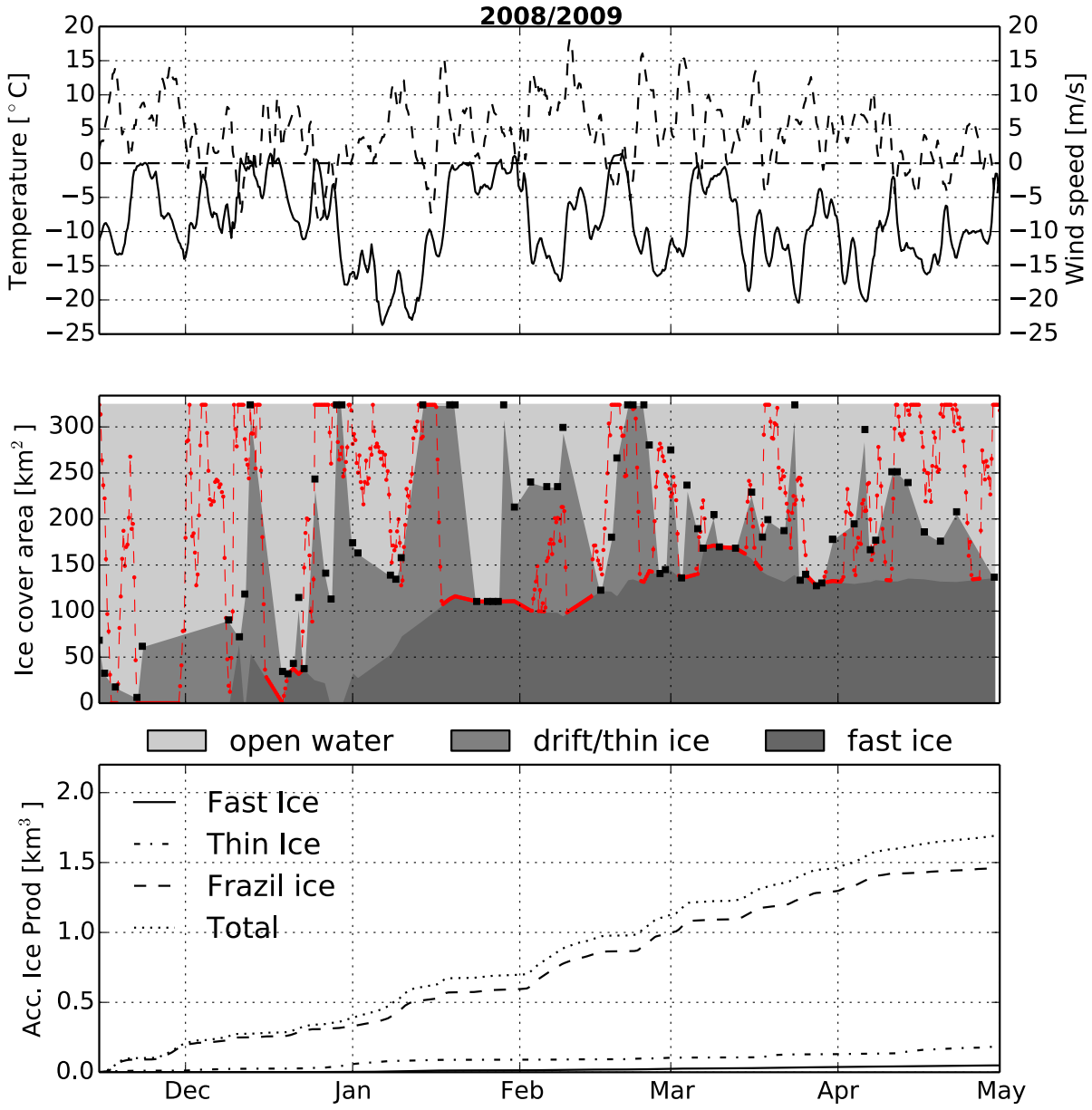

Figure B.4: Model output winters 2009. See caption of B.1 for further explanation

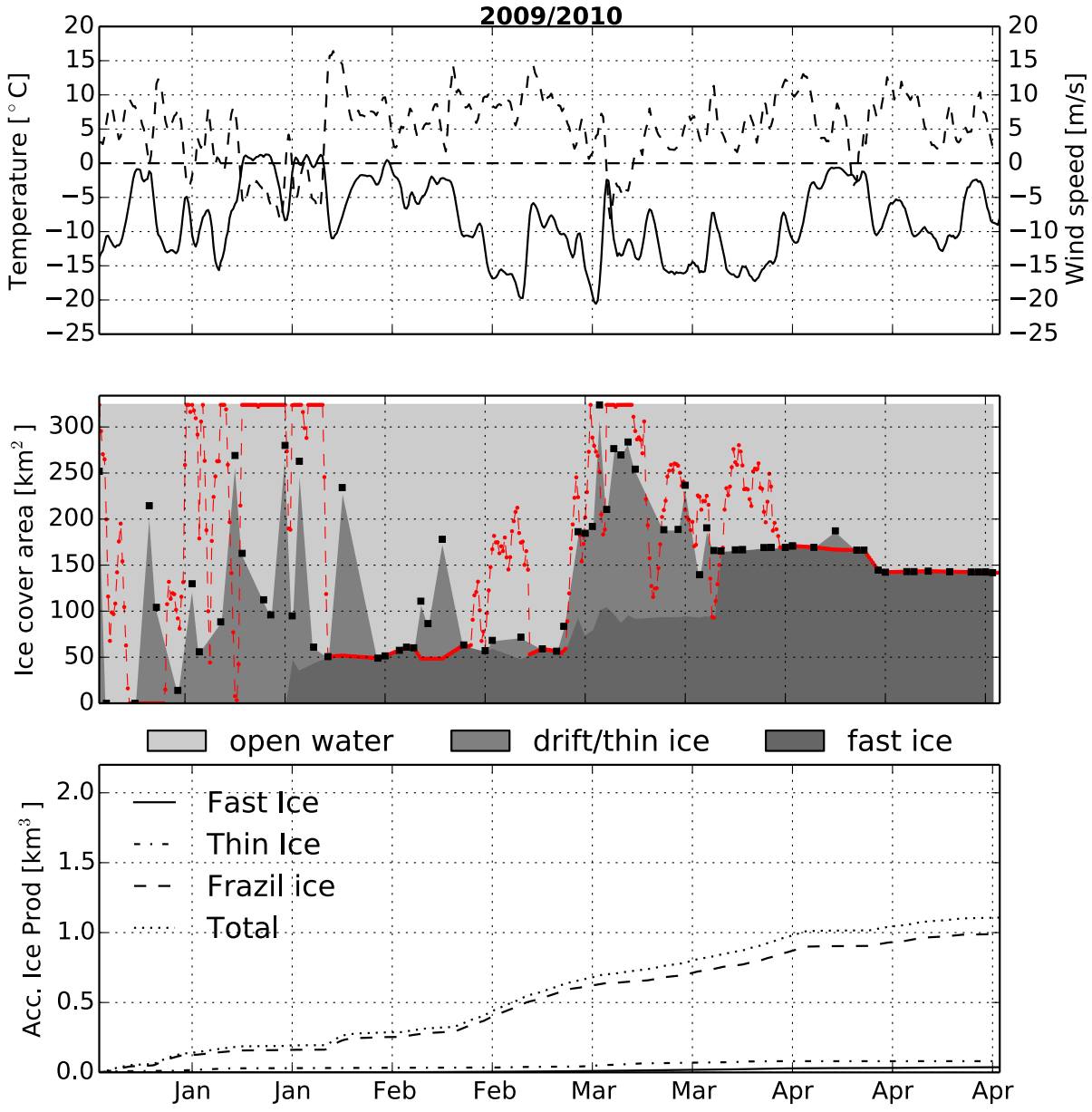

Figure B.5: Model output winters 2010. See caption of B.1 for further explanation

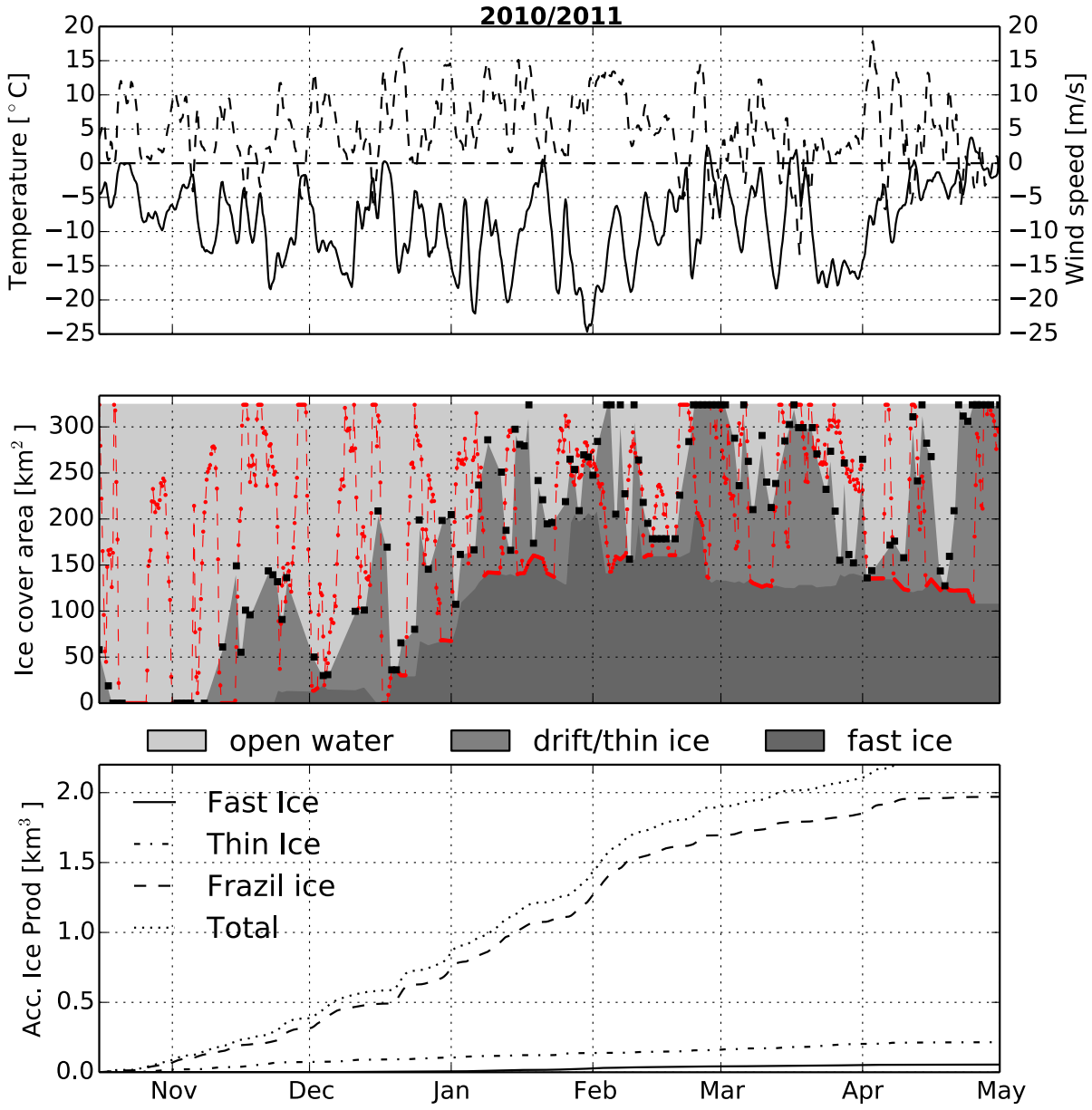

Figure B.6: Model output winters 2011. See caption of B.1 for further explanation

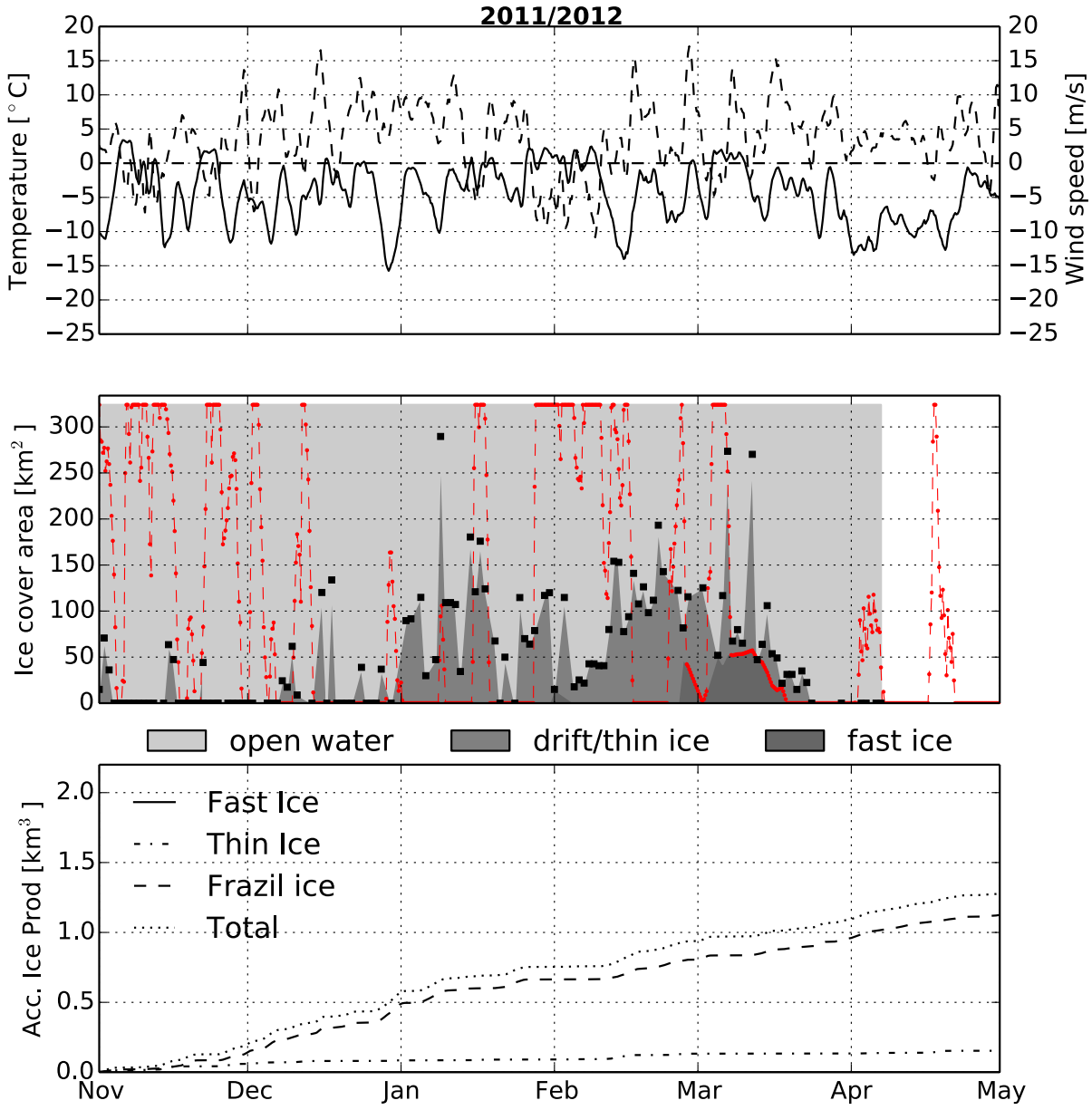

Figure B.7: Model output winters 2012. See caption of B.1 for further explanation

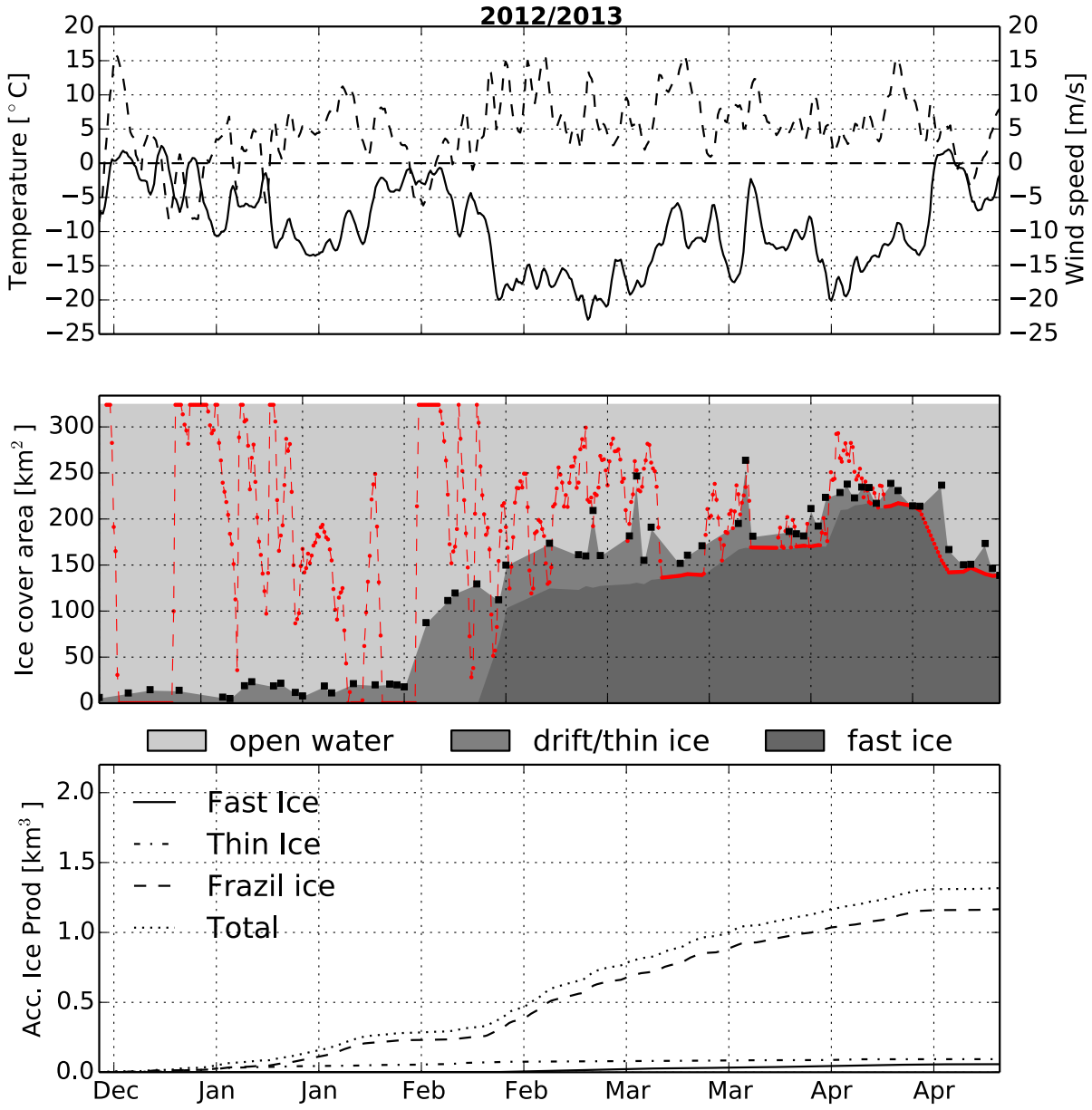

Figure B.8: Model output winters 2013. See caption of B.1 for further explanation

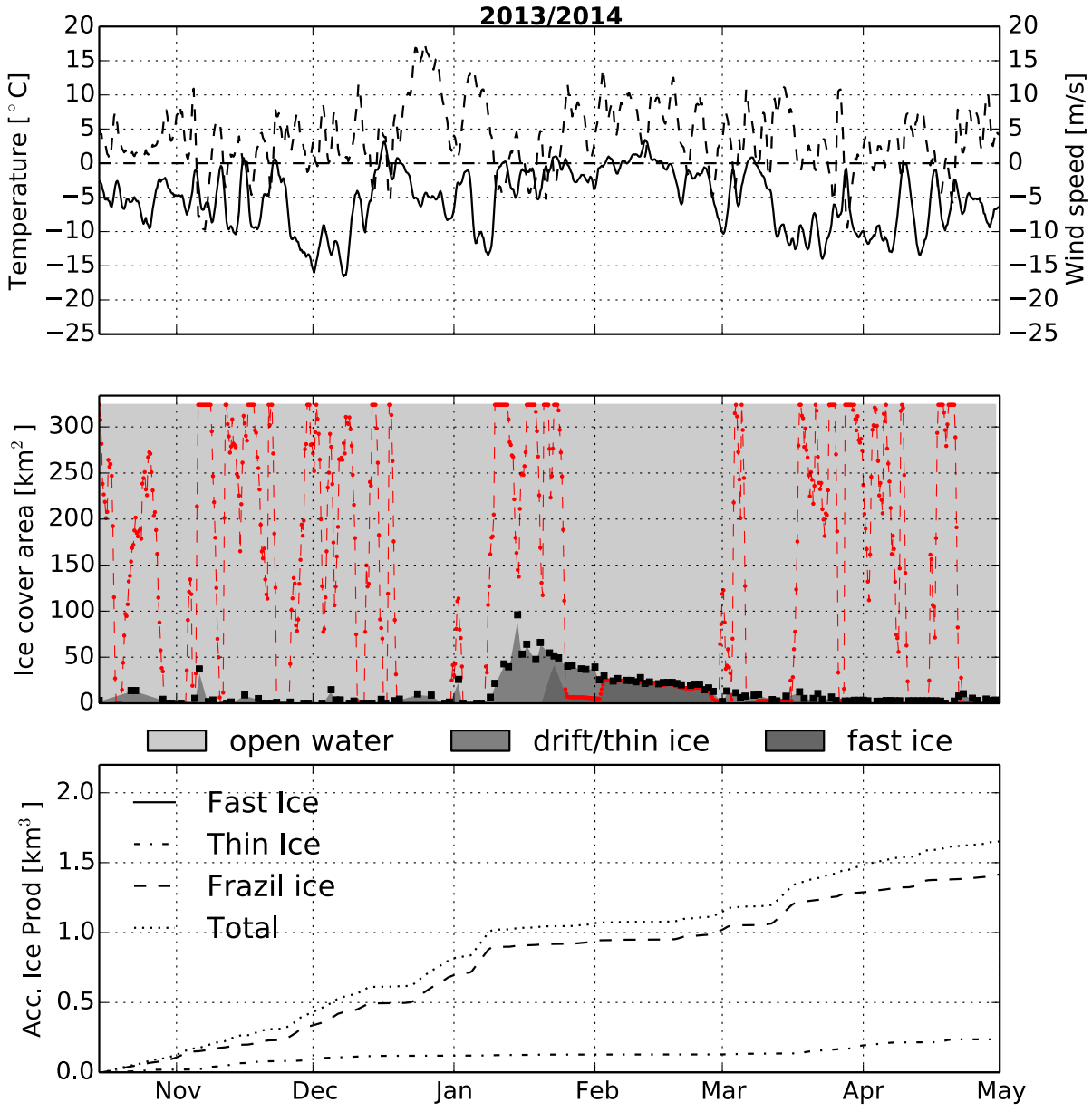

Figure B.9: Model output winters 2014. See caption of B.1 for further explanation

Appendix C

Determine onset of freezing

Ice observation time series are shown in Figure C.1 and C.2 from , data from Muckenhuber et al. (In progress). Blue lines denotes time of which we assume onset of freezing for the model, first drift ice observation. End of modelled period for Brepollen is when 40% fast ice is reached.

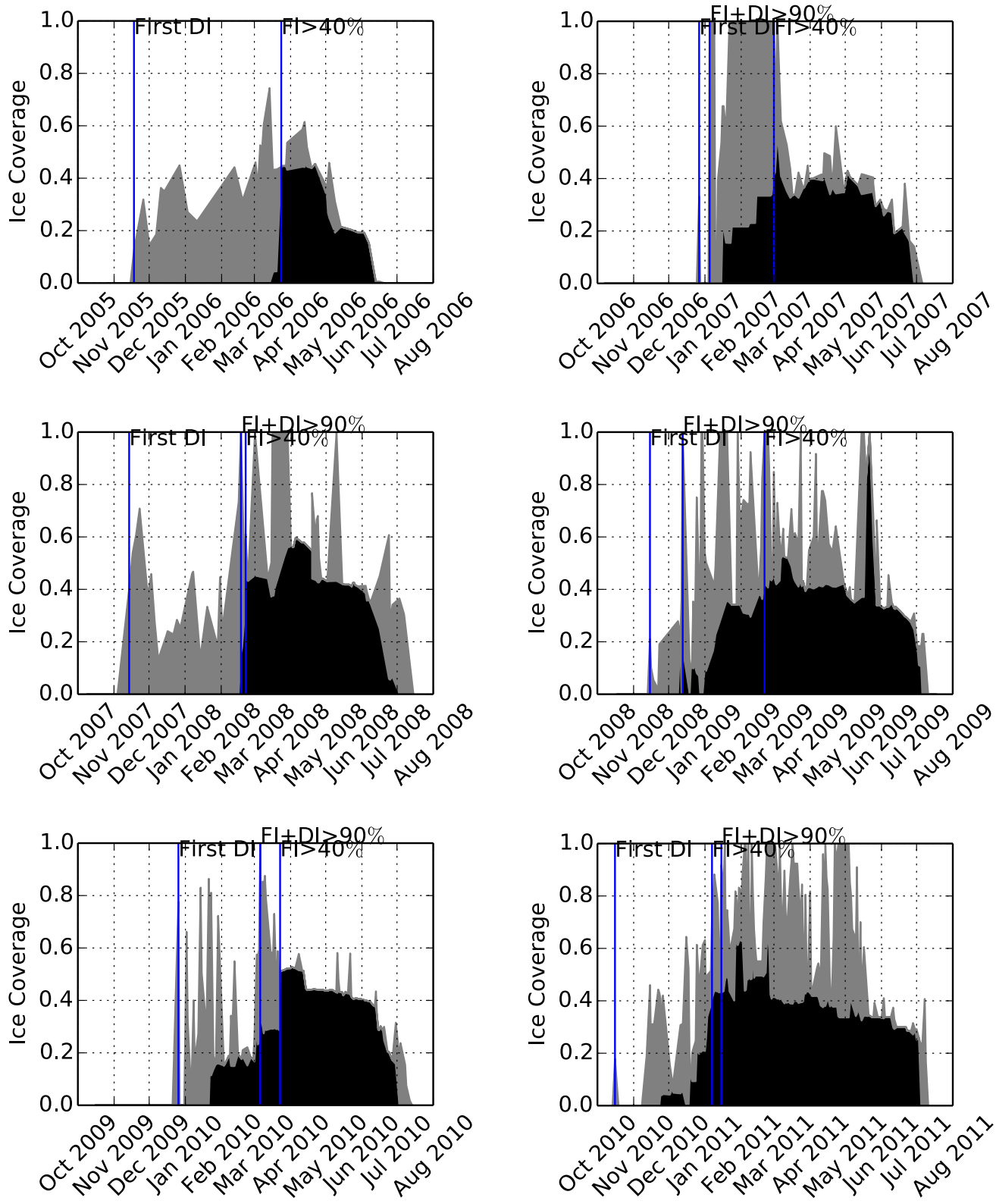

Figure C.1: Ice cover 2006-2011, data from Muckenhuber et al. (In progress). Blue lines corresponding to numbers in Table 3.3

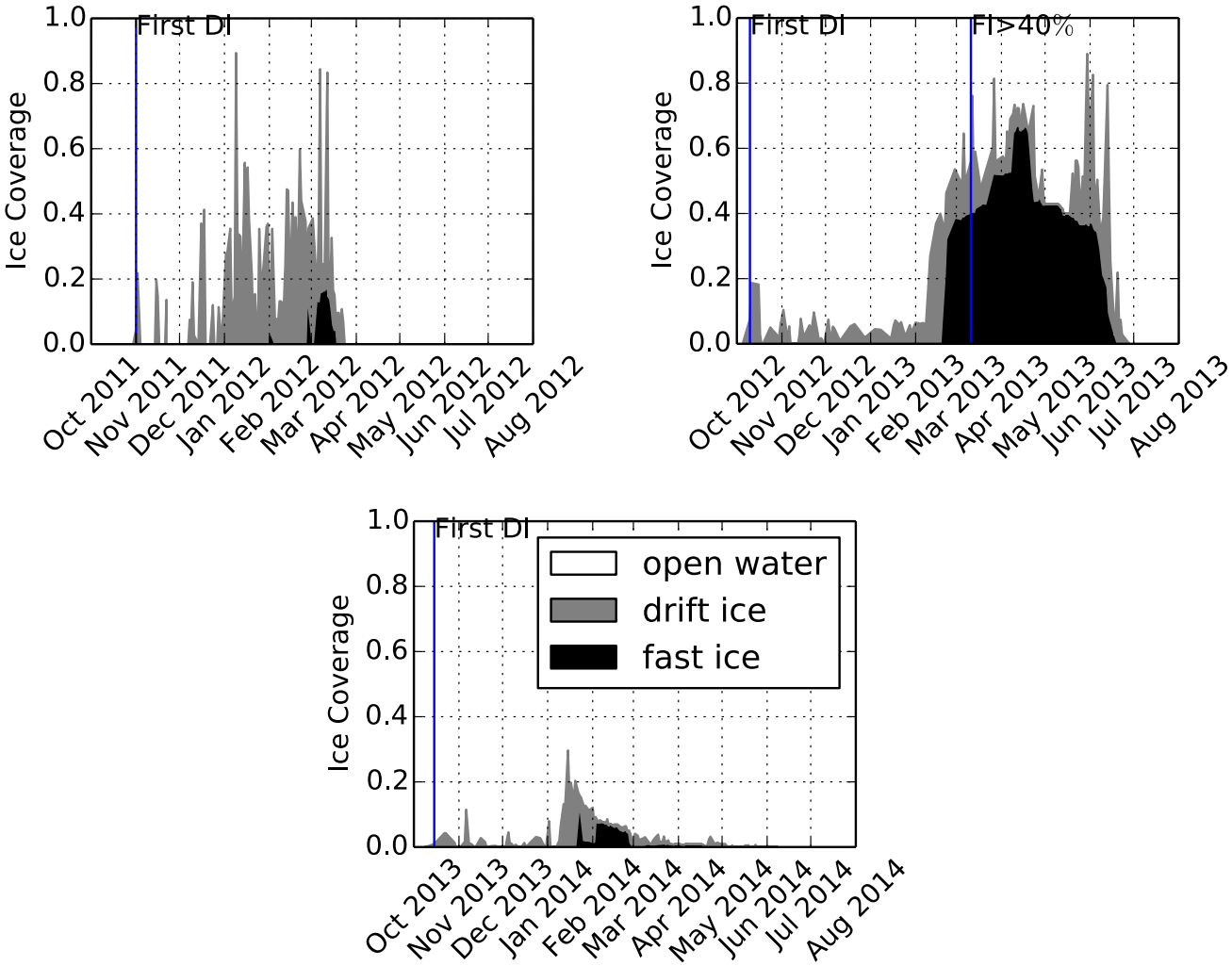

Figure C.2: Ice cover 2012-2014, data from Muckenhuber et al. (In progress). Blue lines corresponding to numbers in Table 3.3

Appendix D

Hypsometric curve for Brepollen

Figure D.1 shows hypsometry for Brepollen is made on the background of bathymetric data from The Norwegian Mapping Authority Hydrographic Service. The surface area do not identically mach the satellite derived surface area, determined by Muckenhuber et al. (In Progress) which is used in the polynya model.

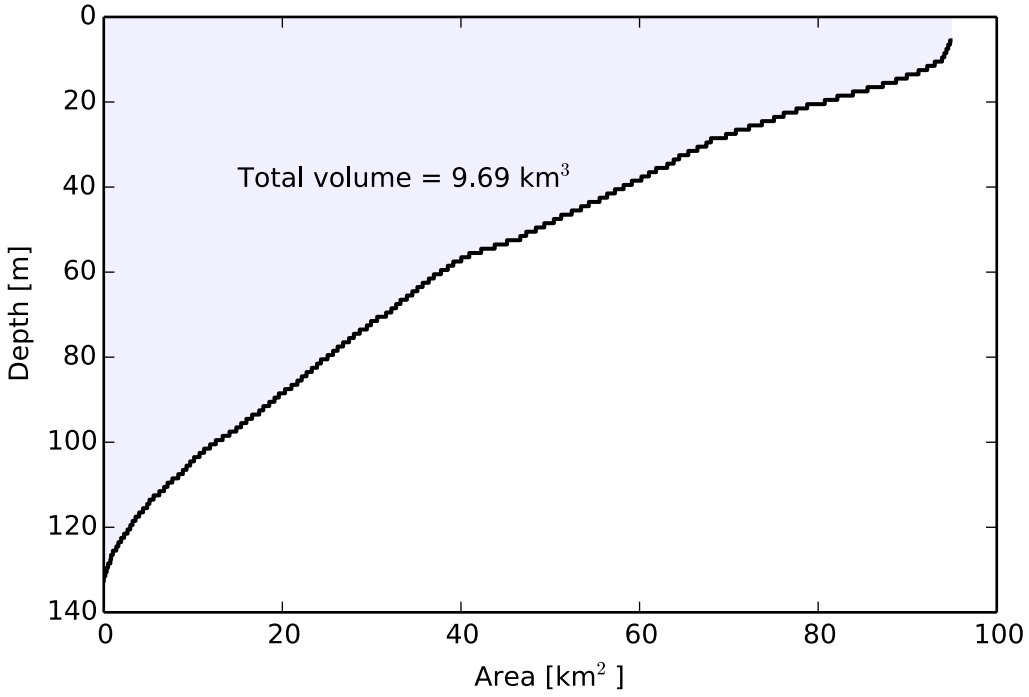

Figure D.1: Hypsometric curve brepollen. The calculation is made for the basin behind the sill south of Treskelodden, thereby including Samarinvågen.

Appendix E

ROMS model results for 2006

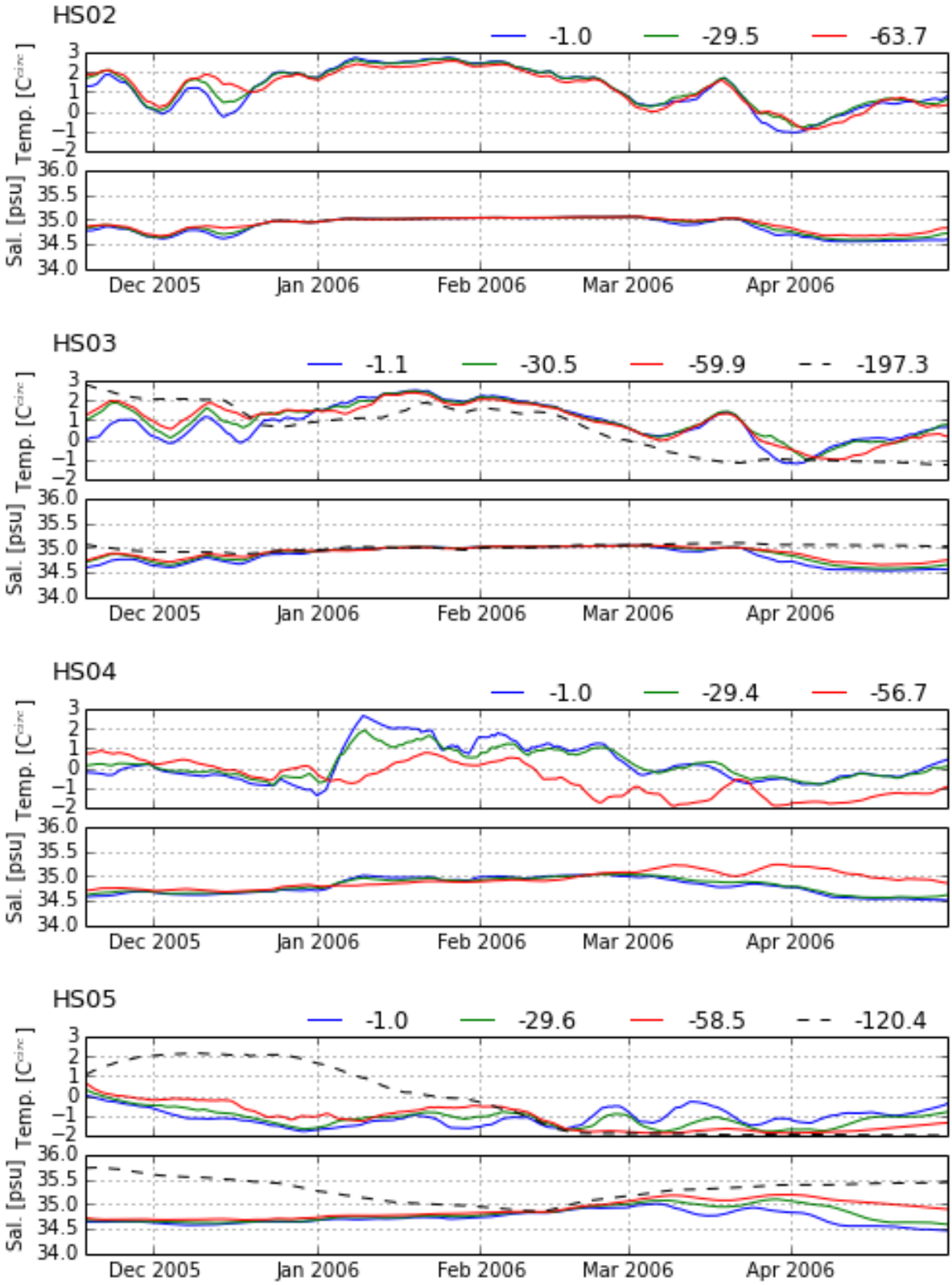

Figure E.1: Temperature and salinity ROMS simulation results from HS02, HS03, HS04 and HS05 for selected depth for the winter season 2006.

Bibliography

Aagaard, K., Coachman, L., and Carmack, E. (1981). On the halocline of the arctic ocean. *Deep Sea Research Part A. Oceanographic Research Papers*, 28(6):529 – 545.

Alam, A. and Curry, J. A. (1998). Evolution of new ice and turbulent fluxes over freezing winter leads. *Journal of Geophysical Research: Oceans*, 103(C8):15783–15802.

Baines, P. G. and Condie, S. (1998). *Observation and Modelling of Antarctic downslope flows: a review in Ocean, ice, and atmosphere: interactions at the Antarctic continental margin*, pages 29–49. American Geophysical Union.

Barber, D. and Massom, R. (2007). Chapter 1 the role of sea ice in arctic and antarctic polynyas. In Smith, W. and Barber, D., editors, *Polynyas: Windows to the World*, volume 74 of *Elsevier Oceanography Series*, pages 1 – 54. Elsevier.

Beszczynska-Møller, A., Fahrbach, E., Schauer, U., and Hansen, E. (2012). Variability in atlantic water temperature and transport at the entrance to the arctic ocean, 1997â2010. *ICES Journal of Marine Science: Journal du Conseil*.

Błaszczyk, M., Jania, A. J., and Leszek, K. (2013). Fluctuations of tidewater glaciers in hornsund fjord (southern svalbard) since the beginning of the 20th century. *Polish Polar Research*, 34:327–.

Bourke, R. H., Weigel, A. M., and Paquette, R. G. (1988). The westward turning branch of the west spitsbergen current. *Journal of Geophysical Research: Oceans*, 93(C11):14065–14077.

Boyd, T. J. and D'Asaro, E. A. (1994). Cooling of the west spitsbergen current: Wintertime observations west of svalbard. *Journal of Geophysical Research: Oceans*, 99(C11):22597–22618.

Brennecke, W. (1921). Die ozeanographischen arbeiten der deutschen antarktischen expedition 1911-1912. *Ark. Deutsch. Seew.,XXXIX*, No. 1.

Budgell, W. (2005). Numerical simulation of ice-ocean variability in the barents sea region. *Ocean Dynamics*, 55(3-4):370–387.

Cavalieri, D. J. and Martin, S. (1994). The contribution of alaskan, siberian, and canadian coastal polynyas to the cold halocline layer of the arctic ocean. *Journal of Geophysical Research: Oceans*, 99(C9):18343–18362.

Cottier, F., Tverberg, V., Inall, M., Svendsen, H., Nilsen, F., and Griffiths, C. (2005). Water mass modification in an arctic fjord through cross-shelf exchange: The seasonal hydrography of kongsfjorden, svalbard. *Journal of Geophysical Research: Oceans*, 110(C12):n/a–n/a.

Cottier, F. R., Nilsen, F., Inall, M. E., Gerland, S., Tverberg, V., and Svendsen, H. (2007). Wintertime warming of an arctic shelf in response to large-scale atmospheric circulation. *Geophysical Research Letters*, 34(10):n/a–n/a.

Cottier, F. R., Nilsen, F., Skogseth, R., Tverberg, V., Skarthhamar, J., and Svendsen, H. (2010). Arctic fjords: a review of the oceanographic environment and dominant physical processes. *Geological Society of London Special Publications*, 344:35–50.

Cushman-Roisin, B. and Beckers, J. M. (2011). Chapter 7 - geostrophic flows and vorticity dynamics. In Cushman-Roisin, B. and Beckers, J.-M., editors, *Introduction to Geophysical Fluid Dynamics Physical and Numerical Aspects*, volume 101 of *International Geophysics*, pages 205 – 238. Academic Press.

Dai, M., Shen, H. H., Hopkins, M. A., and Ackley, S. F. (2004). Wave rafting and the equilibrium pancake ice cover thickness. *Journal of Geophysical Research: Oceans*, 109(C7):n/a–n/a.

Dickson, R. R., Osborn, T. J., Hurrell, J. W., Meincke, J., Blindheim, J., Adlandsvik, B., Vinje, T., Alekseev, G., and Maslowski, W. (2000). The arctic ocean response to the north atlantic oscillation. *J. Climate*, 13(15):2671–2696.

Dmitrenko, I. A., Kirillov, S. A., Rysgaard, S., Barber, D. G., Babb, D. G., Pedersen, L. T., Koldunov, N. V., Boone, W., Crabeck, O., and Mortensen, J. (2015). Polynya impacts on water properties in a northeast greenland fjord. *Estuarine, Coastal and Shelf Science*, 153(0):10 – 17.

Drucker, R., Martin, S., and Moritz, R. (2003). Observations of ice thickness and frazil ice in the st. lawrence island polynya from satellite imagery, upward looking sonar, and salinity/temperature moorings. *Journal of Geophysical Research: Oceans*, 108(C5):n/a–n/a.

Foldvik, A. and Gammelsrød, T. (1988). Notes on southern ocean hydrography, sea-ice and bottom water formation. *Palaeogeography, Palaeoclimatology, Palaeoecology*, 67:3 – 17.

Førland, E. J., Benestad, R., Hanssen-Bauer, I., Haugen, J. E., and Skaugen, T. E. (2011). Temperature and precipitation development at svalbard 1900-2100.

Gade, H. and Edwards, A. (1980). Deep water renewal in fjords. In Freeland, H., Farmer, D., and Levings, C., editors, *Fjord Oceanography*, volume 4 of *NATO Conference Series*, pages 453–489. Springer US.

Gade, H. G. (1986). Features of fjord and ocean interaction. In Hurdle, B., editor, *The Nordic Seas*, pages 183–190. Springer New York.

Gammelsrød, T. and Rudels, B. (1983). Hydrographic and current measurements in the fram strait, august 1981. *Polar Research*, 1(2):115–126.

Gascard, J.-C., Richez, C., and Rouault, C. (1995). New insights on large-scale oceanography in fram strait: The west spitsbergen current. In *Coastal Estuarine Stud.*, volume 49, pages 131–182. AGU, Washington, DC.

Gerland, S. and Hall, R. (2006). Variability of fast-ice thickness in spitsbergen fjords. *Annals of Glaciology*, 44(1):231–239.

Gillibrand, P. A., Turrell, W. R., and Elliott, A. J. (1995). Deep-water renewal in the upper basin of loch sunart, a scottish fjord. *J. Phys. Oceanogr.*, 25(6):1488–1503.

Gordon, A. L. (1998). Western weddel sea thermohaline stratification. *Ocean , Ice, And Atmosphere: Intreaction at the Continental Margin Antarctic Recearch Series*, 75:215–240.

Haarpaintner, J., Gascard, J.-C., and Haugan, P. M. (2001). Ice production and brine formation in storfjorden, svalbard. *Journal of Geophysical Research: Oceans*, 106(C7):14001–14013.

Haidvogel, D., Arango, H., Budgell, W., Cornuelle, B., Curchitser, E., Lorenzo, E. D., Fennel, K., Geyer, W., Hermann, A., Lanerolle, L., Levin, J., McWilliams, J., Miller, A., Moore, A., Powell, T., Shchepetkin, A., Sherwood, C., Signell, R., Warner, J., and Wilkin, J. (2008). Ocean forecasting in terrain-following coordinates: Formulation and skill assessment of the regional ocean modeling system. *Journal of Computational Physics*, 227(7):3595 – 3624. Predicting weather, climate and extreme events.

Hunter, J. (2007). Matplotlib: A 2d graphics environment. *Computing in Science Engineering*, 9(3):90–95.

Inall, M. E. and Gillibrand, P. A. (2010). The physics of mid-latitude fjords: a review. *Geological Society, London, Special Publications*, 344(1):17–33.

Ingvaldsen, R., Reitan, M. B., Svendsen, H., and Asplin, L. (2001). The upper layer circulation in kongsfjorden and krossfjorden-a complex fjord system on the west coast of spitsbergen (scientific paper). *Memoirs of National Institute of Polar Research. Special issue*, 54:393–407.

Jones, E., Oliphant, T., Peterson, P., et al. (2001). SciPy: Open source scientific tools for Python.

Jones, P., Jonsson, T., and Wheeler, D. (1997). Extension to the north atlantic oscillation using early instrumental pressure observations from gibraltar and south-west iceland. *International Journal of Climatology*, 17(13):1433–1450.

Kruszewski, G. (2010). Ice conditions in hornsund during winter season 2009-2010 (sw spitsbergen). *Problemy Klimatologii Polarnej 21*.

Kruszewski, G. (2011). Ice conditions in hornsund and adjecent waters (spitsbergen) during winter season 2010-2011. *Problemy Klimatologii Polarnej 22*.

Leppäranta, M. (2011). *The drift of sea ice*. Springer Science & Business Media.

Martin, S. and Cavalieri, D. J. (1989). Contributions of the siberian shelf polynyas to the arctic ocean intermediate and deep water. *Journal of Geophysical Research: Oceans*, 94(C9):12725–12738.

Maykut, G. A. (1986). The surface heat and mass balance. In Untersteiner, N., editor, *The Geophysics of Sea Ice*, NATO ASI Series, pages 395–463. Springer US.

McDougall, T. and Barker, P. (2011). *Getting Started with TEOS-10 and the Gibbs Seawater (GSW) Oceanographic Toolbox*.

Morales Maqueda, M. A., Willmott, A. J., and Biggs, N. R. T. (2004). Polynya dynamics: a review of observations and modeling. *Reviews of Geophysics*, 42(1):n/a–n/a. RG1004.

Mosby, H. (1934). The waters of the atlantic antarctic ocean. scientific results of the norwegian antarctic expeditions 1927-1928.

Muckenhuber, S., Nilsen, F., Korosov, A., and Sandven, S. (In progress). Sea ice cover in isfjorden and hornsund 2000 - 2014 by using remote sensing.

Myksvoll, M. S., Sandvik, A. D., Asplin, L., and Sundby, S. (2014). Effects of river regulations on fjord dynamics and retention of coastal cod eggs. *ICES Journal of Marine Science: Journal du Conseil*, 71(4):943–956.

Nansen, F. (1906). *Norther Waters: Captain Roald Amundsens Oceanographic Observations in the Arctic Seas in 1901*, volume Matematisk-Naturvidenskabelig Klasse 1,. Videnskab-Selskabets Skrifter 1.

Nansen, F. (1915). *Spitsbergen Waters - Oceanographic observations During the Cruise of the "Veslem¿y" to Spitsbergn 2012*, volume No. 2. Videnskapsselskapets Skrifter 1 Mat.-Naturv. Klasse.

Nilsen, F., Cottier, F., Skogseth, R., and Mattson, S. (2008). Fjord-shelf exchanges controlled by ice and brine production: The interannual variation of atlantic water in isfjorden, svalbard. *Continental Shelf Research*.

Nilsen, F., Skogseth, R., Vaardal-Lund, J., and Inall, M. (In progress). A simple shelf circulation model − intrusion of atlantic water on the west spitsbergen shelf.

Ohshima, K. I., Yoshida, K., Shimoda, H., Wakatsuchi, M., Endoh, T., and Fukuchi, M. (1997). Relationship between the upper ocean and sea ice during the antarctic melting season. *Proceedings of the NIPR Symposium on Polar Meteorology and Glaciology*, 11:267.

OLeary, M. and Christoffersen, P. (2013). Calving on tidewater glaciers amplified by submarine frontal melting. *The Cryosphere*, 7(1):119–128.

Overland, J. E. and Wang, M. (2010). Large-scale atmospheric circulation changes are associated with the recent loss of arctic sea ice. *Tellus A*, 62(1):1–9.

Pavlov, A. K., Tverberg, V., Ivanov, B. V., Nilsen, F., Falk-Petersen, S., and Granskog, M. A. (2013). Warming of atlantic water in two west spitsbergen fjords over the last century (1912-2009). *Polar Research; Vol 32 (2013) incl supplements*, pages –.

Pease, C. H. (1987). The size of wind-driven coastal polynyas. *Journal of Geophysical Research: Oceans*, 92(C7):7049–7059.

Prominska, A., Falck, E., Beszczynska-Møller, A., Walczowski, W., and Sundfjord, A. (Unpublished data). Interannual changes in properties of water in hornsund fjord between 2001 - 2013.

Saloranta, T. M. and Haugan, P. M. (2001). Interannual variability in the hydrography of atlantic water northwest of svalbard. *Journal of Geophysical Research: Oceans*, 106(C7):13931–13943.

Saloranta, T. M. and Haugan, P. M. (2004). Northward cooling and freshening of the warm core of the west spitsbergen current. *Polar Research*, 23(1):79–88.

Saloranta, T. M. and Svendsen, H. (2001). Across the arctic front west of spitsbergen: high-resolution ctd sections from 1998-2000. *Polar Research*, 20(2):177–184.

Schauer, U. (1995). The release of brine-enriched shelf water from storfjord into the norwegian sea. *Journal of Geophysical Research: Oceans*, 100(C8):16015–16028.

Schauer, U. and Fahrbach, E. (1999). A dense bottom water plume in the western barents sea: downstream modification and interannual variability. *Deep Sea Research Part I: Oceanographic Research Papers*, 46(12):2095 – 2108.

Schlichtholz, P. and Goszczko, I. (2005). Was the Atlantic water temperature in the West Spitsbergen Current predictable in the 1990s? , 32:4610.

Skogseth, R., Fer, I., and Haugan, P. M. (2005). *Dense-Water Production and Overflow from an Arctic Coastal Polynya in Storfjorden*, pages 73–88. American Geophysical Union.

Skogseth, R., Haugan, P. M., and Haarpaintner, J. (2004). Ice and brine production in storfjorden from four winters of satellite and in situ observations and modeling. *Journal of Geophysical Research: Oceans*, 109(C10):n/a–n/a.

Smedsrud, L. H. (2011). Grease-ice thickness parameterization. *Annals of Glaciology*, 52(57):77–82.

Smedsrud, L. H., Budgell, W. P., Jenkins, A. D., and Å ndalsvik, B. r. (2006). Fine-scale sea-ice modelling of the storfjorden polynya, svalbard. *Annuals of Glaciology*.

Smedsrud, L. H. and Skogseth, R. (2006). Field measurements of arctic grease ice properties and processes. *Cold Regions Science and Technology*, 44(3):171 – 183.

Smith, S. D., Muench, R. D., and Pease, C. H. (1990). Polynyas and leads: An overview of physical processes and environment. *Journal of Geophysical Research: Oceans*, 95(C6):9461–9479.

Stefan, J. (1891). Ueber die theorie der eisbildung, insbesondere über die eisbildung im polarmeere. *Annalen der Physik*, 278(2):269–286.

Svendsen, H. (1995). Physical oceanography of coupled fjord-coast systems in northern norway with special focus on frontal dynamics and tides. *Ecology of Fjords and Coastal Waters. Elsevier, New York*, pages 149–164.

Svendsen, H., Beszczynska-Møller, A., Hagen, J. O., Lefauconnier, B., Tverberg, V., Gerland, S., Ørbæk, J. B., Bischof, K., Papucci, C., Zajaczkowski, M., Azzolini, R., Bruland, O., Wience, C., Winther, J.-G., and Dallmann, W. (2002). The physical environment of kongsfjorden-krossfjorden, an artic fjord system in svalbard. *Polar Research*, 21:133–166.

Svendsen, H. and Thompson, R. O. R. Y. (1978). Wind-driven circulation in a fjord. *J. Phys. Oceanogr.*, 8(4):703–712.

Swerpel, S. (1985). The hornsund fiord: Water masses. *Polish Polar Research*, 6:475–496.

Tverberg, V., N¿st, O. A., Lydersen, C., and Kovacs, K. M. (2014). Winter sea ice melting in the atlantic water subduction area, svalbard norway. *Journal of Geophysical Research: Oceans*, 119:5945–5967.

Wadhams, P. (1981). The ice cover in the greenland and norwegian seas. *Reviews of Geophysics*, 19(3):345–393.

Walczowski, W. and Piechura, J. (2011). Influence of the west spitsbergen current on the local climate. *International Journal of Climatology*, 31(7):1088–1093.

Walt, S., Colbert, S. C., and Varoquaux, G. (2011). The numpy array: A structure for efficient numerical computation. *Computing in Science & Engineering*, 13(2):22–30.

Weslawski, J. M. and Adamski, P. (1987). Cold and warm years in south spitsbergen coastal marine ecosystem. *Polish Polar Reserch*, 8:96–106.

Williams, W., Carmack, E., and Ingram, R. (2007). Chapter 2 physical oceanography of polynyas. In Smith, W. and Barber, D., editors, *Polynyas: Windows to the World*, volume 74 of *Elsevier Oceanography Series*, pages 55 – 85. Elsevier.

Winsor, P. and Björk, G. (2000). Polynya activity in the arctic ocean from 1958 to 1997. *Journal of Geophysical Research: Oceans*, 105(C4):8789–8803.

WMO, W. M. O. (1970). Sea-ice nomenclature (wmo no. 259 suppl.no.5).

www.myroms.org (n.d.). www.myroms.org.